Control of quantum correlations in hybrid qubit systems

Cristian Edwin Susa Quintero

A thesis submitted at the Universidad del Valle as a partial requirement for the degree of Doctor of Science in Physics

Supervisor
Prof. Dr. John H. Reina E.

Universidad del Valle
Faculty of Natural and Exact Science
Department of Physics
Cali-Colombia
October 2016

To the memory of my grandfather Armando A. Quintero L.

Even when he never understood what I had studied so far, he was always supportive and enthusiastic about the ways of knowledge; followed my progress, and taught me the goodness of politeness.

Acknowledgements

There is an endless list of people and situations that I would like to and must thank so far. However, regardless the order of appearance, I want to sincerely thank Professor John Reina for the great opportunity to work with him, all in all, since an undergraduate, for about seven years, for being patient with my research progress, and for his great advice at both, professional and personal levels.

I also would like to especially acknowledge the QuanTIC group for all the support, fun, discussions, and nice environment that facilitated my work throughout these years.

I thank Vlatko Vedral for the opportunity to work in his Group at Oxford, and would like to specially thank Davide Girolami, with whom I developed the project about complexity and who has been aware of my progress on it so far.

I infinitely thank my parents Pedro and Gloria for their unconditional love and support in all the possible forms, they are the only reason I always try to do my best. I am also specially thankful to my sister for her positive words and for being by my side since I started this endeavour. To my grandparents for trying to understand my path as a physicist.

I thank my wife Lady for taking the decision of learning together about love and sincerity. I am happy to being able to find her and to seeing in our sweet baby Renata, the result of a bit more than ten years of such learning.

To my best friend Carlos Echeverry, who is always in my thoughts, and to his family for their invaluable friendship.

My sincere acknowledgement to the professors in the Department of Physics, who have contributed to my growth as an academic. I acknowledge them for their lectures, criticisms, advice, help, etc. I also thank the secretaries for their administrative help when required.

I thank professors Felipe F. Fanchini, Luis L. Sánchez-Soto, and Richard Hildner for their pertinent work in different stages of my research progress and for sharing nice moments during international conferences.

Last but not least, I thank Colciencias for the full scholarship that allowed me to undertake my graduate studies, and their support for my participation in scientific events, and my research stay at the Clarendon Laboratory, Oxford (U.K.).

Abstract

The principal study reported in this Thesis concerns the investigation of quantum information as a physical resource (e.g., quantum correlations and entanglement) in open quantum systems. We consider a quantum bit (qubit) register interacting with a big reservoir and test the dynamics of quantum correlations and entanglement between the qubits under different physical scenarios. Additionally, in the context of multipartite systems, we extend our knowledge on quantum correlations and introduce a protocol for quantifying quantum complexity. Here, we deal with complexity in terms of the structure of a multiparticle system, i.e., how different the information given by the state of the total system is with respect to the information extracted from the state of the distinct subsystems.

After an introduction to the mathematical tools needed for the computation of the quantifiers of the system's dynamics, in the first part, we discuss the conditional quantum dynamics and the entanglement production that can be achieved with a two-qubit system interacting with a Markovian environment and driven by a continuous coherent laser field. In particular, we focus on arrays of Perylene-Bisimide organic molecules that are currently available and that can be synthesised by our collaborator Richard Hildner at University of Bayreuth, Germany. We show that the molecules can allow the generation of the Swap gate, and bipartite entanglement in a natural way, due to the dipolar interaction between them. We explore some scenarios to process information in terms of the eigenenergies of the associated Hamiltonian and the system's dissipative time evolution. We do so for dimers and trimers (two and three coupled molecules). Furthermore, we explore the way in which the information stored as quantum correlations flows from the qubit system to the environment and viceversa. We show that partial knowledge of the correlations dynamics of the qubit system can be obtained from the correlations between one qubit and the environment, thus remarking the importance of considering the full role of system-environment quantum correlations.

In the second part, we address the role of quantum correlations in a setup comprising quantum emitters coupled to the propagating light on a metallic surface, i.e., the new environment now comprises the plasmons generated on the surface of a metallic one-dimensional waveguide. We demonstrate that it is possible to generate correlations between distant ($\sim 1\mu$m separation) qubits by means of the hybrid qubit-plasmons coupling, and also make use of this physical setup for tailoring entanglement generation. Thus, we report on the robustness of the quantum discord when compared to the entanglement of formation. We also give a dynamical protocol that is able to switch on and off the quantum correlations between the qubits by means of the action of an external field and its interplay with the dipolar interaction generated between the qubits.

In a third part, we investigate the role played by local and nonlocal quantum states on the performance of a bipartite non-zero sum game, and show that input *local* quantum correlations, and *separable* states in particular, suffice to achieve an advantage over any strategy that uses classical resources, thus dispensing with quantum nonlocality, entanglement, or even discord between the players' input states. We recall that quantum information allows the formulation of novel game strategies that lead to new equilibrium points whereby players in some classical games are always outperformed if sharing and processing joint

information ruled by the laws of quantum physics. Thus, we re-examine the question about the actual role played by purely quantum interferences at powering some information-based protocols.

Finally, we deal with the problem of *quantifying complexity* in multipartite systems by linking this concept to that of the correlations that arise between the system parties at different scales of description. We succeeded in identifying a measure of complexity that satisfies the bona fide criteria for multipartite correlations. In doing so, we used information-theoretic tools to build the geometric distance-like metric between the total state and the state reconstructed from the substates of different partitions and that are free of correlations at different scales. After defining our measure of complexity, we computed it on the symmetric multipartite GHZ states and compared it with other measures available in the literature. The main features conveyed by our complexity mesure are that it satisfies the criteria of multipartite correlations, and that it is easier to compute when compared to the results of the existing literature.

Resumen

El estudio principal de esta Tesis concierne a la investigación de la información cuántica como un recurso físico (ej., correlaciones cuánticas y entrelazamiento) en sistemas cuánticos abiertos. Consideramos un registrador de bits cuánticos (qubits) interactuando con su entorno y evaluamos la dinámica de las correlaciones cuánticas y del entrelazamiento entre los qubits bajo diferentes escenarios físicos. Adicionalmente, en el contexto de sistemas multipartitos, extendemos nuestros conocimientos de correlaciones cuánticas e introducimos un protocolo para cuantificar complejidad cuántica. Aquí, tratamos la complejidad en términos de la estructura de un sistema multipartito, es decir, qué tan diferente es la información brindada por el estado del sistema total con respecto a la información extraída del estado de los distintos componentes o subsistemas.

Después de una introducción a las herramientas matemáticas necesarias para el cálculo de los cuantificadores de la dinámica del sistema, en la primera parte, discutimos la dinámica cuántica condicional y la producción de entrelazamiento que puede obtenerse con un sistema de dos qubits interactuando con un entorno Markoviano y dirigido por un campo láser coherente continuo. En particular, nos enfocamos en arreglos de moléculas orgánicas de Perileno-bisimida que están actualmente disponibles y que pueden ser sintetizadas por uno de nuestros colaboradores. Mostramos que las moléculas pueden permitir la generación de la compuerta cuántica Swap, y entrelazamiento bipartito de una forma natural, debido a la interacción dipolar entre las moléculas. Exploramos algunos escenarios para procesar información en términos de las energías propias del Hamiltoniano asociado y la evolución temporal disipativa del sistema. Realizamos el estudio para dímeros y trímeros (dos y tres moléculas acopladas). Además, exploramos la forma en la cual la información almacenada como correlaciones cuánticas, fluye del sistema de qubits al entorno y viceversa. Mostramos que se puede tener un conocimiento parcial de la dinámica de correlaciones del sistema de qubits a partir de las correlaciones entre un qubit y el entorno, así, se enfatiza la importancia de considerar el papel completo de las correlaciones cuánticas sistema-entorno.

En la segunda parte, abordamos el papel de las correlaciones cuánticas en una configuración que comprende emisores cuánticos acoplados a la luz que se propaga sobre una superficie metálica, es decir, el nuevo entorno ahora consiste en los plasmones generados sobre la superficie de una guía de ondas unidimensional metálica. Mostramos que es posible generar correlaciones entre qubits distantes ($\sim 1\mu$m de separación) por medio del acoplamiento del sistema híbrido qubit-plasmones, y también hacemos uso de este sistema físico para dirigir la generación de entrelazamiento. Así, reportamos sobre la robusteza de la discordia cuántica al compararse con el entrelazamiento de formación. Damos también un protocolo dinámico que es capaz de apagar y encender las correlaciones cuánticas entre los qubits por medio de la acción de un campo externo y su interacción con el acople dipolar generado entre los qubits.

En una tercera parte, investigamos el papel desempeñado por estados cuánticos locales y no locales en la ejecución de un juego bipartito de suma no-cero, y mostramos que correlaciones cuánticas locales, y estados separables en particular, son suficientes para alcanzar una ventaja sobre cualquier estrategia que use recursos clásicos, prescindiendo así de nolocalidad cuántica, entrelazamiento, o más aún discordia entre los estados de entrada de los jugadores. Recordamos que la información cuántica permite

la formulación de novedosas estrategias de juego que permiten tener nuevos puntos de equilibrio por los cuales los jugadores en algún juego clásico son superados si se comparte y se procesa información conjunta reglamentada por las leyes de la mecánica cuántica. Así, re-examinamos la pregunta sobre cuál es el papel real de las interferencias puramente cuánticas para mejorar algunos protocolos basados en información.

Finalmente, tratamos el problema de *cuantificar complejidad* en sistemas multipartitos enlazando este concepto con el de correlaciones que surgen entre las partes del sistema a diferentes escalas de descripción. Logramos identificar una medida de complejidad que satisface los criterios de buena fé para correlaciones multipartitas. Para esto, usamos herramientas de la teoría de información para construir la métrica tipo distancia geométrica entre el estado total y el estado reconstruido de los subestados de las diferentes particiones y que son libres de correlaciones a diferentes escalas. Después de definir nuestra medida de complejidad, la calculamos sobre los estados simétricos multipartitos GHZ y la comparamos con otras medidas disponibles en la literatura. Las principales características de nuestra medida de complejidad son que esta satisface los criterios de las correlaciones multipartitas, y que es más fácil de computar cuando se compara con los resultados de la literatura existente.

Contents

Introduction

The quantum properties of physical systems have been studied for many years as crucial resources for quantum processing tasks and quantum information protocols [1, 2, 3, 4, 5]. Among these properties, entanglement [6, 7, 8, 9], non-locality [10, 11], and correlations [12, 13, 14, 15] between quantum objects arise as fundamental features. Non-locality is the most restrictive property known so far. We attribute this property to a quantum state when this can not be described by using a local hidden-variable model [10, 33]. Entangled states constitute a set bigger than non-local states, this means that some entangled states can be local. We say that a state is entangled when it can not be described by means of the states of its components [6, 16]. Finally, quantum correlations are more general than the previous two properties, i. e., almost all quantum states can exhibit quantum correlations [17].

The study of such properties in open quantum systems is a crucial aspect of quantum information science [3, 18, 19], in particular because decoherence appears as a ubiquitous physical process that prevents the realisation of unitary quantum dynamics. It washes out quantum coherence and multipartite correlations, and has long been recognised as a mechanism responsible for the emergence of classicality from events in a purely quantum realm [20]. In fact, it is the influence of harmful errors caused by the interaction of a quantum register (a collection of quantum objects) with its environment [CS7, 20, 21, 22] that precludes the construction of an efficient scalable quantum computer [23, 24]. Existence and behaviour of quantum correlations depend on the actual physical system to be studied, be it quantum dots [25], superconducting qubits [26], atoms and photons [27], or biomolecules [28], they all can support different kind of quantum correlations in different ways.

Nowadays, it is well known that entanglement is not the more general form of correlations between quantum systems, many approaches on measurement-dependent quantum correlations, as it is the case of the original quantum discord [29], have been developed (for a recent review on the applications and the different ways of measuring quantum correlations see [15]). The principal feature of the quantum discord is to differentiate the quantum information stored in a composite state from the information that can be extracted by means of local measurements on one part of the total state [29]. Furthermore, generalisations of the well-known Bell's non-locality have also arisen as distinct forms of non-locality quantifiers [31, 32, 33]. In this Thesis, we focus on discussing the former kind of quantum correlations in open quantum systems. On one hand, we pay attention to the dynamics of entanglement and more general quantum correlations in systems comprising molecules immersed in a host matrix acting as the environment. A particular physical setup underneath this profile is a system made of organic molecules diluted in a protein solvent [35, 36, 34]. They can be modelled as a collection of two-level quantum systems (qubits) interacting with the vacuum electromagnetic field [CS1, CS2]. On the other hand, many works devoted to the study of entanglement and correlations dynamics in open quantum systems are focused on the analysis of the reduced system of interest (the register) and the quantum state of the environment is usually discarded [28, 37, CS4, 38, 39]. There have recently been proposed, however, some ideas for detecting system-environment correlations (see e.g., [40, 41] and references therein). For example, experimental tests of system-environment correlations detection have been recently carried out by means of single trapped ions [42]. The role and effect of the system-environment correlations on the dynamics of open quantum systems have also been studied within the spin-boson model [43], and

as a precursor of a non-Markovian dynamics [CS7, 44]. Here, we also approach the qubit-environment dynamics from a different perspective and show that valuable information about the evolution of quantum entanglement and correlations can be obtained if the distribution of correlations between the register and the environment is better understood. This is described in Chapter 2

Quantum emitters[1] such as single molecules [45, 46] or quantum dots [47, 48, 49] coupled to surface plasmons of conducting nanowires or waveguides have been recently seen as a promising hardware for quantum information processing because of the strong coupling that can be achieved between the emitters and the plasmons [47]. The propagating light along a dielectric/metal interface that results from the optical excitation of the free electrons in the metal, the surface plasmons, can interact with matter [50]. This new light-matter interaction allows the enhancement and control of the coupling between long-distant qubits. This is a key goal in quantum information science for the construction of large quantum networks [4]. Surface plasmons are collective (electron-photon) excitations in dielectric-metal interfaces that have become an important physical resource in many applications in physics, chemistry, and materials science [51, 52]. In particular, the coupling of these excitations with single emitters [53, 54, 55] has attracted substantial attention because it enhances the emission properties of the emitters [56, 57]. The collective spontaneous decay and the plasmon-mediated emitter-emitter coupling have been investigated for a two-qubit system close to a nanowire [58]. Entanglement of two qubits, mediated by a plasmonic waveguide with V-groove shape, has recently been theoretically studied [59] and quantified via the entanglement monotone called concurrence [16]. We extend our discussion on quantum correlations to this emitter-plasmon hybrid system in Chapter 3.

Quantum properties such as entanglement and Bell nonlocality turned out to be of key relevance in the development of quantum information science and technology [CS7, 9, 11]. In game theory, quantisation protocols for strategy games exemplify a physical process whereby entanglement or nonlocality are used as a fundamental resource [60, 61, 62, 31, 63, 64]. This establishes a connection between game theory and quantum information and, as such, introduces the existence of certain advantages over the foregoing classical results [60, 61, 62, 31, 63, 64], and extends the set of cases that find solution to the interaction formalism [65, 66] into the quantum realm [60, 61]. We test the question about the actual role played by purely quantum interferences at powering a bipartite[2] non zero-sum game in Chapter 4.

Understanding the quantum behaviour of many-body (multipartite) systems is also of great relevance for future developments in information science and related areas. Multipartite systems can exhibit new features that are very different to what happens in bipartite systems; for instance, quantum multipartite states can present different kinds of entanglement. The more constituents the system has the more complex its description is. Hence, it seems appropriate to introduce the concept of complexity, as an indicator of how correlated the parts of a multipartite system are. In fact, complexity is a widely discussed concept in several disciplines. A comprehensive definition of complexity states the following: "the minimal knowledge needed to deduce the features of a particular system or phenomenon" [67, 68, 69]. In different contexts, such a statement takes different meanings, yet one can roughly classify the attempts to quantify complexity as the difficulty to describe a process, the ability to predict the dynamics of a system, or its degree of organisation. A non-exhaustive list of more than forty distinct definitions of complexity can be seen in [70]. In Chapter 5, we pay attention to the latter definition, i.e., complexity being a feature of multipartite systems which have properties not deduced from the knowledge of its parts. It is then "natural" to relate the notion of complexity to correlations, and even consider them as equivalent, thus quantifying complexity with a measure of correlations between the system parts.

[1] Quantum emitters are also referred to as qubits, meaning two-level quantum systems. Along this Thesis, we use indistinguishably these two terms.

[2] Bipartite involves two parts. We refer to a bipartite system as a system consisting of two particles with arbitrary dimensions.

Chapter 1
Open quantum systems and quantum correlations

In the real world, physical systems are not completely isolated as they interact with their surroundings (herein referred to as the environment); for instance: atomic systems interacting with the vacuum electromagnetic field, molecules immersed in crystal matrices, quantum emitters in close proximity to structured reservoirs as cavities, surfaces and channels. These sort of physical systems can be modelled in the Shrödinger picture by means of the Hamiltonian theory, thus, the knowledge of the energies associated to both the system of interest and the environment, as well as the energy due to the mutual interaction between them allows us to describe the way in which the system of interest and some interesting properties (herein interpreted as quantum correlations) evolve in time.

Quantum correlations comprise the intriguing and powerful property of entanglement [71] and more general correlations, such as the quantum discord (see section 1.2.3 for definition) [29]. Nowadays, the latter is also considered of great interest in quantum information science and has been experimentally tested to show quantum advantage in several protocols [13, 72].

We briefly introduce the system-environment model in Section 1.1, the master equation formalism is described in Section 1.1.1, and a brief description of the concept of quantum, classical, and total correlations (in an entropic context), as well as that of the entanglement is presented in Section 1.2.

1.1 System plus environment model

Let $\mathcal{H}_S$ be the Hilbert space associated to the system of interest and $\mathcal{H}_\mathcal{E}$ the respective environment Hilbert space, the total (system plus environment) configuration (the universe) lives in a Hilbert space $\mathcal{H}_{Full} = \mathcal{H}_S \otimes \mathcal{H}_\mathcal{E}$. The total Hamiltonian can be written as

$$\hat{H}_{Full} = \hat{H}_S \otimes \mathbb{1}_\mathcal{E} + \mathbb{1}_S \otimes \hat{H}_\mathcal{E} + \hat{H}_{S\mathcal{E}}(t), \tag{1.1.1}$$

where $\hat{H}_{S\mathcal{E}}$ represents the system-environment interaction Hamiltonian (Fig.1.1), $\mathbb{1}_S$ and $\mathbb{1}_\mathcal{E}$ stand for the identity operator of the system of interest and the environment, respectively.

Given an initial condition for the system-environment interaction, the density operator $W(t)$ associated to the universe exhibits a unitary time evolution described by the Liouville-von Neumann equation

$$\dot{W}(t) = -\frac{\mathrm{i}}{\hbar}\left[\hat{H}_{Full}, W(t)\right]. \tag{1.1.2}$$

The open system (S) dynamics can be obtained by tracing out over the degrees of freedom of the environment [73, 74]:

$$\rho(t) = \mathrm{Tr}_\mathcal{E}\{W(t)\}, \tag{1.1.3}$$

such that $\rho(t)$ is the density operator of S at time t.

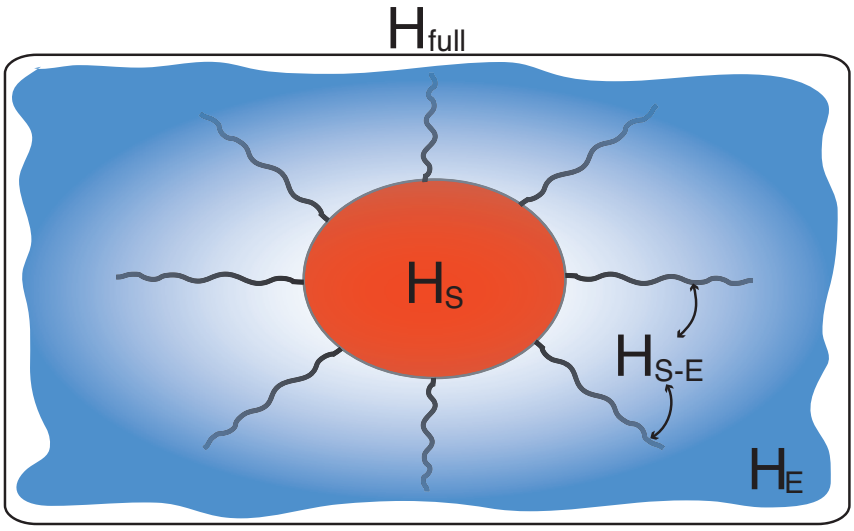

Figure 1.1: Scheme of the system-plus-environment model. $\mathcal{H}_{full}$ is the Hilbert space comprising the quantum system S (the physical system of interest; e.g., an array of two two-level systems—qubits), and the environment E that is considered to be a large reservoir affecting the coherent dynamics of the quantum system.

The way to manage the computation of $\rho(t)$ depends on the physical properties of the full system. In a general framework, we can classify the time evolution of open quantum systems as Markovian and non-Markovian. The former case implies that the environment is considered to be much bigger (as a thermal bath) than the system of interest, such that its state is not affected by the dynamics of the quantum system. On the other hand, a non-Markovian dynamics assumes the environment can be a small structured reservoir with degrees of freedom of the same order of those for the system of interest, which implies that both parts (the system and the environment) are affected by the other such that memory effects have to be taken into account. The physical systems studied in this Thesis can be categorised in the former case whereby the formalism of the master equation in a Markovian approximation (Section 1.1.1) is enough to characterise the dynamics followed by the system.

1.1.1 Markovian master equation

The most significant characteristic of Markovian processes is that they define a semigroup. A semigroup is a set of dynamical maps $\{\Phi(t), t\}$ with the property of being divisible, i.e., $\Phi(t_1)\Phi(t_2) = \Phi(t_1 + t_2)$. The dynamical map $\Phi(t) : \rho(t) = \Phi(t)\rho(0)$ satisfies the complete positivity property; the density operators in all possible extended Hilbert spaces are mapped into density operators in the same extended Hilbert spaces (see, e.g., [74]).

The equation of motion for the reduced system (system of interest) ruling into the Markovian regime is the general Lindblad master equation [74],

$$\dot{\rho}(t) = -\mathrm{i}\left[\hat{H}_{eff}, \rho(t)\right] - \sum_k \frac{\Gamma_k}{2}\left(\left\{A_k^\dagger A_k, \rho(t)\right\} - 2A_k\rho(t)A_k^\dagger\right), \tag{1.1.4}$$

which is derived from Eq. (1.1.2). The first term on the right hand side of Eq. (1.1.4) is the Hamiltonian part that represents a unitary evolution; $\hat{H}_{eff}$ is the effective Hamiltonian of the reduced system which

also includes the information of the interaction with the environment. The second term is the dissipative Lindblad operator and describes the incoherent effects of the environment on the system. The operators A_k take explicit forms depending on the specific system being considered, and the coefficients Γ_k (called the relaxation rates) are positive to ensure the trace-preserving and completely positivity of the master equation. Thus, $\rho(t)$ is the reduced density operator of the system of interest with the information of the environment perturbation.

From a microscopic point of view, the deduction of a Markovian master equation requires some physical assumptions. In briefly, the system-environment interaction is required to be weak, this is called the Born approximation, and non memory effects are taken into account (Markov approach). These two assumption together are referred to as the Born-Markov approximation (see Appendix A for a brief deduction). The two hybrid physical systems studied in this Thesis can be modelled as a two-qubit system interacting with a bigger system represented by radiation fields: the vacuum electromagnetic field (Chapter 2) and the propagating light on a metallic surface (the so-called surface plasmons–Chapter 3). Both configurations can be plugged into the same master equation as follows:

$$\dot{\rho}(t) = \frac{i}{\hbar}\left[\rho(t), \hat{H}_{\text{eff}}\right] - \sum_{i,j=1}^{2} \frac{\Gamma_{ij}}{2}\left(\rho(t)\sigma_{+}^{(i)}\sigma_{-}^{(j)} + \sigma_{+}^{(i)}\sigma_{-}^{(j)}\rho(t) - 2\sigma_{-}^{(i)}\rho(t)\sigma_{+}^{(j)}\right), \tag{1.1.5}$$

where $\sigma_{+}^{(i)} := |1_i\rangle\langle 0_i|$ and $\sigma_{-}^{(i)} := |0_i\rangle\langle 1_i|$ are the new form of operators A_k in Eq. (1.1.4) and are called the raising and lowering operators for qubit i, respectively. They are also written in terms of the Pauli's group $\{\sigma_0, \sigma_x, \sigma_y, \sigma_z\}$ as $\sigma_{\pm} = \sigma_x \pm i\sigma_y$, with:

$$\sigma_0 = \begin{pmatrix} 1 & 0 \\ 0 & 1 \end{pmatrix};\ \sigma_x = \begin{pmatrix} 0 & 1 \\ 1 & 0 \end{pmatrix};\ \sigma_y = \begin{pmatrix} 0 & -i \\ i & 0 \end{pmatrix};\ \sigma_z = \begin{pmatrix} 1 & 0 \\ 0 & -1 \end{pmatrix}, \tag{1.1.6}$$

defined in the computational basis $\{|0\rangle, |1\rangle\}$.

The effective Hamiltonian for the two-qubit system can be written as:

$$\hat{H}_{\text{eff}} = \hat{H}_S + \hat{H}_{\text{d-d}} + \hat{H}_L, \tag{1.1.7}$$

with the respective contributions:

$$\hat{H}_S = -\frac{\hbar}{2}\left(\omega_1\sigma_z^{(1)} + \omega_2\sigma_z^{(2)}\right); \tag{1.1.8}$$

$$\hat{H}_{\text{d-d}} = \frac{1}{2}\hbar V(\sigma_x^{(1)} \otimes \sigma_x^{(2)} + \sigma_y^{(1)} \otimes \sigma_y^{(2)}); \tag{1.1.9}$$

$$\hat{H}_L = \hbar\ell^{(1)}\left(\sigma_{-}^{(1)}e^{i\omega_L t} + \sigma_{+}^{(1)}e^{-i\omega_L t}\right) + \hbar\ell^{(2)}\left(\sigma_{-}^{(2)}e^{i\omega_L t} + \sigma_{+}^{(2)}e^{-i\omega_L t}\right), \tag{1.1.10}$$

where $\omega_{1(2)}$ stands for the transition frequency between the ground $|0\rangle$ and excited $|1\rangle$ states of qubit 1(2). $\hat{H}_L$ contains the interaction between the qubits and an external coherent field, here always considered as a continuos laser of frequency ω_L and amplitude $\ell^{(i)}$ (Rabi oscillations). $\hbar\ell^{(i)} = -\hat{\mu}_i \cdot \mathbf{E}_i$ is the light-matter coupling with $\mathbf{E}_i$ being the amplitude of the coherent field acting on the i-th qubit. V is the strength of the dipole-dipole (d-d) coupling between qubits coming as a coherent effect from the system-environment interaction.

On the other hand, the coefficients Γ_{ij} in Eq. (1.1.5) define the individual spontaneous emission rates (Γ_{11} and Γ_{22}), and the collective damping rates ($\Gamma_{12} = \Gamma_{21}^{*}$), respectively.

This collective damping and the d-d coupling are important physical parameters in our study of quantum correlations in open quantum systems. Hence, their explicit forms depend on the physical

origin of the system-environment interaction; we consider the pair of emitters (qubits) interacting with the infinite modes of the vacuum electromagnetic field in Chapter 2, and then, we modify the environment to be a bath made of plasmons generated by the light propagation on a metal surface of a waveguide in Chapter 3.

1.2 Quantum information and correlations

In information theory, entropy is a key concept to denote both classical and quantum information. Entropy is the information we gain, on average, when we learn either the value of a random variable X, in classical theory, or the density matrix ρ in the quantum regime. In this section, we first introduce the concept of measurement throughout the third postulate of quantum mechanics and then briefly present the formalism to calculate classical, quantum and total correlations in quantum states.

1.2.1 Quantum measurements

In quantum mechanics, measurements are described by a collection of operators $\{M_i\}$ which maps a quantum state ρ into a statistical ensamble of states $\{p_i, \rho_i\}$ [3]. The index i stands for the measurement outcome that takes place, that is, after one measures the state ρ, it is led to the state $\rho_i = \frac{M_i \rho M_i^\dagger}{p(i)}$, with propability $p(i) = \mathrm{Tr}(M_i \rho M_i^\dagger)$. The measurement operators are required to satisfy the completeness relation $\sum_i M_i^\dagger M_i = \mathbb{1}$.

A mathematical framework for the analysis of measurements is the formalism of Positive Operator-Valued Measures (POVMs). For a set of measurement operators M_i, the set of POVMs is defined as $E_i = M_i^\dagger M_i$, and the probability to obtain the outcome i is $p(i) = \mathrm{Tr}(E_i \rho E_i)$. From its definition, E_i is a positive operator and satisfies the completeness relation $\sum_m E_m = \mathbb{1}$. A possible construction of POVM measurements is to consider an ancilla state which is measured by operators M_i after the bigger state ρ_{SA} evolves into a unitary evolution that couples the system and the ancilla. It is known that tracing out the degrees of freedom of the ancilla system makes the state ρ to evolve into $\mathrm{Tr}(\rho_{SA,i}) = \frac{1}{p_i} E_i \rho E_i$. The particular case of considering projective measurements is referred to as von Neumann measurements.

1.2.2 Entanglement

Entanglement is a crucial feature of quantum phenomena, sometimes referred to as the fingerprint of quantum mechanics. It has been arduously explored as a precious resource for performing quantum computing and quantum communication protocols [3] both theoretically [6, 7, 37, 59] and experimentally[8, 9, 27].

A state ρ_A is said to be mixed if it is written as $\rho_A = \sum_i p_A^i |\psi_A^i\rangle\langle\psi_A^i|$, where $|\psi_A^i\rangle \in \mathcal{H}_A$ is a pure state. For a bipartite system, we say that a mixed state ρ is *separable* if it is of the form

$$\rho_{AB} = \sum_i c_{AB}^i \rho_A^i \otimes \rho_B^i \,, \tag{1.2.1}$$

where ρ_A^i and ρ_B^i are, in general, mixed states in $\mathcal{H}_A$ and $\mathcal{H}_B$, respectively. If ρ_{AB} is *pure*, then, the separability (1.2.1) reduces to $|\Psi\rangle_{AB} = \sum_i a_i |i\rangle_A \otimes \sum_j b_j |j\rangle_B$. A state that is not possible to write in the form (1.2.1) is to be referred to as entangled.

Despite the diversity of entanglement metrics, the entanglement of formation (EoF) is one of the most prominent, and free of ambiguity, measurement of entanglement for bipartite states. The EoF of a density matrix ρ_{AB} is defined as [16]:

$$E(\rho_{AB}) = \min_{\{p_i,\psi_i\}} \sum_i p_i S(|\psi_i\rangle), \tag{1.2.2}$$

where the minimisation is carried out over all the possible pure states[1] decomposition of ρ_{AB}; $\rho_{AB} = \sum_i p_i |\psi_i\rangle\langle\psi_i|$, and $S(|\psi_i\rangle) = -\mathrm{Tr}(\rho_A^i \log_2 \rho_A^i) = -\mathrm{Tr}(\rho_B^i \log_2 \rho_B^i)$ is the von Neumann entropy of each subsystem, with $\rho_{A(B)}^i = \mathrm{Tr}_{B(A)}(|\psi_i\rangle\langle\psi_i|)$. For the particular case of two-qubit systems, the EoF has an analytical solution for both pure and mixed states [16].

For pure states, the EoF can be written as

$$E(\psi_{AB}) = \mathfrak{E}(C(\psi_{AB})), \tag{1.2.3}$$

where the concurrence is defined as $C(\psi_{AB}) =\mid \langle\psi_{AB}|\psi_{AB}\rangle \mid$, and the function $\mathfrak{E}$ is given by

$$\mathfrak{E}(C) = h\left(\frac{1+\sqrt{1-C^2}}{2}\right), \tag{1.2.4}$$

where $h(x) = -x\log_2 x - (1-x)\log_2(1-x)$ denotes the binary entropy function. $\mathfrak{E}$ monotonically increases from 0 to 1 as the concurrence C ranges from 0 to 1. This explains why C can be used as an alternative entanglement quantifier. It should be stressed that only the EoF is an entanglement metric, and C gets its meaning via its relation to the EoF.

For mixed states the EoF is written as [16]

$$E(\rho_{AB}) = \mathfrak{E}(C(\rho_{AB})). \tag{1.2.5}$$

Consider, in descending order, the eigenvalues λ_i of the matrix $\sqrt{\rho_{AB}\tilde{\rho}_{AB}}$, where $\tilde{\rho}_{AB} = (\sigma_y \otimes \sigma_y)\bar{\rho}_{AB}(\sigma_y \otimes \sigma_y)$, $\bar{\rho}_{AB}$ is the elementwise complex conjugate of ρ_{AB}. The concurrence C is defined as

$$C(\rho_{AB}) = \max\{0, \lambda_1 - \lambda_2 - \lambda_3 - \lambda_4\}, \tag{1.2.6}$$

where the λ_i's are as defined above or, equivalently (also in descending order), the square root of the eigenvalues of the non-Hermitian matrix $\rho_{AB}\tilde{\rho}_{AB}$ [16].

1.2.3 Quantum discord and total correlations

In classical information theory, the joint information of two random variables can be obtained by means of the mutual information (MI). Let X and Y be two random variables with Shannon entropies $H(X) = -\sum_x p_x \log p_x$ and $H(Y) = -\sum_y p_y \log p_y$, respectively. The MI is defined as,

$$I(X:Y) = H(X) + H(Y) - H(X,Y). \tag{1.2.7}$$

Using Bayes's rules, the conditional probability is given by $p_{(X|Y=y)} = p_{(X,Y=y)}/p_{(Y=y)}$, therefore, the MI reads

$$I(X:Y) = H(X) - H(X|Y), \tag{1.2.8}$$

[1]The notation $|\psi_i\rangle$ (instead of $|\psi_S^i\rangle$) is used when the system (S) which is referred to is clear. The same simplification will be made for density matrices.

where $H(X|Y)$ is the conditional entropy.

The MI in its representation (1.2.7) has a counterpart in the quantum world written in terms of the von Neumann entropy instead of the Shannon entropy. This is called the quantum mutual information (QMI) and reads as,

$$\mathcal{I}_{AB}(\rho_{AB}) = S(\rho_A) + S(\rho_B) - S(\rho_{AB}), \tag{1.2.9}$$

where $S(\rho) = -\mathrm{Tr}(\rho \log_2 \rho)$. This intrinsic quantity is nothing to do with measurements. However, a fact that arises when trying to get the quantum version of equation (1.2.8) is that it is not always identical to $\mathcal{I}_{AB}(\rho_{AB})$. The reason is that, getting a quantum conditional entropy implies to perturbe (measure) the state of one subsystem (say B) to know the state of the other subsystem (say A).

Ollivier and Zurek [29] proposed a generalisation of Eq. (1.2.8) assuming a complete unidimensional projective measurement made on subsystem B, with projectors $\{\Pi_j^B\}$ satisfying $\sum (\Pi_j^B)^\dagger \Pi_j^B = \mathbb{1}$. The generalisation of Eq. (1.2.8) thus provides another way of writing the QMI (which in general does not coincide with that of Eq. (1.2.9)):

$$J_{\{\Pi_j^B\}}(\rho_{AB}) = S(\rho_A) - S(\rho_{A|\{\Pi_j^B\}}), \tag{1.2.10}$$

where the conditional entropy $S(\rho_{A|\{\Pi_j^B\}}) = \sum_j p_j S(\rho_{A|\Pi_j^B})$, with probability $p_j = \mathrm{Tr}(\Pi_j^B \rho_{AB} \Pi_j^B)$, and the density matrix after the measurements have been performed on subsystem B is given by

$$\rho_{A|\Pi_j^B} = \frac{\Pi_j^B \rho_{AB} \Pi_j^B}{\mathrm{Tr}(\Pi_j^B \rho_{AB} \Pi_j^B)}. \tag{1.2.11}$$

Equation (1.2.10) gives the amount of information gained about A after a measure has been carried out on B.

Following this line of discussion, and given that Eqs. (1.2.9) and (1.2.10) are not always equivalent, they proposed as a measure of quantum correlations, the so-called quantum discord (QD) as the minimum difference between Eq. (1.2.9) and Eq. (1.2.10):

$$\begin{aligned} \delta_{AB}^{\leftarrow}(\rho_{AB}) &= \min_{\{\Pi_j^B\}} \left(\mathcal{I}_{AB}(\rho_{AB}) - J(\rho_{AB})_{\{\Pi_j^B\}} \right) \\ &= S(\rho_B) - S(\rho_{AB}) + \min_{\{\Pi_j^B\}} \sum_j p_j S(\rho_{A|\Pi_j^B}), \end{aligned} \tag{1.2.12}$$

where $S(\rho_{A|\Pi_j^B})$ is the entropy associated with the density matrix of subsystem A after the measure. Some properties can be inferred from Eq. (1.2.12): i) For pure states, $\delta_{AB}^{\leftarrow} = S(\rho_B)$, ii) $\delta_{AB}^{\leftarrow} = 0$ if and only if $\rho_{AB} = \sum_j \Pi_j^B \rho_{AB} \Pi_j^B$, iii) $0 \leq \delta_{AB}^{\leftarrow} \leq S(\rho_B)$ and iv) $\delta_{AB}^{\leftarrow}$ is an entanglement monotone on pure states.

At the same time, Henderson and Vedral [30] proposed a measure of classical correlations (CC) in quantum states by imposing, on the conditional entropy (1.2.10), the criteria that a well-defined measure of correlations should satisfy. However, they considered a set of positive operator valued measures (POVM) instead of projective measurements. Hence, this quantity is interpreted as the maximum extractable classical information from A, when a set of POVM ($\{\mathcal{M}_i\}$) has been performed on B, and is written as,

$$\begin{aligned} \mathcal{J}_{AB}^{\leftarrow}(\rho_{AB}) &= \max_{\{\mathcal{M}_i^B\}} J_{\{\mathcal{M}_i^B\}}(\rho_{AB}) \\ &= S(\rho_A) - \min_{\{\mathcal{M}_i^B\}} \sum_i p_i S(\rho_{A|\Pi_i^B}). \end{aligned} \tag{1.2.13}$$

Briefly, a measure of CC should incorporate the following: i) $\mathcal{J}^{\leftarrow}_{AB} = 0$ if and only if $\rho_{AB} = \rho_A \otimes \rho_B$ (uncorrelated states), and ii) $\mathcal{J}^{\leftarrow}_{AB}$ is non-increasing, and invariant under local unitary operations. It is worth noting that the set of POVM that maximises the CC given by Eq. (1.2.13) turns out to be a complete unidimensional projective measurement $\{\Pi^B_j\}$ [75]. This implies that joining Eq. (1.2.12) and Eq. (1.2.13), the QD can be defined as,

$$\delta^{\leftarrow}_{AB} = \mathcal{I}_{AB} - \mathcal{J}^{\leftarrow}_{AB}. \tag{1.2.14}$$

Hence, we say that the QMI is a measure of total correlations in a quantum state [76]. Both QD and CC are antisymmetric by definition, i.e., they depend on what subsystem the measures are taken on. Without loss of generality, we always consider in this Thesis that B is the measured subsystem. From the appearance of the QD, several alternative quantum correlations quantifiers based on local disturbance on quantum states have been developed so far (see e.g. [14, 15]). Despite this, throughout this Thesis, we make use of the definition (1.2.12) to quantify quantum correlations.

Chapter 2
Conditional dynamics, entanglement and correlations in molecular systems

In this chapter we report on the conditional dynamics and entanglement generation in PBI dimers and trimers. The standard formalism of the collective effects on a two-qubit system immersed in a common reservoir or environment is briefly presented in section 2.1. The study of a particular physical setup of dimers and trimers of organic molecules is discussed in section 2.2. Then, in section 2.3 we present an analysis about the way in which the different kind of correlations are "distributed" between the qubits and the environment.

2.1 Interacting qubits under a common reservoir

Initially, we consider that the quantum system S in Fig. 1.1 consists of two qubits which are allowed to interact with each other through a common reservoir $\mathcal{E}$ modelled as a zero temperature environment. The formalism briefly described here is the basis of the developments in sections 2.2 and 2.3, as well as of those presented in Chapter 3.

The total Hamiltonian of the full system (Eq. (1.1.1)) has the following contributions from the environment and the system-environment interaction,

$$H_{\mathcal{E}} = \sum_{\vec{k}s} \hbar\omega_{\vec{k}s}(\hat{a}^{\dagger}_{\vec{k}s}\hat{a}_{\vec{k}s} + 1/2), \tag{2.1.1}$$

$$H_{S\mathcal{E}} = -\mathrm{i}\hbar\sum_{i=1}^{2}\sum_{\vec{k}s}\left(\boldsymbol{\mu}_i \cdot \boldsymbol{u}_{\vec{k}s}(\vec{r}_i)\sigma_{+}^{(i)}\hat{a}_{\vec{k}s} + \boldsymbol{\mu}_i^{*}\cdot\boldsymbol{u}_{\vec{k}s}(\vec{r}_i)\sigma_{-}^{(i)}\hat{a}_{\vec{k}s} - \mathrm{H.c.}\right). \tag{2.1.2}$$

The Hamiltonian for the pair of qubits remains as in Eq. (1.1.8). $\hat{a}_{\vec{k}s}$ ($\hat{a}^{\dagger}_{\vec{k}s}$) are the annihilation (creation) operators of the mode k with polarisation s and frequency $\omega_{\vec{k}s}$, the light-matter coupling is $\boldsymbol{\mu}_i \cdot \boldsymbol{u}_{\vec{k}s}(\vec{r}_i)$, with $\boldsymbol{u}_{\vec{k}s}(\vec{r}_i) = (\omega_{\vec{k}s}/2\epsilon_0\hbar\vartheta)^{1/2}\boldsymbol{\varepsilon}_{\vec{k}s}\exp\mathrm{i}\vec{k}\cdot\vec{r}_i$, ϵ_0 the vacuum permittivity, ϑ the quantisation volume, and $\boldsymbol{\varepsilon}_{\vec{k}s}$ the unitary vector of the field mode. For the sake of completeness, we also allow for an external qubit control whereby the qubits can be optically-driven by a coherent laser field as in Eq. (1.1.10). The two emitters are separated by the vector $\boldsymbol{r}_{12}$ and are characterised by transition dipole moments $\boldsymbol{\mu}_i \equiv \langle 0_i|\hat{D}_i|1_i\rangle$, with dipole operators $\hat{D}_i$.

Under these considerations, the master equation (1.1.5) and the effective Hamiltonian (1.1.7) hold

with the collective contributions:

$$V = \frac{3\sqrt{\Gamma_1\Gamma_2}}{4}\Big\{ [\hat{\mu}_1 \cdot \hat{\mu}_2 - (\hat{\mu}_1 \cdot \hat{\mathbf{r}}_{12})(\hat{\mu}_2 \cdot \hat{\mathbf{r}}_{12})] \frac{\cos z}{z} + [\hat{\mu}_1 \cdot \hat{\mu}_2 - 3(\hat{\mu}_1 \cdot \hat{\mathbf{r}}_{12})(\hat{\mu}_2 \cdot \hat{\mathbf{r}}_{12})] \left(\frac{\cos z}{z^3} + \frac{\sin z}{z^2} \right) \Big\}, \quad (2.1.3)$$

$$\gamma = \frac{3\sqrt{\Gamma_1\Gamma_2}}{2}\Big\{ [\hat{\mu}_1 \cdot \hat{\mu}_2 - (\hat{\mu}_1 \cdot \hat{\mathbf{r}}_{12})(\hat{\mu}_2 \cdot \hat{\mathbf{r}}_{12})] \frac{\sin z}{z} + [\hat{\mu}_1 \cdot \hat{\mu}_2 - 3(\hat{\mu}_1 \cdot \hat{\mathbf{r}}_{12})(\hat{\mu}_2 \cdot \hat{\mathbf{r}}_{12})] \left(\frac{\cos z}{z^2} - \frac{\sin z}{z^3} \right) \Big\}, \quad (2.1.4)$$

where $z = nk_0 r_{12}$, $k_0 = \omega_0/c$, $\omega_0 = (\omega_1+\omega_2)/2$, n is the refraction index of the medium (environment), $\hat{\mu}_i$ is the unitary vector of the dipole moment i, and $\hat{\mathbf{r}}_{12}$ is the unitary vector along the separation between the qubits. The individual spontaneous emission ($\Gamma \equiv \Gamma_{11} = \Gamma_{22}$) can be computed by means of the Einstein's coefficients: $\Gamma_{ii} = nA_i/2 = n\omega_i^3|\boldsymbol{\mu}_i|^2/6\pi\hbar\epsilon_0 c^3$, and the collective damping ($\gamma \equiv \Gamma_{12} \in \Re$).

2.2 Entanglement generation and control of quantum dynamics in organic molecules

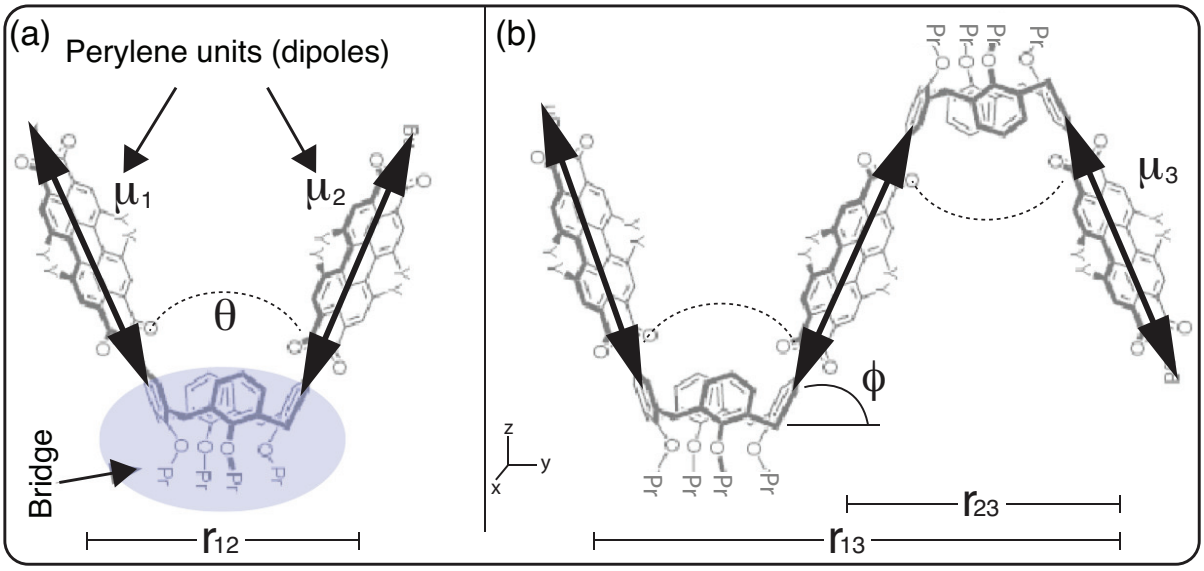

Figure 2.1: Planar configuration of dipoles associated to the (a) PBI dimer (two dipoles) and (b) trimer. They are physically linked by tetrakis(propyloxy)-calix[4]arene bridges that allow the control of the angle between adjacent units and their corresponding separation. $\boldsymbol{\mu}_i$ corresponds to the dipolar moment of the i-th monomer with electronic transition frequency ω_i. θ is the angle between units 1 and 2 (also 2 and 3), and ϕ is the angle between unit 2 and the vector along the inter-separation direction. Units 1 and 3 are parallel to each other. The monomer separation vectors are such that $|\boldsymbol{r}_{12}| = |\boldsymbol{r}_{23}| = |\boldsymbol{r}_{13}|/2$.

Exploring entanglement generation in quantum physical systems is of great interest for the development of novel technologies. In this chapter we present results on entanglement generation and control

with two (section 2.2.1) and three (section 2.2.4) coupled qubits. The real physical system comprises Perylene-Bisimide (PBI) molecules immersed in a protein solvent. For the single-molecule spectroscopy experiments, the molecules are immobilised in a host (hexadecane for instance) such that a well-defined nanoenvironment is provided [34]. The PBI chromophores concentration is about 10^{-10} mol/L and the experiments are carried out at 1.5 K approximately [34]. These molecules are currently synthesised and highly controlled by our collaborator Richard Hildner in Bayreuth, Germany [34, 35, 36].

Under the aforementioned conditions, these organic molecules can be considered as a collection of two-level emitters (also referred to as units) at low temperature, so we associate a dipole moment $\boldsymbol{\mu}_i$ to each unit with frequency ω_i. Figure 2.1(a) shows the particular configuration of a dimer composed of two units or monomers separated a distance $\boldsymbol{r}_{12}$ and with an opening angle θ. The corresponding setup for a trimer is shown in Fig. 2.1(b). The units are connected by a tetrakis(propyloxy)-calix[4]arene bridge that allows the experimentalists to control the mutual separation and the orientation of the dipoles. According to some experimental results on the spontaneous emission and dipole-dipole interaction of these molecules (see for instance Ref. [35]), it is possible to assure a Born-Markov approximation (Appendix A).

2.2.1 Dimer entanglement generation

The matrix representation of the bare Hamiltonian H_{eff} (1.1.7) for the d-d interacting qubits in the computational basis of product states reads ($\hbar = 1$)

$$H_{\text{eff}} = \begin{pmatrix} -\omega_0 & 0 & 0 & 0 \\ 0 & -\Delta_-/2 & V & 0 \\ 0 & V & \Delta_-/2 & 0 \\ 0 & 0 & 0 & \omega_0 \end{pmatrix}, \tag{2.2.1}$$

where $\omega_0 = (\omega_1 + \omega_2)/2$, $\Delta_- = \omega_1 - \omega_2$ is the molecular detuning, and V the d-d interaction strength (2.1.3).

The eigenvalues and normalised eigenvectors of this matrix are:

$$\begin{aligned} &E_1 = -\omega_0; \quad |E_1\rangle = |00\rangle; \\ &E_2 = -\Delta^*; \quad |E_2\rangle = -\tfrac{2\Delta^*+\Delta_-}{2\sqrt{\Delta^*(2\Delta^*+\Delta_-)}}|01\rangle + \tfrac{V}{\sqrt{\Delta^*(2\Delta^*+\Delta_-)}}|10\rangle; \\ &E_3 = \Delta^*; \quad\ |E_3\rangle = \tfrac{2\Delta^*-\Delta_-}{2\sqrt{\Delta^*(2\Delta^*-\Delta_-)}}|01\rangle + \tfrac{V}{\sqrt{\Delta^*(2\Delta^*-\Delta_-)}}|10\rangle; \\ &E_4 = \omega_0; \quad\ |E_4\rangle = |11\rangle, \end{aligned} \tag{2.2.2}$$

where $\Delta^* = \sqrt{V^2 + (\Delta_-/2)^2}$. From Eq. (2.2.2) we can distinguish three regions defined by the parameters Δ_- and V: (i) When $V/\Delta_- \ll 1$, almost independent qubits, the two intermediate states reduce to the two computational basis states $|01\rangle$ and $|10\rangle$. In an experimental sense, we say that the excitation is localised on molecule 2 or 1, respectively. (ii) When $V/\Delta_- \gg 1$, or for identical qubits ($\omega_1 = \omega_2$), these two intermediate states become maximally entangled as the magnitude of all the four coefficients goes to $1/\sqrt{2}$. In this case, we cannot say which molecule is excited as the excitation is delocalised on both molecules. And, (iii) when $\Delta_-/V \sim 1$, the molecules do not join neither the weak nor the strong coupling regime, so the two intermediate states become partially entangled. The degree of entanglement reached by them depends on the value of these two parameters. Despite the fact that Δ_- is not controllable experimentally, the fraction can be tailored by modifying the inter-molecule distance and the dipole orientation (for the particular PBI molecules, this is possible by means of the connecting bridge as shown in Fig. 2.1). A full discussion on the dissipative dynamics, the control of entanglement

and quantum correlations in two-qubit systems, in the three different aforementioned regions, can be found in [CS1, CS2].

In terms of the eigensystem (2.2.2), we first analyse the scenario $V/\Delta_- = 0.1$; with $V = 1200$ GHz, $\Delta_- = 12000$ GHz, $\omega_1 = 712$ THz and $\omega_2 = 700$ THz. The values of V and Δ_- come from some recent experiments carried out in [35, 77]. We assure that the rotating wave approximation holds, as the average frequency ω_0 is about two orders of magnitude greater than Δ_- ($\Delta_-/\omega_0 = 0.017$):

$$\begin{array}{ll} E_1 = -706\,\text{THz}; & |E_1\rangle = |00\rangle; \\ E_2 = -6118.82\,\text{GHz}; & |E_2\rangle = -0.9951|01\rangle + 0.0985|10\rangle; \\ E_3 = 6118.82\,\text{GHz}; & |E_3\rangle = 0.0985|01\rangle + 0.9951|10\rangle; \\ E_4 = 706\,\text{THz}; & |E_4\rangle = |11\rangle. \end{array}$$

This result says that the eigenstates are basically the computational basis as the two intermediate eigenstates reduce to the standard basis states $|E_2\rangle \to |01\rangle$ and $|E_3\rangle \to |10\rangle$, up to a global phase. This is in agreement with the fluorescence spectra reported in [35, 77] and does not present an interesting scenario to further develop.

In a second instance, we explore the case $V/\Delta_- = 1$; we reduce the molecular detuning to $\Delta_- = 1200$ GHz and keep the rest of parameters as before (now, $\Delta_-/\omega_0 = 0.0017$):

$$\begin{array}{ll} E_1 = -706\,\text{THz}; & |E_1\rangle = |00\rangle; \\ E_2 = -1341.64\,\text{GHz}; & |E_2\rangle = -0.8507|01\rangle + 0.5257|10\rangle; \\ E_3 = 1341.64\,\text{GHz}; & |E_3\rangle = 0.5257|01\rangle + 0.8507|10\rangle; \\ E_4 = 706\,\text{THz}; & |E_4\rangle = |11\rangle. \end{array}$$

Hence, we have a reasonable superposition between the states $|01\rangle$ and $|10\rangle$ such that there exists a degree of entanglement in the two intermediate eigenstates. As expected, the greater the fraction V/Δ_- is, the more entangled the intermediate eigenstates are.

According to this energy scheme, we can generate coherent transitions between some of the eigenstates as shown in Fig. 2.2 for the particular transition $|E_1\rangle \leftrightarrow |E_3\rangle$. We generate the transition in presence of dissipation with spontaneous emission Γ and collective damping γ. In the left panel we plot $\text{Tr}(\rho(t)|E_1\rangle\langle E_1|) = \langle E_1|\rho(t)|E_1\rangle$ (blue) and $\text{Tr}(\rho(t)|E_3\rangle\langle E_3|)$ (brown), where $\rho(t)$ is the density matrix after solving the master equation of the open system when the initial state is $|00\rangle$. This dynamics is induced by a coherent laser field with amplitude $\ell = 1$ GHz and a frequency $\omega_L = |E_3 - E_1|$ (the same result holds for stronger laser amplitudes). As expected, in the stationary regime the system goes to an equally distributed population between the two involved eigenstates, i.e., the stationary state is the statistical mixture $1/2|E_1\rangle\langle E_1| + 1/2|E_3\rangle\langle E_3|$. This can be checked following the dynamics of the respective coherence $|E_1\rangle\langle E_3|$, or equivalently, the coherences $|00\rangle\langle 01|$ and $|00\rangle\langle 10|$ (right panel of Fig. 2.2). The upper panel corresponds to the first numerical example, $V/\Delta_- = 0.1$, and the lower panel shows the case $V/\Delta_- = 1$. In the latter case, we have a mixture of a separable state ($|00\rangle$) and an entangled state $|E_3\rangle = 0.5257|01\rangle + 0.8507|10\rangle$. Despite of this entanglement, this mixture is still a local state in the Bell's sense. The total time for this oscillatory evolution is ~ 52 ns corresponding to about $10 \times (1/\Gamma)$.

Quantum logic gates dynamics

The fact of having a d-d interaction between the monomers indicate that the system can "naturally" generate the Swap gate which flips the two intermediate states of the 4-dimensional basis, $|01\rangle \leftrightarrow |10\rangle$.

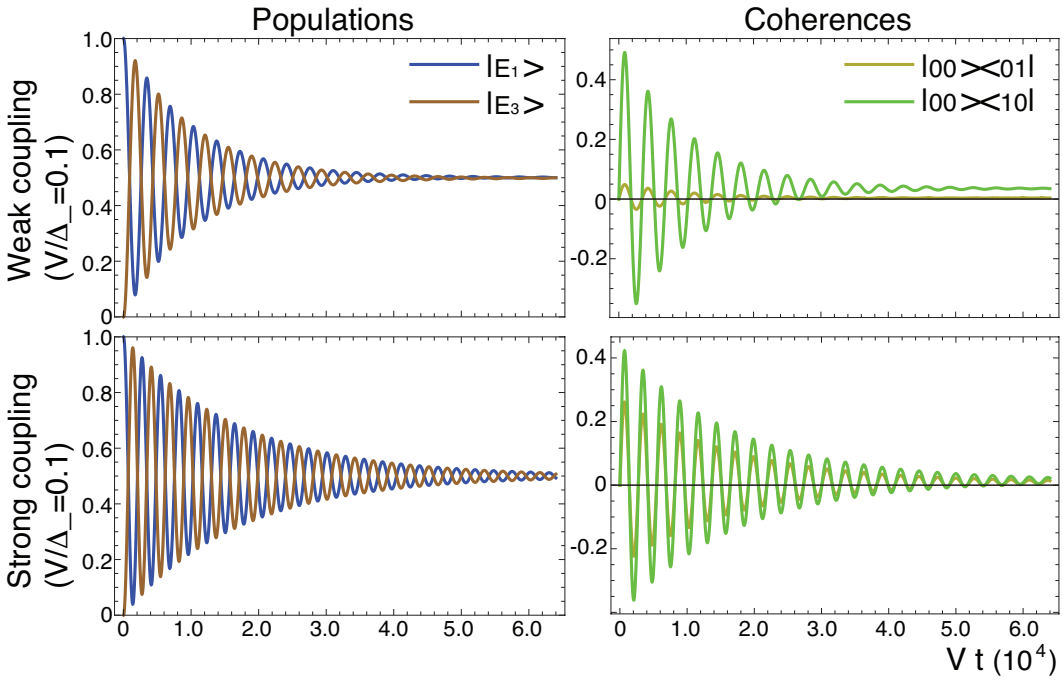

Figure 2.2: Expected values (left panel) and some coherences (right panel) dynamics for the transition $|E_1\rangle \leftrightarrow |E_3\rangle$ under the action of a coherent (continuous) laser $\ell = 1$ GHz and $\omega_L = E_3 - E_1$. Upper panel: $V/\Delta_- = 0.1$, lower panel: $V/\Delta_- = 1$. The plotted coherences are $|00\rangle\langle 01|$ and $|00\rangle\langle 10|$. $V = 1200$ GHz, dissipation $\Gamma = 172.4$ MHz, and collective damping $\gamma = -86.2$ MHz.

Its matrix representation reads

$$U_{\text{Swap}} = \begin{pmatrix} 1 & 0 & 0 & 0 \\ 0 & 0 & 1 & 0 \\ 0 & 1 & 0 & 0 \\ 0 & 0 & 0 & 1 \end{pmatrix}. \tag{2.2.3}$$

Here we show a particular scenario in which the dimer can be driven from the ground state to $|01\rangle$, so then it naturally creates the swap gate. Figure 2.3 shows the simple two-step process to perform the Swap gate as follows: Step 1; the $|00\rangle \rightarrow |01\rangle$ transition is carried out, by applying a laser pulse $(\pi/2\ell_2)$ on qubit 2 with $\ell_2 = 1000$ GHz and $\Delta_2 = 0$, with high fidelity (Fig. 2.3(c)). Step 2; after getting $|01\rangle$ the laser on qubit 2 is turned off such that the dimer evolves under the action of the d-d interaction for a time $t_{\text{swap}} = \pi/(2V)$, after this time, the dimer is naturally in the $|10\rangle$ state (main plot of Fig. 2.3(b) shows the populations of this evolution, and the inset is the dynamics of the coherence $\rho_{01,10}$). Figure 2.3(d) is the corresponding fidelity $\mathcal{F}(\rho,\sigma) = \text{Tr}\left[\sqrt{\sqrt{\sigma}\rho\sqrt{\sigma}}\right]$, where σ is the expected state at the end of the gate and ρ is the actual state of the dissipative evolution. The time axis has been plotted in V units and corresponds to a total time of ~ 2.68 ps, such that the swap-gate step has been carried out in ~ 1.16 ps with $\mathcal{F} = 1$. The used parameters are: $\Gamma = 172.4$ MHz, $V = 1355.816$ GHz (computed with Eq. (2.1.3) for an opening angle of 120^{o} and dipole moments of 10 D), and $\gamma = -86.187$ MHz. It is worth noting that after the step 1, the swap gate holds (the dynamics exhibits coherent oscillations) for times up to two orders of magnitude longer than ~ 1.16 ps, in particular, the coherent oscillations lose a 5% of fidelity at around $t = 250\ t_{\text{swap}}$, i.e., for $t = 290$ ps (not shown). This decay is due to the slow

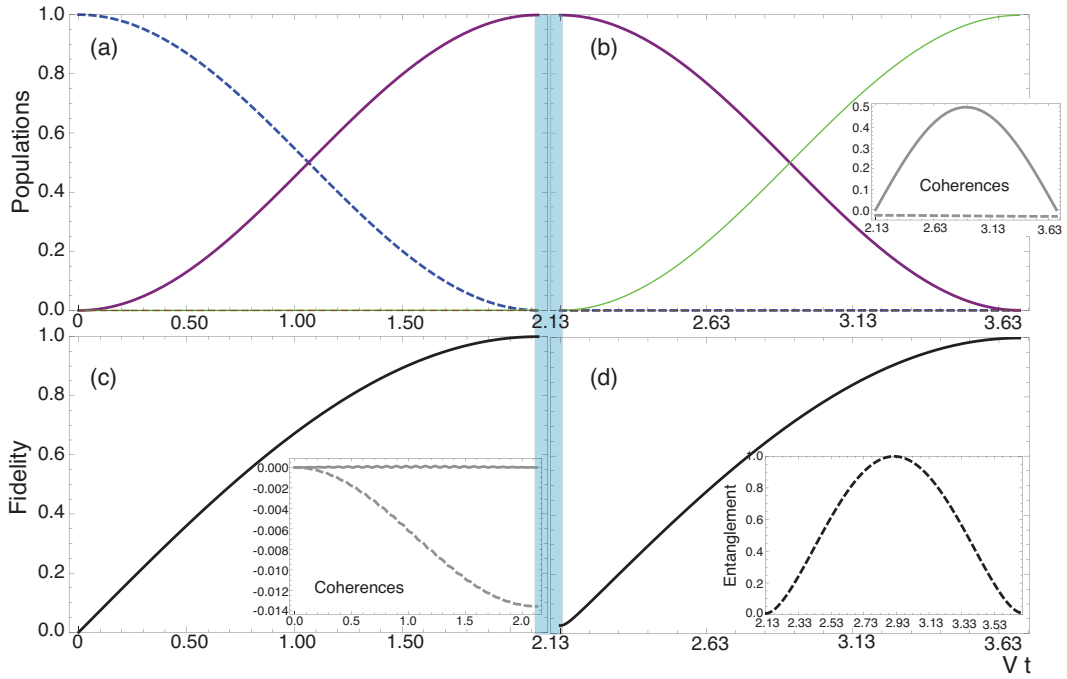

Figure 2.3: Realisation of a swap gate. (a) $|00\rangle \rightarrow |01\rangle$ transition by applying a laser pulse ($\pi/2\ell_2$) on qubit 2 with $\ell_2 = 1000$ GHz, $\Delta_2 = 0$ and $\Delta_1 = 100$ THz. $\rho_{00,00}$ (dashed-blue), $\rho_{01,01}$ (solid-purple), $\rho_{10,10}$ (thin-solid-green) and $\rho_{11,11}$ (thin-dashed-brown). (b) Main: naturally generated swap gate due to the d-d interaction, here the laser has been turned off. The inset shows $\mathcal{R}e\left[\rho_{01,10}\right]$ (dashed-gray) and $\mathcal{I}m\left[\rho_{01,10}\right]$ (solid-gray) of the relevant coherence. (c) The main plot is the fidelity of the first step and the inset is the evolution of the coherence $\rho_{01,10}$ for this step. (d) Main: fidelity associated to the generation of the swap gate; the gate time is $t_{\rm swap} = \pi/2V$. Inset: evolution of the EoF in the swap-gate process. $V = 1355.816$ GHz, $\Delta_- = 14.2717$ GHz, $\Gamma = 172.4$ MHz, and $\gamma = -86.187$ MHz. The time is given in units of V.

nanosecond spontaneous emission.

Two important byproducts of this conditional dynamics arise: Firstly, thanks to the local action of the laser field on qubits, it is posible to perform arbitrary rotations on each qubit, particularly, note that if we apply the same laser pulse on qubit 2 but just for the half of the time reported in Fig. 2.3(a), the dimer arrives to the state $1/\sqrt{2}(|00\rangle + i|01\rangle)$, which means that the qubit 2 is driven to the superposition $1/\sqrt{2}(|0\rangle + e^{i\pi/2}|1\rangle)$, this transformation up to a local phase shift is equivalent to the Hadamard gate $H = 1/\sqrt{2}(\sigma_z + \sigma_x)$, a landmark of the local (one-qubit) unitary transformations. Secondly, looking at the inset of Fig. 2.3(d), it is clear that the swap gate can be managed to generate entanglement in the dimer as shown by the highest value of the EoF at time $t_{\rm swap}/2$. For the case in Fig. 2.3 we have used a fraction $V/\Delta_- = 95$, thus showing the versatility of the dimer setup to generate single- as well as two-qubit quantum gates. Regarding the feasibility of reproducing this scenario experimentally, we notice that, even though it might be not so easy to flip the state of one monomer without affecting its neighbour's state (as they are so close to each other), it is possible to excite different samples of dimers and 'catch' one in the desired state, e.g. $|01\rangle$.

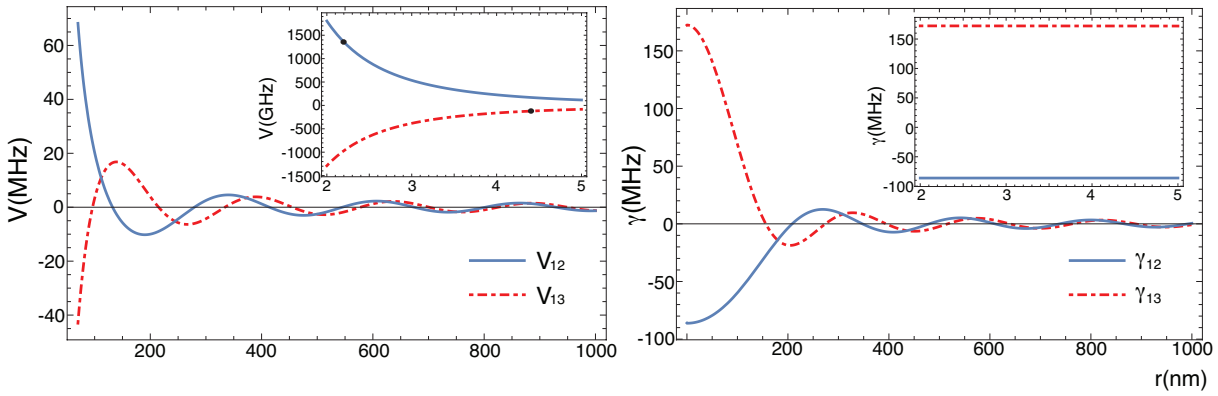

Figure 2.4: (Left panel) d-d interactions V_{12} (solid) and V_{13} (dashed). (Right panel) collective damping γ_{12} (solid) and γ_{13} (dashed). The two black dots in the inset on left panel show the specific inter-qubit separation for the computed values in the main text.

2.2.2 Trimer entanglement generation

The extension to the three-qubit case leads us to understand the possible generated entanglement in a bigger setup. The new Hamiltonian is an 8×8 matrix and has some new extra parameters. To derive analytical expressions for the eigensystem of this bigger setup, we consider the following: Qubit 1 and qubit 3 (the outer ones) have the same transition frequency ω such that $\Delta_- = \omega_2 - \omega$, where ω_2 is the transition frequency of the intermediate qubit. Due to the spacial symmetry of the considered planar setup shown in Fig. 2.1(b), we also have that $V_{12} = V_{23} = V$ and $V > V_{13}$. Under this assumption, and without loss of generality, the effective three-qubit bare Hamiltonian reads

$$H_{\text{trimer}} = \begin{pmatrix} -\frac{3}{2}\omega_0 & 0 & 0 & 0 & & 0 & 0 & 0 \\ 0 & -\omega_2/2 & V & 0 & V_{13} & 0 & 0 & 0 \\ 0 & V & -\frac{1}{2}(\omega-\Delta_-) & 0 & V & 0 & 0 & 0 \\ 0 & 0 & 0 & \omega_2/2 & 0 & V & V_{13} & 0 \\ 0 & V_{13} & V & 0 & -\omega_2/2 & 0 & 0 & 0 \\ 0 & 0 & 0 & V & 0 & \frac{1}{2}(\omega-\Delta_-) & V & 0 \\ 0 & 0 & 0 & V_{13} & 0 & V & \omega_2/2 & 0 \\ 0 & 0 & 0 & 0 & 0 & 0 & 0 & \frac{3}{2}\omega_0 \end{pmatrix}, \quad (2.2.4)$$

where $\omega_0 = (\omega_1 + \omega_2 + \omega_3)/3 = (2\omega + \omega_2)/3$, and the molecular detuning $\Delta_- := \omega_2 - \omega \ll \omega$. Figure 2.4 shows the general behaviour of the collective parameters in the trimer system. The left panel shows the behaviour of V_{12} (solid curve) and V_{13} (dashed curve) as functions of the corresponding mutual separation $\boldsymbol{r}_{12}$ and $\boldsymbol{r}_{13}$, respectively, from 70 nm to 1000 nm, the inset shows a zoom of the range $[2\,\text{nm}, 5\,\text{nm}]$. The two black dots in the inset of the left panel represent the separation distance between monomers 1 and 2, or equivalently, 2 and 3 (2.2 nm), and between monomers 1 and 3 (4.4 nm), respectively. The computation of the collective parameters through Eq. (2.1.3) and (2.1.4) gives the following values: $V_{12} = V_{23} \approx 1355.816$ GHz, $\gamma_{12} = \gamma_{23} \approx -86.187$ MHz, $V_{13} \approx -121.947$ GHz and $\gamma_{13} \approx 172.139$ MHz [1]. The corresponding behaviour of γ_{12} and γ_{13} is shown on the right panel.

[1] We keep the subscripts in γ_{ij} to avoid confusions, as in the trimer case we have two different collective damping rates. The same observation is kept for the d-d interaction.

The eigensystem for this Hamiltonian reads

$$\begin{array}{ll}
E_1 = -\frac{3}{2}\omega_0; & |E_1\rangle = |000\rangle; \\
E_2 = -(\omega_2/2 + V_{13}); & |E_2\rangle = \frac{1}{\sqrt{2}}(-|001\rangle + |100\rangle); \\
E_3 = -\frac{1}{2}(\omega - V_{13} + \Delta^-); & |E_3\rangle = \frac{2V}{\sqrt{2\Delta^-(\Delta^- + V_{13} - \Delta_-)}}(|001\rangle + |100\rangle) - \sqrt{\frac{\Delta^- + V_{13} - \Delta_-}{2\Delta^-}}|010\rangle; \\
E_4 = -\frac{1}{2}(\omega - V_{13} - \Delta^-); & |E_4\rangle = \frac{2V}{\sqrt{2\Delta^-(\Delta^- - V_{13} + \Delta_-)}}(|001\rangle + |100\rangle) + \sqrt{\frac{\Delta^- - V_{13} + \Delta_-}{2\Delta^-}}|010\rangle; \\
E_5 = \frac{1}{2}(\omega + V_{13} - \Delta^+); & |E_5\rangle = \frac{2V}{\sqrt{2\Delta^+(\Delta^+ + V_{13} + \Delta_-)}}(|011\rangle + |110\rangle) - \sqrt{\frac{\Delta^+ + V_{13} + \Delta_-}{2\Delta^+}}|101\rangle; \\
E_6 = \frac{1}{2}(\omega + V_{13} + \Delta^+); & |E_6\rangle = \frac{2V}{\sqrt{2\Delta^+(\Delta^+ - V_{13} - \Delta_-)}}(|011\rangle + |110\rangle) + \sqrt{\frac{\Delta^+ - V_{13} - \Delta_-}{2\Delta^+}}|101\rangle; \\
E_7 = \omega_2/2 - V_{13}; & |E_7\rangle = \frac{1}{\sqrt{2}}(-|011\rangle + |110\rangle); \\
E_8 = \frac{3}{2}\omega_0; & |E_8\rangle = |111\rangle,
\end{array} \tag{2.2.5}$$

where $\Delta^{\pm} = \sqrt{8V^2 + (V_{13} \pm \Delta_-)^2}$. To see the order of magnitude of the eigenenergies and the coefficients in the eigenstates, we choose as a particular example the following parameters: $V/\Delta_- = 0.1$; $V = 1200$ GHz, $V_{13} = -120$ GHz, $\Delta_- = 12000$ GHz, $\omega = 700$ THz and $\omega_2 = 712$ THz ($\Delta_-/\omega_0 = 0.017$). The eigensystem reads

$$\begin{array}{ll}
E_1 = -1056\,\text{THz}; & |E_1\rangle = |000\rangle; \\
E_2 = -355880\,\text{GHz}; & |E_2\rangle = \frac{1}{\sqrt{2}}(-|001\rangle + |100\rangle); \\
E_3 = -356353\,\text{GHz}; & |E_3\rangle = 0.7005(|001\rangle + |100\rangle) - 0.1361|010\rangle; \\
E_4 = -343767\,\text{GHz}; & |E_4\rangle = 0.0962(|001\rangle + |100\rangle) + 0.9907|010\rangle; \\
E_5 = 343762\,\text{GHz}; & |E_5\rangle = 0.0981(|011\rangle + |110\rangle) - 0.9903|101\rangle; \\
E_6 = 356118\,\text{GHz}; & |E_6\rangle = 0.7003(|011\rangle + |110\rangle) + 0.1387|101\rangle; \\
E_7 = 356120\,\text{GHz}; & |E_7\rangle = \frac{1}{\sqrt{2}}(-|011\rangle + |110\rangle); \\
E_8 = 1056\,\text{THz}; & |E_8\rangle = |111\rangle.
\end{array} \tag{2.2.6}$$

For a smaller molecular detuning such that: $V/\Delta_- = 1$; $V = 1200$ GHz, $V_{13} = -120$ GHz, $\Delta_- = 1200$ GHz, $\omega = 700$ THz and $\omega_2 = 701.2$ THz ($\Delta_-/\omega_0 = 0.0017$), the values for the eigensystem are

$$\begin{array}{ll}
E_1 = -1050.6\,\text{THz}; & |E_1\rangle = |000\rangle; \\
E_2 = -350480\,\text{GHz}; & |E_2\rangle = \frac{1}{\sqrt{2}}(-|001\rangle + |100\rangle); \\
E_3 = -351881\,\text{GHz}; & |E_3\rangle = 0.5836(|001\rangle + |100\rangle) - 0.5646|010\rangle; \\
E_4 = -348239\,\text{GHz}; & |E_4\rangle = 0.3992(|001\rangle + |100\rangle) + 0.8254|010\rangle; \\
E_5 = 348159\,\text{GHz}; & |E_5\rangle = 0.4174(|011\rangle + |110\rangle) - 0.8072|101\rangle; \\
E_6 = 351721\,\text{GHz}; & |E_6\rangle = 0.5708(|011\rangle + |110\rangle) + 0.5902|101\rangle; \\
E_7 = 350720\,\text{GHz}; & |E_7\rangle = \frac{1}{\sqrt{2}}(-|011\rangle + |110\rangle); \\
E_8 = 1050.6\,\text{THz}; & |E_8\rangle = |111\rangle.
\end{array} \tag{2.2.7}$$

Following the same procedure as that for the dimer case, we can excite different transitions between the eigenstates with a coherent external field. We plot the system dynamics by exciting the transition $|E_1\rangle \leftrightarrow |E_3\rangle$ with a weak laser ($\ell = 1$GHz), we assume the initial state is $|E_1\rangle \equiv |000\rangle$. This transition occurs coherently as shown by the time evolution of the expected values $\langle E_1|\rho(t)|E_1\rangle$ (blue) and $\langle E_3|\rho(t)|E_3\rangle$ (brown) in the left panel of Fig. 2.5. The stationary state is a statistical mixture of the two involved states. A similar result is obtained when exciting the transition with a stronger laser amplitude $\ell = 120$ GHz (inset). For the first instance, we have $V/\Delta_- = 0.1$ (see Eq. (2.2.6)) such that the

eigenstates are made of up to pairwise entangled states and there are not tripartite entangled eigenstates. This means that the three PBI molecules are not entangled at the same time, but just two of them exhibit entanglement and their state is separable with respect to the other monomer.

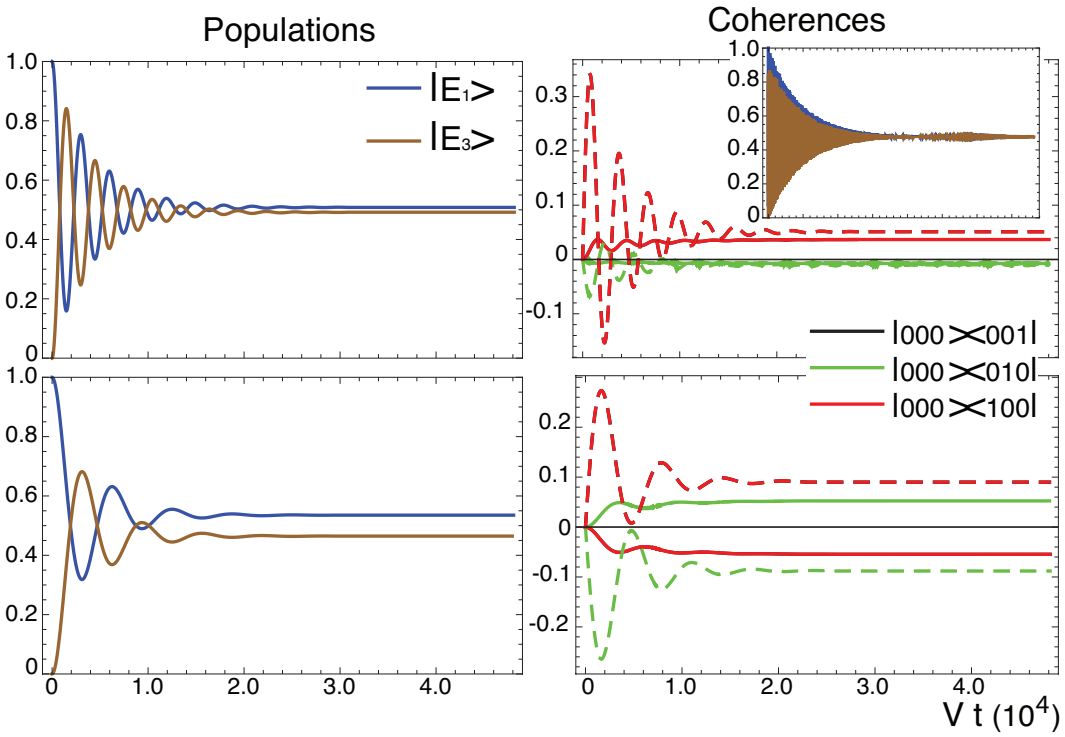

Figure 2.5: Expected values for the transition $|E_1\rangle \leftrightarrow |E_3\rangle$ under the action of a coherent (continuous) laser $\ell = 1$ GHz. Upper panel: $\Delta_- = 12000$ GHz and $\omega_L = E_3 - E_1 = 699647$ GHz. Lower panel: $\Delta_- = 1200$ GHz and $\omega_L = E_3 - E_1 = 698719$ GHz. Left panel: Populations $|E_1\rangle\langle E_1|$ and $|E_3\rangle\langle E_3|$. Right panel: Real (solid) and Imaginary (dashed) part of the three corresponding coherences (Red and black curves are superposed). The inset shows the same populations as in the upper-left panel but with a laser amplitude $\ell = 120$ GHz. The rest of parameters are $V = 1200$ GHZ, $V_{13} = -120$ GHz, $\Gamma = 172.4$ MHz, $\gamma_{12} = \gamma_{23} = -86.2$ MHz, and $\gamma_{13} = 172.1$ MHz.

The situation differs when setting a ratio $V/\Delta_- = 1$ (Eq. (2.2.7)), in this case, the four intermediate eigenstates are reasonable superpositions of three orthonormal states such that they exhibit tripartite entanglement, in fact, the eigenstate $|E_3\rangle$ corresponds to the W state $1/\sqrt{3}(|001\rangle - |010\rangle + |100\rangle)$. Such tripartite entanglement is still lightly present in the stationary regime as some of the coherences of the transition $|E_1\rangle \leftrightarrow |E_3\rangle$ are different from zero (lower-right panel of Fig. 2.5). This implies that the stationary state is not only classically correlated (a diagonal matrix) but still has quantum correlations.

Bare entanglement dynamics

The time evolution of the density matrix elements for the trimer can be numerically computed by means of the natural extension of the master equation (1.1.5) using the new Hamiltonian (2.2.4), and adding the Γ_3 and γ_{13} terms to the Lindblad operator.

To investigate the entanglement that the trimer system can generate and support, we recall that there are two representative kinds of entanglement in a three-qubit system: i) W states, also referred to as

Dicke states, and ii) Greenberger-Horne-Zeilinger (GHZ) states. The important remark is that these two classes of entangled states are inequivalent to each other, i.e., they can not be obtained from the other by means of local operations and classical communication [78]. This is of course a completely distinct scenario than that of the dimer in which there is just one kind of entanglement.

The representative W state is of the form (with rank 3):

$$|W\rangle = \frac{1}{\sqrt{3}}\left(|001\rangle + |010\rangle + |100\rangle\right),$$

and the rank-2 GHZ state is written as:

$$|GHZ\rangle = \frac{1}{\sqrt{2}}\left(|000\rangle + |111\rangle\right).$$

Due to the structure of the trimer Hamiltonian, this system can naturally generate entangled states of the W class thanks to the dipole interaction between the subunits. This can be numerically studied by exploring the natural dynamics of the trimer. For the sake of simplicity, we continue using the bare Hamiltonian (2.2.4).

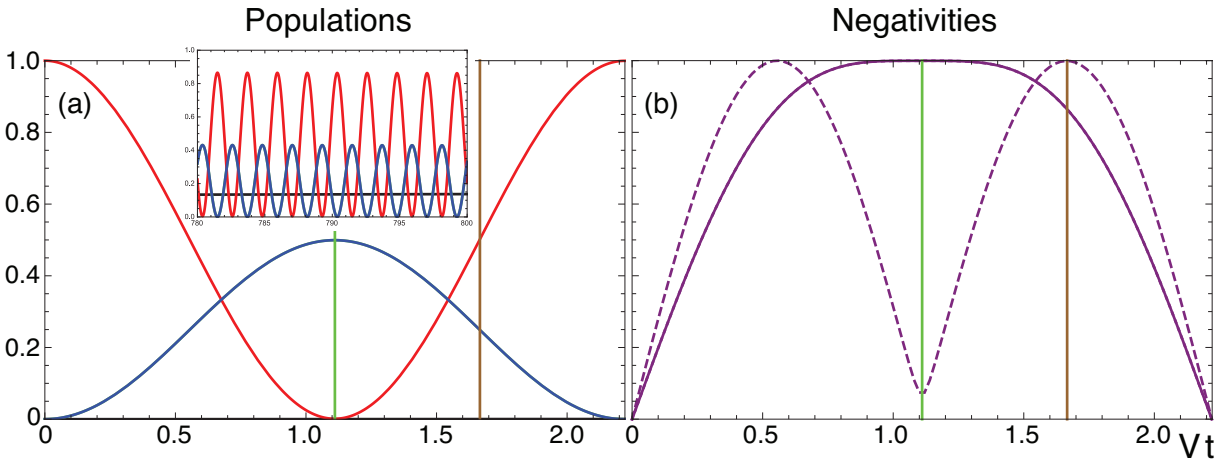

Figure 2.6: Generation of pairwise (bipartite) entangled and W-like states by means of the d-d interactions. (a) Main: Populations $\rho_{000,000}$ (black), $\rho_{010,010}$ (red), $\rho_{100,100}$ (blue) and $\rho_{001,001}$ (green). Inset: Same populations for $t_V \in [780, 800]$ (two orders of magnitude greater than the time in the main plot and one order of magnitude smaller than t_Γ). Green vertical line at $t_{pw} = \pi/\sqrt{8V^2 + (V_{13} - \Delta_-)^2} \approx \pi/2\sqrt{2}V$ indicates the generation of a pairwise entangled state, and the brown line at $t_{\mathcal{W}} = 3t_{pw}/2 \approx 3\pi/4\sqrt{2}V$ highlights the generation of the $|\mathcal{W}\rangle$ state (see main text for full description). (b) Negativity with respect to the partition $\{1|23\}$ (solid), $\{2|13\}$ (dashed) and $\{3|12\}$ (dotted). Parameters: $V \approx 1355.816$ GHz, $V_{13} \approx -121.947$ GHz ($|V_{13}| \sim 0.09V$), $\Gamma_{12} = \Gamma_{23} \approx -86.187$ MHz, $\Gamma_{13} \approx 172.139$ MHz, and $\Delta_- = 10$ GHz ($\sim 0.007V$), no laser turned on. $\omega_2 > \omega_1 = \omega_3$ (similar results are obtained for different choices of these frequencies–not shown).

Pairwise as well as W-like entangled states are naturally generated as shown in Fig. 2.6 when the trimer initiates in the $|010\rangle$ state, i.e., the sandwiched monomer (qubit 2) is in its excited state and the other two are in their ground state. After leaving the system to evolve alone by means of the dipole interactions the system arrives almost perfectly to the pairwise entangled state $1/\sqrt{2}(|100\rangle + b|001\rangle) \equiv$

$|\Psi^+\rangle_{13} \otimes |0\rangle_2$ (see vertical green line in Fig. 2.6), this corresponds to a maximally entangled state of the partition $\{13\}$ (qubits 1 and 3) tensor product the ground state of qubit 2. This state is created after a time $t_{pw} = \pi/\Delta^-$ (Δ^- given in Eq. (2.2.5)). This behaviour is expected according to the swapping effect due to V and the fact that $V/\Delta_- \gg 1$ ($V_{13}/\Delta_- > 1$) which is experimentally feasible. Curves of $\rho_{100,100}$ and $\rho_{001,001}$ superpose to each other (Fig. 2.6(a)). The inset shows the coherent dynamics of populations for two orders of magnitude greater than the time in the main plot.

This fast dynamics is even more interesting as it exhibits a huge family of W-like states: It is easy to show that under this evolution the only states evolving different from zero are those in the mixture $\rho_W(t) = p_1(t)|000\rangle\langle 000| + p_2(t)|W^*(t)\rangle\langle W^*(t)|$, where $|W^*(t)\rangle = a_1(t)|100\rangle + a_2(t)|010\rangle + a_3(t)|001\rangle$, with $|a_1(t)|^2 + |a_2(t)|^2 + |a_3(t)|^2 = 1$ and $a_2(0) = 1$, are W-like states. Given the fact that $p_1(t) \ll p_2(t)$ for times smaller than the relaxation time due to spontaneous emission ($t_\Gamma \sim 10^3 t_V$), being t_V the time in units of the V interaction, it is basically the state $\rho_W(t) \to |W^*(t)\rangle\langle W^*(t)|$ the one present during the dynamics in this time regime.

The entanglement of this evolution has been caught throughout the negativity [79, 80] due to its operational interpretation and easiness of computation. Negativity can be defined as: $\aleph(\rho) = \max\{0, -2\zeta_{min}\}$, where ζ_{min} is the smallest eigenvalue of the partial transposed matrix ρ^{T_A}, with elements $\langle i_A j_B|\rho^{T_A}|k_A l_B\rangle \equiv \langle k_A j_B|\rho|i_A l_B\rangle$, of the density matrix ρ with respect to the subsystem A. For our three-qubit system, the partitions $\{1|23\}$, $\{2|13\}$ and $\{3|12\}$ are required and their respective negativities have been plotted in Fig. 2.6(b), as expected, the negativities for $\{1|23\}$ and $\{3|12\}$ have the same behaviour due to the entanglement between qubit 1 and 3. It is clear that the representative $|W\rangle$ state belongs to the family of the generated entangled $\rho_W(t)$ states. In Fig. 2.6(a), this former state occurs when the three corresponding populations take the same value. On the other hand, exploring the non-trivial behaviour of the negativity for the partition $\{2|13\}$, we find that at the instance in which it gets its maximum value (see e.g., the brown line at $t_{\mathcal{W}} = (3/2)t_{pw} = 3\pi/2\Delta^-$ in Fig. 2.6) the system generates the state

$$|\mathcal{W}\rangle = \frac{1}{2}\left(|100\rangle + \sqrt{2}e^{-i0.48903\pi}|010\rangle + |001\rangle\right).$$

This particular state is of great interest as it belongs to a subclass of W-like states that have been proven to be useful for teleportation and superdense coding [81].

2.2.3 Discussion

We point out that the study of entanglement generation in PBI molecules here reported corresponds to the particular scenario shown in Fig. 2.1; a planar configuration with an opening angle $\theta = 120^{\text{o}}$ for adjacent molecules. However, as mentioned before, the inter-emitter separation as well as the orientation of the dipole associated to each molecule can be modified by means of the linking bridge such that different values of the collective effects (2.1.3) and (2.1.4) can be obtained. For instance, molecules orientation could be moved such that their dipoles are parallel to each other, this would allow the molecules to exhibit a stronger dipolar interaction and as a consequence more entanglement between them.

Our results on both dimer and trimer entanglement generation reveal that the dynamics of the PBI molecules is highly coherent on the picosecond scale because the relaxation time of their excited states lies in the nanosecond time scale. This means that the gate operations carried out in picoseconds are much faster than the life time of the molecules and are, to a very good approximation, coherent operations.

Our study can also be extended to multipartite settings as these molecules can be synthesised to form long-chain configurations, where energy transfer (weak coupling regime) and coherent transport of excitation energy (strong coupling regime) are two interesting physical processes that rely on the d-

d interaction between molecules, therefore depending on the entanglement present in the dimer/trimer states [82].

2.3 Flow of information between the qubit-system and its environment

Entanglement shared by qubits is a key resource for quantum information and quantum computation tasks. However, it is clear that this entanglement is highly related to the way in which qubits interact with their surrounding. In this section, we explore the distribution of entanglement and more general quantum correlations, in the tripartite two-qubit-plus-environment system. We consider arbitrary qubits instead of the molecules used in section 2.2, as our interest is to study the flow of information through the components of the full system as depicted in Fig. 2.7.

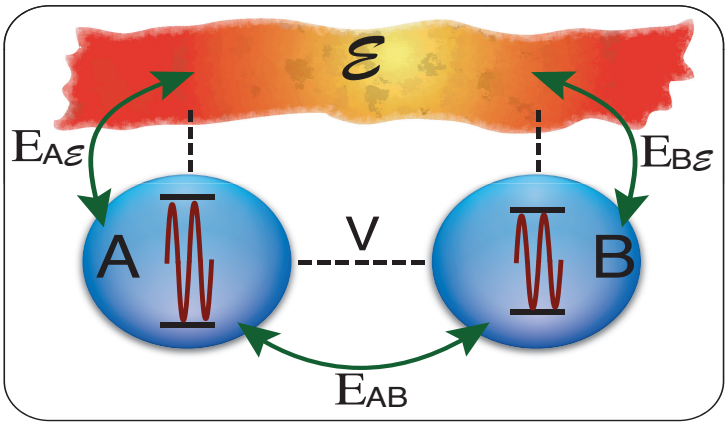

Figure 2.7: Schematics of the considered $AB\mathcal{E}$ physical system and the flow of quantum information: qubits interacting with a dissipative environment, which are allowed to be optically-driven via an external laser excitation.

2.3.1 Koashi-Winter monogamic relations

It is a known fact that a quantum system composed by many parts cannot freely share entanglement or quantum correlations between its parts [83, 84, 85, 86, 87, 88]. Indeed, there are strong constrains on how these correlations can be shared, which gives rise to what is known as monogamy of quantum correlations. We use monogamic relations to demonstrate that the way that quantum correlations are distributed in a quantum register is constrained by the way in which each subsystem gets correlated with the reservoir [83, 89, 90], and that an optimisation of the interqubit entanglement and correlations can be devised via a quantification of the information flow between each qubit and its environment.

We consider a bipartite AB system (the qubits) interacting with a third subsystem $\mathcal{E}$ (the environment). We begin by assuming that the *whole* '$AB\mathcal{E}$ system' is described by an initial pure state $W(0) \equiv \rho_{AB\mathcal{E}}(0) = \rho_{AB}(0) \otimes \rho_{\mathcal{E}}(0)$; i.e., at $t = 0$, the qubits and the environment density matrices, ρ_{AB} and $\rho_{\mathcal{E}}$, need to be pure. This is a particular initial condition and has to be understood not to be

always required to solve the master equation (1.1.5), for instance, in Chapter 3 we considered initial mixed states for the subsystem AB.

The global $AB\mathcal{E}$ evolution is derived from Eq. (1.1.2) and reads:

$$\rho_{AB\mathcal{E}}(t) \;=\; e^{-\frac{i}{\hbar}\hat{H}t}\rho_{AB\mathcal{E}}(0)e^{\frac{i}{\hbar}\hat{H}t}, \tag{2.3.1}$$

where $\hat{H}$ is given by Eq. (1.1.1). Since $\rho_{AB\mathcal{E}}(0)$ is pure, $\rho_{AB\mathcal{E}}(t)$ is also pure for all time and hence we can calculate the way that AB gets entangled with the environment directly from the entropy. For the EoF $E_{(AB)\mathcal{E}}$, for example, this is given by the von Neumann entropy $E_{(AB)\mathcal{E}} = S(\rho_{AB}) = S(\rho_{\mathcal{E}})$ [3, 91]. In order to quantify the way in which A (B) gets entangled with $\mathcal{E}$, we calculate $E_{A\mathcal{E}}$ ($E_{B\mathcal{E}}$) by means of the Koashi-Winter (KW) theorem [83, 90] established as a trade-off between the EoF and the CC defined by Henderson and Vedral [30]. They proved that [90]:

Theorem: *When $\rho_{AB'}$ is B-complement to ρ_{AB},*

$$E(\rho_{AB}) + \mathcal{J}^{\leftarrow}_{AB'}(\rho_{AB'}) = S(\rho_A), \tag{2.3.2}$$

where ***B-complement*** means that there exist a tripartite pure state $\rho_{ABB'}$ such that $\mathrm{Tr}_B[\rho_{ABB'}] = \rho_{AB'}$ and $\mathrm{Tr}_{B'}[\rho_{ABB'}] = \rho_{AB}$, where $S_A := S(\rho_A)$ is the von Neumann entropy of the density matrix $\rho_A \equiv \mathrm{Tr}_B[\rho_{AB}] = \mathrm{Tr}_{B'}[\rho_{AB'}]$, $E(\rho_{AB}) \equiv E_{AB}$ is the EoF (1.2.5), and $\mathcal{J}^{\leftarrow}_{AB'}$ leads the CC (1.2.13).

Proof: we briefly reproduce the proof of the KW relation (2.3.2) whose complete version can be straightforwardly followed in [90]. By starting with the definition of the EoF,

$$E_{AB} = \min_{\{p_i,|\psi_i\rangle\}} \sum_i p_i S\left(\mathrm{Tr}_B[|\psi_i\rangle\langle\psi_i|]\right), \tag{2.3.3}$$

where the minimum is over the ensamble of pure states $\{p_i, |\psi_i\rangle\}$ satisfying $\sum_i p_i|\psi_i\rangle\langle\psi_i| = \rho_{AB}$, it is possible to show, after some algebra, that

$$\mathcal{J}^{\leftarrow}_{AB'} \geq S_A - \sum_i p_i S\left(\mathrm{Tr}_B[|\psi_i\rangle\langle\psi_i|]\right), \tag{2.3.4}$$

for the CC (1.2.13).

Conversely, from the definition of CC [30]:

$$\mathcal{J}^{\leftarrow}_{AB'} = \max_{\{M_k^{B'}\}} \left[S_A - \sum_k p_k S(\rho_{A|k}) \right], \tag{2.3.5}$$

where $\rho_{A|k} = \mathrm{Tr}_{B'}\left[\left(\mathbb{1}_A \otimes M_k^{B'}\right)\rho_{AB'}\right]/p_k$ is the state of party A after the set of measurements $\{M_k^{B'}\}$ has been done on party B' with probability $p_k = \mathrm{Tr}\left[\left(\mathbb{1}_A \otimes M_k^{B'}\right)\rho_{AB'}\right]$. Let us assume that $\{M_i^{B'}\}$ is the set achieving the maximum in equation (2.3.5) such that one can write $\mathcal{J}^{\leftarrow}_{AB'} = S_A - \sum_i p_i S(\rho_{A|i})$, as the operators $M_i^{B'}$ may be of rank larger than one, by decomposing them into rank-1 nonnegative operators such that $M_i^{B'} = \sum_j M_{ij}^{B'}$, one can show the following

$$E_{AB} \leq \sum_{ij} p_{ij} S\left(\mathrm{Tr}_{B'}[|\phi_{ij}\rangle\langle\phi_{ij}|]\right), \tag{2.3.6}$$

where $\{p_{ij}, |\phi_{ij}\rangle\}$ is an ensamble of pure states with $\sum_{ij} p_{ij}|\phi_{ij}\rangle\langle\phi_{ij}| = \rho_{AB'}$ as the set of measurements $\{M_{ij}^{B'}\}$ is applied to the pure tripartite state $\rho_{ABB'}$. The relationship between the sets $\{M_i^{B'}\}$ and $\{M_{ij}^{B'}\}$ is through: $p_i = \sum_j p_{ij}$ and $p_i\rho_{A|i} = \sum_j p_i\rho_{A|\{ij\}}$.

Noting that $S_A - \sum_{ij} p_{ij} S(\rho_{A|\{ij\}}) \geq S_A - \sum_i p_i S(\rho_{A|i}) \equiv \mathcal{J}^{\leftarrow}_{AB'}$ due to the concavity of the von Neumann entropy, but that the opposite inequality arises by the own definition of the CC, one concludes that $S_A - \sum_{ij} p_{ij} S(\rho_{A|\{ij\}}) = \mathcal{J}^{\leftarrow}_{AB'}$. Then, by putting together the results of equations (2.3.4) and (2.3.6), one achieves the equation (2.3.2) $\square$.

By introducing the definition of QD (1.2.12) into Eq. (2.3.2), one gets

$$E_{AB} - \delta^{\leftarrow}_{AB'} = S_{A|B'}, \tag{2.3.7}$$

with $S_{A|B'} = S_{AB'} - S_{B'}$ the conditional entropy. Noting that $S_{A|B'} = -S_{A|B}$ because the tripartite state $\rho_{ABB'}$ is pure, and changing the subscript B' to $\mathcal{E}$, Eq. (2.3.7) gives rise to the expression for $\delta^{\leftarrow}_{A\mathcal{E}}$ in Eq. (2.3.8) (The second expression is obtained by moving the subscripts):

$$\delta^{\leftarrow}_{A\mathcal{E}} = E_{AB} + S_{A|B};\ \delta^{\leftarrow}_{B\mathcal{E}} = E_{AB} + S_{B|A}. \tag{2.3.8}$$

Hence, we compute the QD between each subsystem and the environment by means of the EoF between the two qubits. Continuing moving the subscripts and applying the definition of CC to the appropriate partition, we can also compute the EoF between each qubit and the environment. We do so by means of the QD as:

$$E_{A\mathcal{E}} = \delta^{\leftarrow}_{AB} + S_{A|B};\ E_{B\mathcal{E}} = \delta^{\leftarrow}_{BA} + S_{B|A}. \tag{2.3.9}$$

Since the tripartite state $AB\mathcal{E}$ remains pure for all time t, we can calculate, even without any knowledge about $\mathcal{E}$, the dynamics of quantum correlations between each subsystem and the environment. We note that, in general, $\delta^{\leftarrow}_{A\mathcal{E}} \neq \delta^{\leftarrow}_{\mathcal{E}A}$ and $\delta^{\leftarrow}_{B\mathcal{E}} \neq \delta^{\leftarrow}_{\mathcal{E}B}$, i.e., these quantities are not symmetric. Directly from the KW relations, such asymmetry can be understood due to the different behaviour exhibited by the EoF and the QD for the AB partition; e.g., $\delta^{\leftarrow}_{\mathcal{E}A} = \delta^{\leftarrow}_{BA} + S_{A|B}$, such that $\delta^{\leftarrow}_{A\mathcal{E}} \neq \delta^{\leftarrow}_{\mathcal{E}A}$ when $\delta^{\leftarrow}_{BA} \neq E_{AB}$ (the equality holds for pure states). In our setup the AB partition goes into a mixed state due to the dissipative effects and the qubits detuning [46, CS1]. In our calculations, the behaviour of $\delta^{\leftarrow}_{i\mathcal{E}}$ and $\delta^{\leftarrow}_{\mathcal{E}i}$, $i = A, B$, is similar, so we only compute, without loss of generality, those correlations given by equations (2.3.8). An important aspect to be emphasised on the KW relations concerns its definition in terms of the EoF. Although the original version of the KW relation is given in terms of the EoF and CC defined in terms of the von Neumann entropy, this is not a necessary condition. Indeed, similar monogamic relations can be determined by any concave measure of entanglement. In this sense, it can be defined a KW relation in terms of the tangle or even the concurrence, since they both obey the concavity property. For instance, in Ref. [92] the authors use the KW relation in terms of the linear entropy to show that the tangle is monogamous for a system of N qubits. Here we use EoF and QD given their nice operational interpretations, but we stress that this is not a necessary condition.

In order to impose the pure initial condition to the $AB\mathcal{E}$ system required to use the KW relations, we suppose that the quantum register is in a pure initial state and that we have a zero temperature environment. Thus,

$$\rho_{AB\mathcal{E}}(0) = \rho_{AB} \otimes |0\rangle_{\mathcal{E}}\langle 0|. \tag{2.3.10}$$

However, we note that a less controllable and different initial state for the environment can be considered since an appropriate purification of the environment $\mathcal{E}$ with a new subsystem $\mathcal{E}'$ could be realised. Despite this, for the sake of simplicity in calculating the quantum register dynamics, we consider a zero temperature environment.

The master equation (1.1.5) gives a solution for $\rho_{AB}(t)$ that becomes mixed since it creates quantum correlations with the environment. We pose the following questions: i) How does each qubit get entangled with the environment? ii) How does this depend on the energy mismatch between A and B?, and iii) on the external laser pumping?

2.3.2 Register-environment quantum correlations

To begin with the quantum dynamics of the qubit-environment correlations, we initially consider resonant qubits, $\omega_1 = \omega_2 \equiv \omega_0$. In the absence of optical driving, there is an optimal inter-emitter separation R_c which maximises the correlations [93]. In Fig. 2.8 we plot the $\delta^{\leftarrow}_{A\mathcal{E}}$, $\delta^{\leftarrow}_{AB}$ and $E_{A\mathcal{E}}$ as functions of the interqubit separation $k_0 r$ at $t = \Gamma^{-1}$. The maximum value reached by each correlation is due to the behaviour of the collective damping γ, which reaches its maximum negative value at the optimal separation $k_0 R_c \simeq 0.674$, as shown in Fig. 2.8, with $k_0 = \omega_0/c$. This is due to the fact that the initial state $|\Psi^+\rangle = \frac{1}{\sqrt{2}}(|01\rangle + |10\rangle)$ decays at the rate $\Gamma + \gamma$ (see equations (2.3.11) with $\alpha = 1/2$), and hence the maximum life-time of $|\Psi^+\rangle$ is obtained for the most negative value of γ, i. e., for any time t, the correlations reach their maxima precisely at the interqubit distance R_c (the same result holds for the $B\mathcal{E}$ bipartition, not shown).

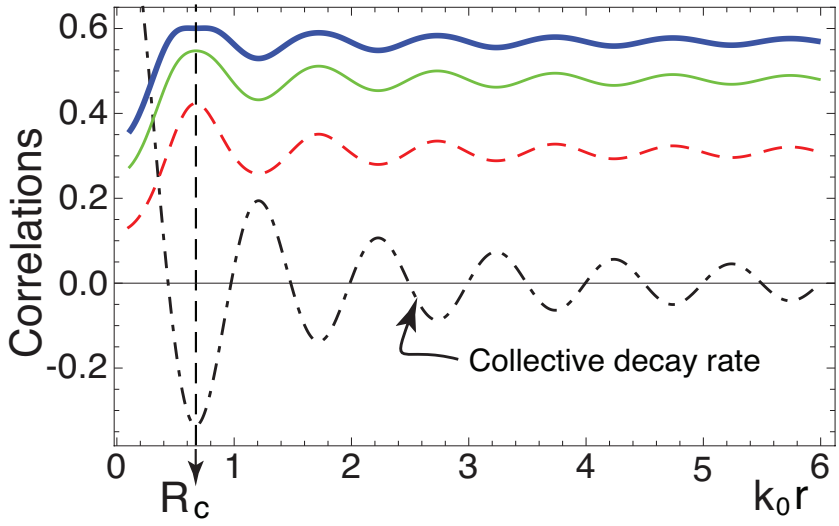

Figure 2.8: $\delta^{\leftarrow}_{AB}$ (dashed-red line), $\delta^{\leftarrow}_{A\mathcal{E}}$ (solid-green line), and $E_{A\mathcal{E}}$ (solid-blue line); initial state $|\Psi^+\rangle = (|01\rangle + |10\rangle)/\sqrt{2}$, at $t = \Gamma^{-1}$. The dotted-dashed curve shows the variation in the collective decay rate γ due to changes in the interqubit separation r. The vertical line signals the optimal $r = R_c \simeq 0.674\, k_0^{-1}$.

We stress that it is the collective damping and *not* the dipolar interaction that defines the distance R_c. For a certain family of initial states (which includes $|\Psi^+\rangle$), the free evolution of the emitters is independent of the interqubit interaction V [CS2]: for the initial states $|\Psi(\alpha)\rangle = \sqrt{\alpha}|01\rangle + \sqrt{1-\alpha}|10\rangle$, $\alpha \in [0,1]$, equation (1.1.5) admits an analytical solution and the non-trivial density matrix elements read

$$\begin{aligned}
\rho_{00,00}(t) &= 1 - \rho^{+}_{01,01}(t) - \rho^{-}_{10,10}(t), \qquad (2.3.11)\\
\rho_{01,10}(t) &= \frac{e^{-\Gamma t}}{2}\left[2\sqrt{\alpha(1-\alpha)}\cosh(\gamma t) - \sinh(\gamma t) + \mathrm{i}(2\alpha-1)\sin(2Vt)\right],\\
\begin{bmatrix} \rho^{+}_{01,01}(t) \\ \rho^{-}_{10,10}(t) \end{bmatrix} &= \frac{e^{-\Gamma t}}{2}\left[\pm(2\alpha-1)\cos(2Vt) + \cosh(\gamma t) - 2\sqrt{\alpha(1-\alpha)}\sinh(\gamma t)\right],
\end{aligned}$$

with $\rho_{10,01}(t) = (\rho_{01,10}(t))^*$. This solution implies that the density matrix dynamics dependence on V vanishes for $\alpha = 1/2$ ($|\Psi^+\rangle$), and hence the damping γ becomes the only collective parameter responsible for the oscillatory behaviour of the correlations, as shown in Fig. 2.8. A similar analysis can be derived for the initial states $|\Phi(\beta)\rangle = \sqrt{\beta}|00\rangle + \sqrt{1-\beta}|11\rangle$ [93]. Such β states are not, in general,

'naturally' supported by the system Hamiltonian since they are not eigenstates of $\hat{H}_S$, and hence, they exhibit a 'detrimental' behaviour for $\delta^{\leftarrow}_{AB}$ and E_{AB} (not shown).

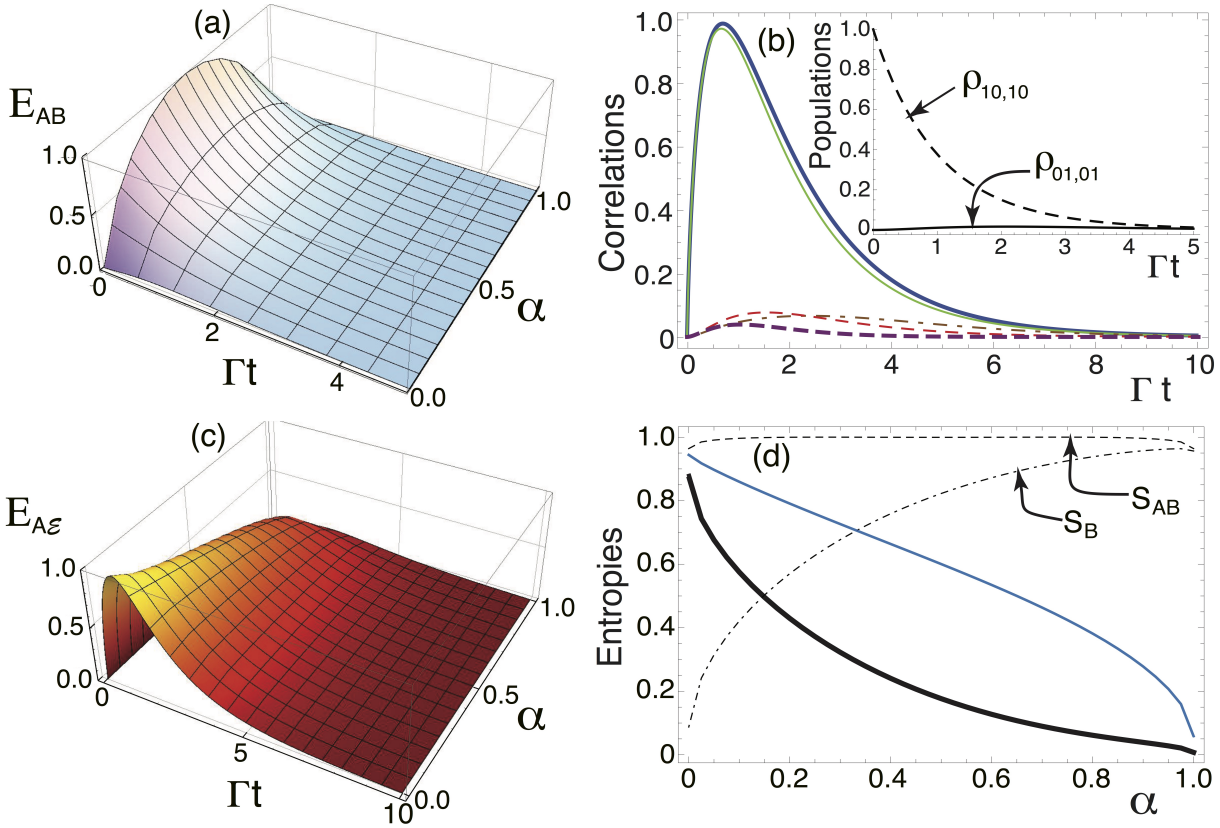

Figure 2.9: (a) Qubit-qubit (E_{AB}), and (c) qubit-environment ($E_{A\mathcal{E}}$) Entanglement dynamics for the α initial states. (b) $\delta^{\leftarrow}_{AB}$ (dashed-red curve), $\delta^{\leftarrow}_{A\mathcal{E}}$ (solid-green curve), $\delta^{\leftarrow}_{B\mathcal{E}}$ (dotted-dashed-brown curve), E_{AB} (dashed-purple curve) and $E_{A\mathcal{E}}$ (solid-blue curve). Inset; populations $\rho_{01,01}$ (solid) and $\rho_{10,10}$ (dashed), $\alpha = 0$. (d) Conditional entropy $S_{A|B}$ (thick-black curve), and $S_{M_i^B}$ (thin-blue curve) for qubit initial states α, $t = \Gamma^{-1}$. $r = R_c$.

We now consider the qubits full time evolution and calculate the correlations dynamics for the whole spectrum of initial states $|\Psi(\alpha)\rangle$, $0 \leq \alpha \leq 1$. The emitters' EoF E_{AB} exhibits an asymptotic decay for all α values, with the exception of the two limits $\alpha \to 0$ and $\alpha \to 1$, for which the subsystems begin to correlate with each other and the entanglement increases until it reaches a maximum before decaying monotonically, as shown in Fig. 2.9(a). The AB QD also follows a similar behaviour; this can be seen in Fig. 2.9(b) for $\alpha = 0$. Initially, at $t = 0$, $E_{A\mathcal{E}}$ (Fig. 2.9(c)) equals zero because of the separability of the tripartite $AB\mathcal{E}$ state at such time. After this, the EoF between A and $\mathcal{E}$ increases to its maximum, which is reached at a different time ($t \sim \Gamma^{-1}$) for each α, and then decreases asymptotically. The simulations shown in Figs. 2.9(a) and (c) have been performed for the optimal inter-emitter separation R_c. These allow to access the dynamical qubit information (quantum correlations) exchange between the environment and each subsystem for suitable qubit initialisation.

Figure 2.9(a) shows the EoF between identical emitters: E_{AB} is symmetric with respect to the initialisation $\alpha = 1/2$, i.e., the behaviour of E_{AB} is the same for the separable states $|01\rangle$ and $|10\rangle$. In contrast, Fig. 2.9(c) exhibits a somewhat different behaviour for the entanglement $A\mathcal{E}$, which is not sym-

metric with respect to α: the maximum reached by $E_{A\mathcal{E}}$ increases as α tends to 0 (the QD $\delta^{\leftarrow}_{A\mathcal{E}}$ follows the same behaviour–not shown). The dynamical distribution of entanglement between the subsystem A and the environment $\mathcal{E}$ leads to the following: it is possible to have near zero interqubit entanglement (e.g., for the $\alpha = 1$ initialisation) whilst the entanglement between one subsystem and the environment also remains very close to zero throughout the evolution.

This result stresses the sensitivity of the qubit-environment quantum correlations distribution to its qubit initialisation. To understand why this is so (cf. states $|01\rangle$ and $|10\rangle$), we analyse the expressions for $\delta^{\leftarrow}_{A\mathcal{E}}$ and $E_{A\mathcal{E}}$. From equations (2.3.9) and equations (2.3.8), and since E_{AB} and $\delta^{\leftarrow}_{AB}$ are both symmetric, the asymmetry of $\delta^{\leftarrow}_{A\mathcal{E}}$ and $E_{A\mathcal{E}}$ should follow from the conditional entropy $S_{A|B} = S(\rho_{AB}) - S(\rho_B)$. This is plotted in the thick-black curve in Fig. 2.9(d). The behaviour of the conditional entropy is thus reflected in the dynamics of quantum correlations between A and $\mathcal{E}$, and this can be seen if we compare the behaviour of $E^{\leftarrow}_{A\mathcal{E}}$ around $t = \Gamma^{-1}$ throughout the α-axis in Fig. 2.9(c), with that of $S_{A|B}$ shown in Fig 2.9(d). Since this conditional entropy gives the amount of partial information that needs to be transferred from A to B in order to know ρ_{AB}, with a prior knowledge of the state of B [94], we have shown that this amount of information may be extracted from the dynamics of the quantum correlations generated between qubits and their environment.

Interestingly, by replacing the definition of $\delta^{\leftarrow}_{AB}$ [29] into the first equality of equations (2.3.9), we find that the EoF of the $A\mathcal{E}$ partition is exactly the post-measure conditional entropy of the AB partition,

$$E_{A\mathcal{E}} = S_{M_i^B} \equiv \min_{M_i^B} \Big[\sum_i p_i S\left(\rho_{A|i}\right) \Big], \tag{2.3.12}$$

that is, the EoF between the emitter A and its environment is the conditional entropy of A after the partition B has been measured, and hence the asymmetric behaviour of $E_{A\mathcal{E}}$ can be verified by plotting this quantity, as shown by the thin-blue curve of Fig. 2.9(d). A physical reasoning for the asymmetric behaviour of the $A\mathcal{E}$ correlations points out that for $\alpha \to 0$ the state $|10\rangle$ has higher weights throughout the whole dynamics. For instance, for $\alpha = 0$ the subsystem B always remains close to its ground state, and transitions between populations $\rho_{01,01}$ and $\rho_{10,10}$ do not take place, as it is shown in the inset of Fig. 2.9(b). This means that the partition B keeps almost inactive during this specific evolution and therefore does not share much information, neither quantum nor locally accessible with partition A and the environment $\mathcal{E}$. This can be seen from the QD $\delta^{\leftarrow}_{B\mathcal{E}}$, which is plotted as the dotted-dashed-brown curve of Fig. 2.9(b). We stress that this scenario allows A to get strongly correlated with the environment $\mathcal{E}$.

Although $E_{A\mathcal{E}}$ and $\delta^{\leftarrow}_{A\mathcal{E}}$ are not 'symmetric' with respect to α, it is the way in which the information (correlations) is transferred from the qubits to the environment, the quantity that recovers the symmetry exhibited by E_{AB} (see Fig. 2.9(a) and (c)). In other words, if the initial state were $|01\rangle$, or in general, $\alpha \to 1$, the partition A would remain almost completely inactive and the flow of information would arise from the bipartite partition $B\mathcal{E}$ instead of $A\mathcal{E}$. A simple numerical computation for $\alpha = 0$ at $t = \Gamma^{-1}$ shows that

$$\rho_A = \begin{pmatrix} 0.62 & 0 \\ 0 & 0.38 \end{pmatrix} \quad \text{and} \quad \rho_B = \begin{pmatrix} 0.99 & 0 \\ 0 & 0.01 \end{pmatrix}, \tag{2.3.13}$$

with $S_A = 0.96$ and $S_B = 0.09$, respectively. This means that the state of subsystem B is close to a pure state (its ground state), and no much information about it may be gained. Instead, almost all the partial information on the state of A can be caught regardless of whether the system B is measured or not. From this simple reasoning, and by means of the KW relations, the results shown in Fig. 2.9 arise. The opposite feature between ρ_A and ρ_B occurs for $\alpha = 1$, and in this case, it is the partition $B\mathcal{E}$ that plays the strongest correlation role.

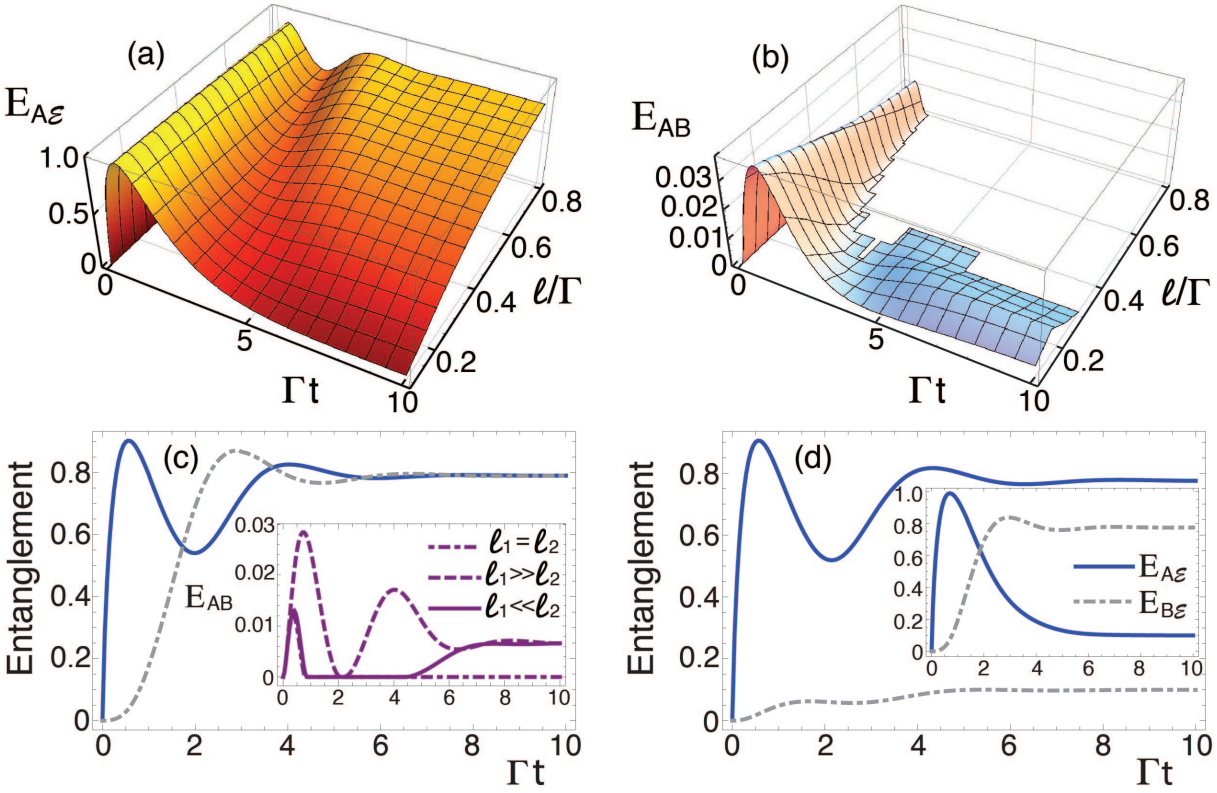

Figure 2.10: Dynamics of EoF (a) $A\mathcal{E}$ and (b) AB as functions of the laser intensity ℓ. Main (c) $A\mathcal{E}$ (solid) and $B\mathcal{E}$ (dotted-dashed), $\ell_1 \equiv \ell_2 = \ell = 0.8\Gamma$; the inset plots E_{AB} for three scenarios, main (d) $\ell_1 = 0.8\Gamma$, $\ell_2 = 0$; the inset plots $\ell_2 = 0.8\Gamma$, $\ell_1 = 0$. $\rho_{10,10}(0) = 1$, and $r = R_c$.

2.3.3 Information flow in laser-driven resonant qubits

The laser Hamiltonian $\hat{H}_L$ conveys an additional degree of control of the qubits information (quantum correlations) flow. Let us consider a continuous laser field acting with the same amplitude, $\ell_1 = \ell_2 \equiv \ell$, on the two emitters, and in resonance with the emitters transition energy, $\omega_L = \omega_0$. In the absence of an external field, the subsystem A gets the strongest correlated with the environment for the initial pure state $|10\rangle$ in the relevant time regime (see Fig. 2.9(c)), but this correlation monotonically decays to zero in the steady-state regime. In Fig. 2.10 we see the effect of the laser driving for the initial state $|10\rangle$, for qubits separated by the optimal distance $r = R_c$. The laser field removes the monotonicity in the quantum correlations decay between A and $\mathcal{E}$, and, as shown in Fig. 2.10(a), the more intense the laser radiation (even at the weak range $\ell \leq \Gamma$), the more entangled the composite $A\mathcal{E}$ partition becomes. This translates into a dynamical mechanism in which the qubit register AB gets rapidly disentangled and, even at couplings as weak as $\ell \sim 0.4\Gamma$, the qubits exhibit early stage disentanglement, as shown in Fig. 2.10(b). This regime coincides with the appearance of oscillations in the $A\mathcal{E}$ entanglement (see Fig. 2.10(a)), and steady nonzero $A\mathcal{E}$ entanglement translates into induced interqubit (AB) entanglement suppression by means of the laser field.

By tailoring the laser amplitude we are able to induce and control the way in which the qubits get correlated with each other and with the environment. Figures 2.10(c) and (d) show three different scenarios in terms of such amplitude. In panel (c) we plot $E_{A\mathcal{E}}$ (solid-blue curve) and $E_{B\mathcal{E}}$ (dashed-dotted-grey

curve) for the symmetric light-matter interaction ($\ell_1 = \ell_2 \equiv \ell = 0.8\Gamma$), which leads to the entanglement sudden death (ESD) phenomenon in the partition AB (see graph (b)), as well as to a symmetric qubit-environment correlation in the stationary regime. However, as can be seen in main graph (d), where we have assumed $\ell_1 >> \ell_2$, the breaking of this symmetry completely modifies the qubit-environment entanglement, and now it is qubit A that gets strongly correlated with the environment, while qubit B remains weakly correlated during the dynamics. The opposite arises for $\ell_1 << \ell_2$ (inset of panel (d)): $E_{B\mathcal{E}}$ becomes much higher than $E_{A\mathcal{E}}$, which decays monotonically after reaching its maximum. Remarkably, we notice that these two asymmetric cases lead a nonzero qubit-qubit entanglement as shown in the inset of graph (c), where equal steady entanglement is obtained. It means that the qubits early stage disentanglement [38, 39] can be interpreted in terms of the entanglement distribution between the qubits and the environment. We interpret this behaviour as the flow and distribution of entanglement in the different partitions of the whole tripartite system [95], and hence this result shows that an applied external field may be used to dictate the flow of quantum information within the full tripartite system.

2.3.4 Flow of information in detuned qubits

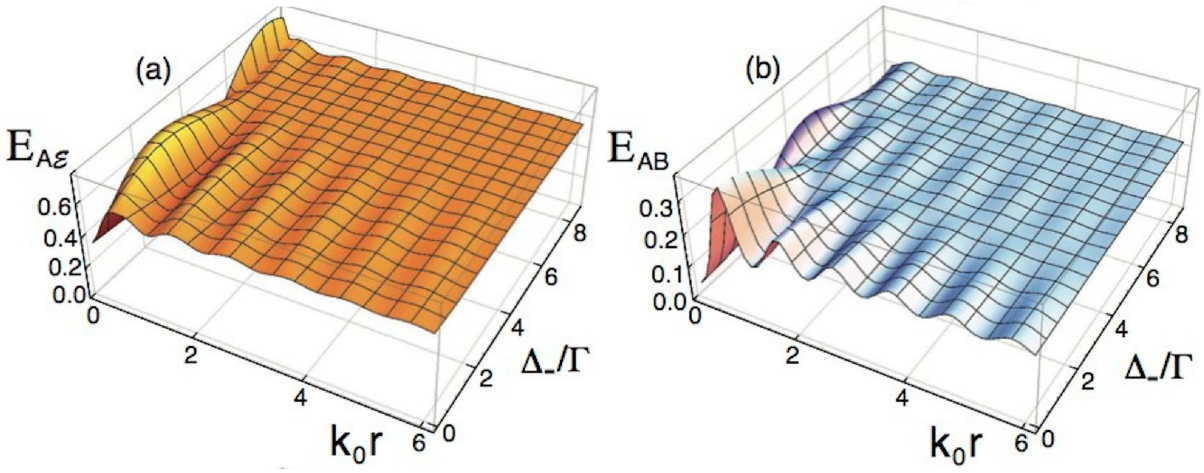

Figure 2.11: (a) $E_{A\mathcal{E}}$, and (b) E_{AB} dependence on the inter-emitter distance r for frequency detuning $\Delta_- \equiv \omega_1 - \omega_2$, and qubits initial state $|\Psi^+\rangle$, $t = \Gamma^{-1}$.

We now consider a more general scenario in which each two-level emitter is resonant at a different transition energy, and hence a molecular detuning $\Delta_- = \omega_1 - \omega_2$ arises; $\omega_0 \equiv (\omega_1 + \omega_2)/2$. Such a detuning substantially modifies the qubit-qubit and qubit-environment correlations. Since $\Delta_- \neq 0$, the $\alpha = 1/2$-time independence of equations (2.3.11) with respect to V no longer holds, and the critical distance R_c of Fig. 2.8 becomes strongly modified: the information flow exhibits a more involved dynamics precisely at distances $r < R_c$, and the intermediate sub- and super-radiant states are no longer the maximally entangled Bell states.

As shown in Fig. 2.11, the oscillations of the EoF of $A\mathcal{E}$ and AB (and their maxima) start to decrease and become flat as the molecular detuning rises ($\Delta_- = 0$ corresponds to the case shown in Fig. 2.8). This means that now, it is not only the collective decay rate, γ, that modulates the behaviour of the quantum correlations, but also the interplay between the detuning Δ_- and the d-d interaction V. Note from Fig. 2.11 that the critical distance R_c, for which both the correlations of partition AB and those of

$A\mathcal{E}$ get their maxima, disappears with the inclusion of the molecular detuning. Furthermore, E_{AB} and $E_{A\mathcal{E}}$ exhibit maxima at different inter-emitter distances as the detuning increases, i. e., E_{AB} remains global maximum for resonant qubits ($\Delta_- = 0$) whereas $E_{A\mathcal{E}}$ reaches its global maximum for a certain $\Delta_- \neq 0$ (e.g., $\Delta_-/\Gamma = 8$ at $k_0 r \sim 0.1$), a value for which E_{AB} is stationary for almost all interqubit separation r.

To complete the analysis of the general tripartite $AB\mathcal{E}$ system, we now consider that the asymmetric (detuned) qubits are driven by an external laser field on resonance with the average qubits transition energy, $\omega_0 = \omega_L$, as shown in Fig. 2.12 for the two-qubit initial state $|\Psi^+\rangle$. We have plotted the EoF dynamics E_{AB}, $E_{A\mathcal{E}}$, and $E_{B\mathcal{E}}$. Fig. 2.12(a) shows the EoF evolution for two identical emitters in the absence of the external driving. The molecular detuning, and the laser excitation have been included in graphs (b) and (c), respectively. The panel (d) shows the EoF evolution under detuning and laser driving. The monotonic decay of E_{ij} for resonant qubits in Fig. 2.12(a) is in clear contrast with the E_{ij}-oscillatory behaviour due to the qubit asymmetry, as plotted in Fig. 2.12(b). A non-zero resonant steady entanglement is obtained thanks to the continuos laser excitation (Fig. 2.12(c) and (d)). These graphs have been compared with that of the clockwise flow of pairwise locally inaccessible information $\mathcal{L}_{\circlearrowleft} = \delta^{\leftarrow}_{B\mathcal{E}} + \delta^{\leftarrow}_{AB} + \delta^{\leftarrow}_{\mathcal{E}A}$ [95], as shown in the long-dashed black curve.

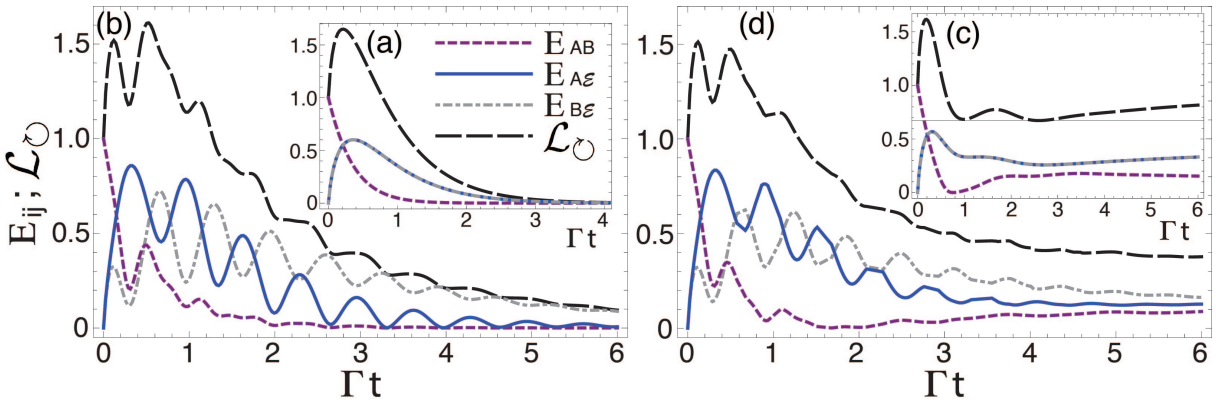

Figure 2.12: EoF dynamics E_{AB}, $E_{A\mathcal{E}}$, $E_{B\mathcal{E}}$, and the flow of quantum information $\mathcal{L}_{\circlearrowleft}$. (a) identical, and (b) detuned emitters, $\Delta_- = 8\Gamma$; no laser excitation. $\ell = 0.8\Gamma$ and $\omega_0 = \omega_L$-laser-driven (c) identical, and (d) detuned emitters, $\Delta_- = 8\Gamma$. The initial state $|\Psi^+\rangle$, and $k_0 r = 0.1$.

2.3.5 Discussion

We can now interpret the entanglement dynamics of the AB partition by means of the dynamics of the clockwise QD distribution in the full tripartite system ($\mathcal{L}_{\circlearrowleft}$), and that of the entanglement of $A\mathcal{E}$ and $B\mathcal{E}$ partitions. From the conservation law [83] between the distribution of the EoF and QD followed from Eqs. (2.3.9) and (2.3.8), and noting that $\mathcal{L}_{\circlearrowleft} = \mathcal{L}_{\circlearrowleft}$ for pure states [95], where $\mathcal{L}_{\circlearrowleft} = \delta^{\leftarrow}_{BA} + \delta^{\leftarrow}_{\mathcal{E}B} + \delta^{\leftarrow}_{A\mathcal{E}}$, a direct connection between qubit-qubit entanglement and qubit-environment entanglement can be established [95]:

$$E_{AB} = \mathcal{L}_{\circlearrowleft} - E_{A\mathcal{E}} - E_{B\mathcal{E}}. \tag{2.3.14}$$

We note from equation (2.3.14) and from the pairwise locally inaccessible information that by knowing $\delta^{\leftarrow}_{AB}$ (or $\delta^{\leftarrow}_{BA}$), we can exactly compute the qubit-qubit entanglement in terms of the system bipartitions $A\mathcal{E}$ and $B\mathcal{E}$. In particular, we show how a profile of the qubit-qubit entanglement might be

identified from the partial information obtained from $E_{A\mathcal{E}}$ and $E_{B\mathcal{E}}$, as indicated in the right-handside of equation (2.3.14). It is also shown in Figs. 2.12(b) and (d) whereby the local minima of E_{AB} occur at times for which the extrema of $E_{A\mathcal{E}}$ and $E_{B\mathcal{E}}$ take place. However, it is interesting to note that $\mathcal{L}_{\circlearrowleft}$, which gives a global information of the whole tripartite system (the distribution of the QD), can be extracted directly from the quantum state of the register. This fact can be demonstrated by replacing equation (2.3.12), and its equivalent formula for the bipartition $B\mathcal{E}$ ($E_{B\mathcal{E}} = S_{M_i^A} \equiv \min_{M_i^A} \sum_i p_i S(\rho_{B|i})$), into equation (2.3.14):

$$\mathcal{L}_{\circlearrowleft} = E_{AB} + S_{M_i^A} + S_{M_i^B}. \tag{2.3.15}$$

This relation means that the entanglement of partition AB plus *local accessible* information of subsystems A and B, i.e. the post-measured conditional entropies $S_{M_i^A}$ and $S_{M_i^B}$, give complete information about the flow of the locally inaccessible (quantum) information, which is a global property of the tripartite system.

An advantage of using the information gained from the system-environment correlations to get information about the reduced system's entanglement dynamics is that new interpretations and understanding of the system dynamics may arise. For instance, in Ref. [96], this fact has been used to propose an alternative way of detecting the non-Markovianity of an open quantum system by testing the accessible information flow between an ancillary system and the local environment of the apparatus (the open) system.

Chapter 3
Correlations in a hybrid quantum emitter-plasmon system

The main physical aspect analysed in this Chapter is the interaction between the emitters and the plasmons that propagate on the surface of a metallic channel. Thinking in a possible physical implementation of the results presented in this Chapter, we have in mind the organic molecules we studied in Chapter 2 as the emitter located near the metallic surface. As mentioned in Section 1.1.1, the properties of the collective effects signal the behaviour of the quantum correlations through the dissipative dynamics of the emitters. We study the quantum correlations, and conditional dynamics in the hybrid emitter-plasmon setup, for long distant (about $1\,\mu$m) emitters, as follows: In section 3.1 we briefly describe surface plasmons. In section 3.2 we indicate the explicit form of both the d-d interaction and the collective damping assisted by plasmons, and compare their behaviour with the respective quantities in absence of plasmons. A discussion on the correlations dynamics is presented in section 3.3. Finally, a laser-assisted mechanism for switching on/off the emitters correlations that works for both resonant and detuned emitters is presented in section 3.4.

3.1 Surface plasmon excitations

One of the major difficulties of nano-escale optical design is the confinement of light in regions smaller than the diffraction limit, i.e. light cannot be focused in regions smaller than $\sim \lambda/2n$ by means of conventional optical devices, where λ is the wavelength of light and n the refraction index of the medium [50]. Although it is possible to create optical devices in the nano-scale, as slab waveguides and fibres, the light is poorly confined.

One solution that emerged to this problem was to focus the light with metallic nano-structures. An incident light excites the free electrons on the metallic surface (this is another example of light-matter interaction), and creates charge density oscillations that, coupled to the electromagnetic wave, may propagate along the metal/dielectric interface. This new physical object is called surface plasmons (SP) [51, 50] and has found novel applications as for example interferometers, sensors and magneto-optic storage [51, 97, 98].

Confinement and propagation of SP has become an area of great interest not just in physics but also chemistry, material science and engineering. Many structures to guide SP have been developed: dielectric slab between two metal slabs, encased slot, V-groove and wedge waveguides, just to name a few [50, 102]. Particularly, great advantages of V-groove waveguides are their strong localisation and relatively large propagation distances ($\sim 10\mu$m). Furthermore, the enhancement of collective effects of a two-emitter system located close to the waveguide, and the possibility of generate entanglement between

the emitters at large mutual separation distances have also been explored [58, 59].

We study the effects that SP produce on the dynamics of quantum and classical correlations in a couple of emitters. In order of doing so, we consider a V-groove structure (Fig. 3.1(a)) as the channel that mediates the effective interaction between the emitters. Our main interest is not the detailed description of the Maxwell's equations solution for SP propagation, we crudely discuss about the dispersion relation of the surface propagating light.

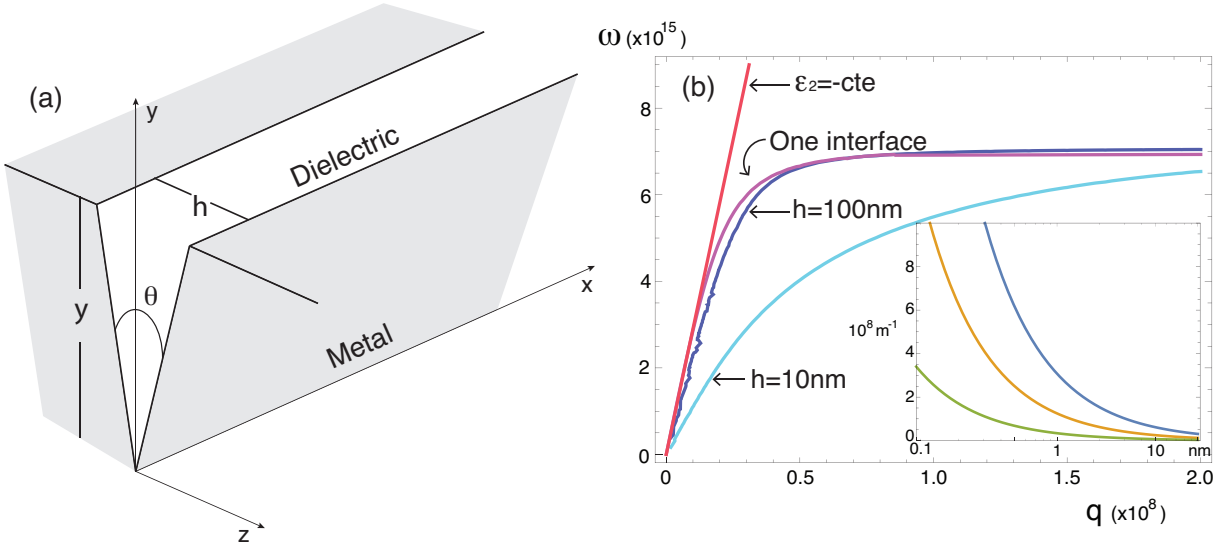

Figure 3.1: (a) V-groove nano waveguide structure: opening angle $\tan\theta/2 = h/2y$. (b) Dispersion relation (frequency ω vs wave vector q) for two different gaps h, and for the one single interface case. Inset: Wave vector as a function of the gap h for (blue) $e_1 = -6.5$ and $\lambda = 459.2$ nm, (orange) $e_1 = -16$ and $\lambda = 632.8$ nm and (green) $e_1 = -58.8$, and $\lambda = 1.127\,\mu$m. $\epsilon_1 = 1$ for the three cases.

To easily understand the V-groove SP dispersion relation, we consider that the opening angle of the channel $\tan\theta/2 = h/2y$ is such that $h/2y \ll 1$ holds, where h is the gap on the top of the channel and y is the depth as shown in Fig. 3.1(a). Under this assumption (equivalent to consider an infinite depth), we can treat the V-groove as a metal-insulator-metal multilayer. The dispersion relation for the symmetric SP in this sort of configurations [99], is written as,

$$\tanh\frac{\alpha_1 h}{2} = -\frac{\alpha_2\epsilon_1}{\alpha_1\epsilon_2}, \tag{3.1.1}$$

where $\alpha_i = \sqrt{q^2 - k_0^2\epsilon_i}$, k_0 is the vacuum wave number and $\epsilon_1(\epsilon_2)$ stands for the electric permittivity of the insulator(metal). The permittivity of the metal is complex $\epsilon_2 = e_1 + ie_2$, such that $e_1 < 0$ and $|e_1| \gg e_2$. These conditions are required for exciting SP and avoiding strong dissipation into the metal.

Figure 3.1(b) shows the dispersion relation (3.1.1) assuming the Drude's model for metals $e_1 = 1 - (\omega_p/\omega)^2$, being ω_p the plasma frequency, and for two values of the gap h; as expected, for increasing h, the dispersion relation approaches the dispersion exhibited for a single metal-insulator interface (purple line in Fig. 3.1(b)). We also plot the straight light line given by the dispersion relation between two materials with constant permittivities (we assumed $\epsilon_2 = e_1 = -16$ in this case). The behaviour of the wave vector q as a function of the gap h is also shown in the inset of Fig. 3.1(b). The wave vector increases rapidly when the opening angle in the groove tends to zero. We illustrate this behaviour for three values of the metal permittivity.

These propagating SP can interact with matter, in the following section we illustrate how the collective properties of two emitters located close to the plasmonic waveguide are modified due to the SP.

3.2 Quantum emitters coupled to surface plasmons

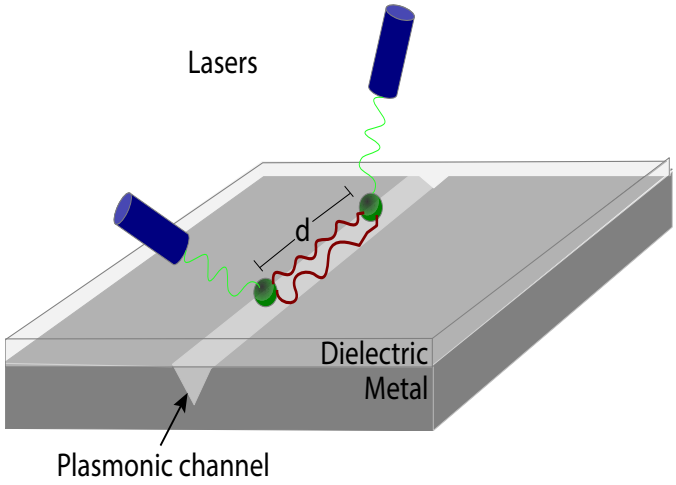

Figure 3.2: Schematic representation of the physical setup comprising two separate emitters located in a dielectric host near a metallic surface that allows the propagation of surface plasmons. d stands for the inter-emitter separation, red curves indicate that emitters can interact to each other by means of the plasmonic channel, and the blue cylinders point to the possibility of an external field control on both emitters.

We continue considering our qubits to be atom-like (small) emitters with an operational wavelength in the optical frequency regime (we use $\lambda_0 \sim 640$ nm), but now coupled to a plasmonic waveguide (for a schematic illustration see Fig. 3.2). This coupling is also considered to be weak enough [58, 59, 100] such that the master equation in the Born-Markov and rotating wave approximations (Eq. 1.1.5) is still valid [CS1, CS2, 46, 58]. The strength of the effective d-d interaction can be now calculated as,

$$V = \frac{1}{\pi\epsilon_0 c^2\hbar}\mathcal{P}\int_0^\infty d\omega \frac{\omega^2 \mathrm{Im}[\boldsymbol{\mu}_1^* \boldsymbol{G}(\omega, \mathbf{r}_1, \mathbf{r}_2)\boldsymbol{\mu}_2]}{\omega - \omega_0}, \tag{3.2.1}$$

where $\omega_0 = (\omega_1 + \omega_2)/2$ and $\mathcal{P}$ denotes the principal part of the integral. The second term of Eq. (1.1.5) accounts for the dimer's incoherent effects that arise from radiation into the vacuum, dissipation through losses in the metal, and the excitation of the SP that propagates on the metallic surface [59, 101]. If the losses in the metal are negligible, the two remaining dissipative channels to be accounted for are captured by

$$\Gamma_{ij} = \frac{2\omega_0^2}{\epsilon_0 c^2 \hbar}\mathrm{Im}[\boldsymbol{\mu}_i^* \boldsymbol{G}(\omega_0, \mathbf{r}_i, \mathbf{r}_j)\boldsymbol{\mu}_j], \tag{3.2.2}$$

where, as before, $\Gamma_{11} = \Gamma_{22} \equiv \Gamma_p$, and $\Gamma_{12} = \Gamma_{21}^* \equiv \gamma_p$ are the individual and collective spontaneous emission rates, respectively [46, CS2], and $i, j = 1, 2$.

The emitter-plasmon dissipative coupling renders new d-d strength V_p and collective damping rates γ_p. If we consider that the emitters dipoles are equally oriented and are located at the same distance to

the surface of the metal, and that the emitters most relevant dissipative contribution is due to the plasmon modes. An exact calculation of V_p (Eq. (3.2.1)) and γ_p (Eq. (3.2.2)) follows from the Green's functions of the plasmon excitations [56, 58, 59],

$$V_p = \frac{\Gamma_p}{2}\beta e^{-\frac{\lambda_p}{2L}\zeta}\sin(2\pi\zeta); \tag{3.2.3}$$

$$\gamma_p = \Gamma_p\beta e^{-\frac{\lambda_p}{2L}\zeta}\cos(2\pi\zeta), \tag{3.2.4}$$

where the wavelength of plasmons $\lambda_p \equiv 2\pi/k_p$, k_p is the plasmon wave vector, $\zeta \equiv d/\lambda_p$, d gives the distance between emitters, L is the propagation length of the plasmons, and β is called the spontaneous emission factor (or simply, the β-factor) that gives the probability of emitting SP. As our principal aim is to focus on correlations and their properties through the dynamics of the system, and bearing in mind that plasmonic nanostructures and their applications convey a vast area of research [102, 103], we do not explicitly enter the aforementioned Green's function formalism and start from the results for the collective parameters. For details on analytical and numerical treatments of these collective effects, the reader is referred to Refs. [47, 56, 58, 59, 50].

Equations (3.2.3) and (3.2.4) are valid for high β-factors ($\beta \equiv \Gamma_p/\Gamma_T$, $\Gamma_T = \Gamma + \Gamma_p$), which means that the emitters main dissipative mechanism is due to the propagating plasmons on the metallic surface, and hence the fraction of emitted radiation by the plasmonic propagating mode $\beta \mapsto 1$. This factor depends on the vertical distance between the emitters and the metallic surface. Here, we consider a V-groove geometry as our plasmonic waveguide, for which the plasmonic excitations have been shown to substantially enhance the interqubit interaction (Λ-wedge geometries also exhibit similar properties) [56, 57], thus validating both Eq. (3.2.3) and Eq. (3.2.4). In particular, for the V-groove channel, β-factors ~ 0.91 (and higher) are expected for an emitter-metal vertical separation above the bottom of the V-channel waveguide of about 160 nm, and a depth of the channel of 140 nm [59, 56]. For such a channel depth, it has been reported [59, 56] that shorter emitter-metal distances (< 80 nm) imply a reduction in the β-factor since the losses into the metal become appreciable. On the other hand, larger emitter-metal distances (> 180 nm), also diminish the β-factor since radiation into the vacuum becomes the major decay contribution [59, 56]. In addition, the 'plasmonic approximation' given by Equations (3.2.3) and (3.2.4) works well for emitter-emitter separations larger than $\sim \lambda_p/4$ [59, 58], and in this case $|\gamma_p| \leq \Gamma_p$ and $|V_p| \leq \Gamma_p/2$. Below such distance, the vacuum electromagnetic fluctuations become more significant and modify the collective parameters.

The behaviour of the collective parameters is shown in Fig. 3.3 as follows: Fig. 3.3(a) shows the d-d interaction strength (Eq. (2.1.3)) and the collective damping rate (Eq. (2.1.4)) for emitters interacting with the vacuum electromagnetic field (no plasmons in action), Fig. 3.3(b) shows the respective collective parameters when emitters undergo the presence of plasmons (equations (3.2.3) and (3.2.4)).

For the sake of comparison, we plot in Fig. 3.3 the especial case of two emitters whose dipole moment vectors are parallel to each other and perpendicular to the inter-emitter separation vector. As shown by the dashed region ($d \leq \lambda/4$), where the plasmon approximation does not work, the collective parameters can take high values compared with the individual spontaneous emission; $\gamma \sim \Gamma$ and $V \geq \Gamma$, for the vacuum electromagnetic field-emitter scenario (Fig. 3.3(a)). However, these quantities rapidly go to zero when going out from this region and are about one order of magnitude less than Γ for distances around one wavelength. The opposite happens in the plasmon-assisted scenario in which the collective damping can reach values close to Γ_p for distances up to two wavelengths, whilst the d-d interaction persists about $\Gamma_p/2$ in the same inter-emitter separation domain (Fig. 3.3(b)).

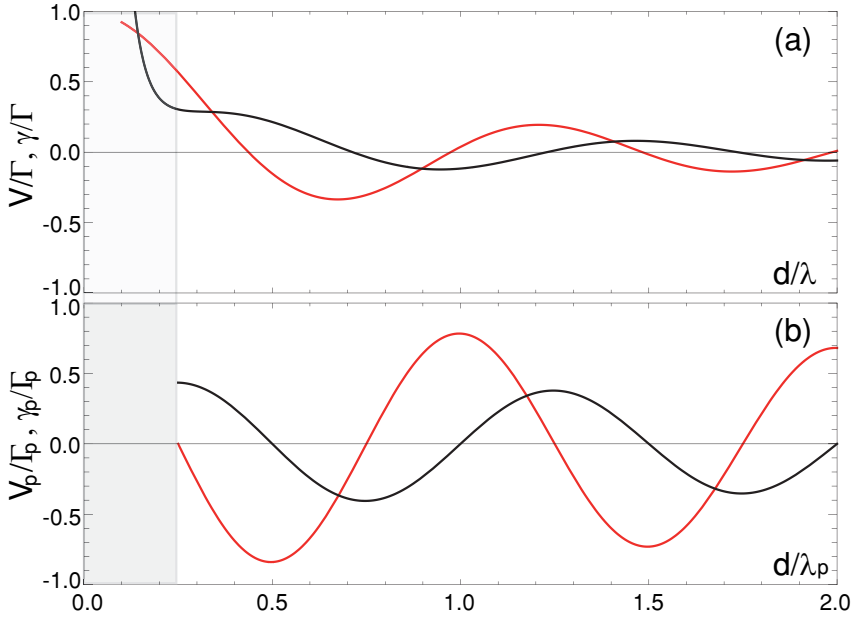

Figure 3.3: Behaviour of the d-d interaction strength and the collective damping in both scenarios studied in this Thesis: (a) Emitters coupled to the vacuum electromagnetic field, and (b) emitters coupled to surface plasmon polaritons.

3.3 Dynamics of correlations: Quantum discord vs entanglement of formation

We calculate the exact dynamics of correlations by solving the master equation (1.1.5), and taking into account the definitions introduced in section 1.2. Before discussing the implications of the plasmon effects on the different kind of correlations, we first present correlations for emitters uncoupled to the plasmons. In terms of the collective effects (Eq. (2.1.3) and Eq. (2.1.4)), the dynamics depends on the separation between emitters and also on the orientation of their dipole moments.

A typical situation where the d-d interaction is much greater than the incoherent part $V \gg \Gamma \geq \gamma$ (Fig. 3.4(a)) can be observed, for example, in systems as those studied in Chapter 2, that basically correspond to diluted molecules in a dispersive matrix; a rich entanglement and quantum discord dynamics for this sort of systems has been arguably explored [CS1, CS2]. Figure 3.4(a) shows that correlations reach high values and oscillate rapidly because of the strong d-d interaction energy V; however, the correlations decay within a short time and the system becomes uncorrelated quite rapidly.

A different scenario, depicted in Fig. 3.4(b), considers a pair of dipoles parallel to each other and perpendicular to their separation vector, which allows the calculation of the collective parameters V (Eq. (2.1.3)) and γ Eq. (2.1.4). Although the correlations initially show smaller values than before, their monotonic behaviour persists for a longer time.

The influence of the plasmonic waveguide is illustrated in Fig. 3.5, and can be directly compared with the results in Fig. 3.4. According to the relations derived from Equations (3.2.3) and (3.2.4) [58, 59], one of the parameters V_p or γ_p can, in principle, be maximised by 'switching off' the other one. For the inter-qubit distance $d = \frac{3}{4}\lambda_p$ (Fig. 3.5(b)), the plasmonic modes allow for an effective enhancement of correlations, as can be seen from a direct comparison between the inset of figure 3.5(b) and figure 3.4(b).

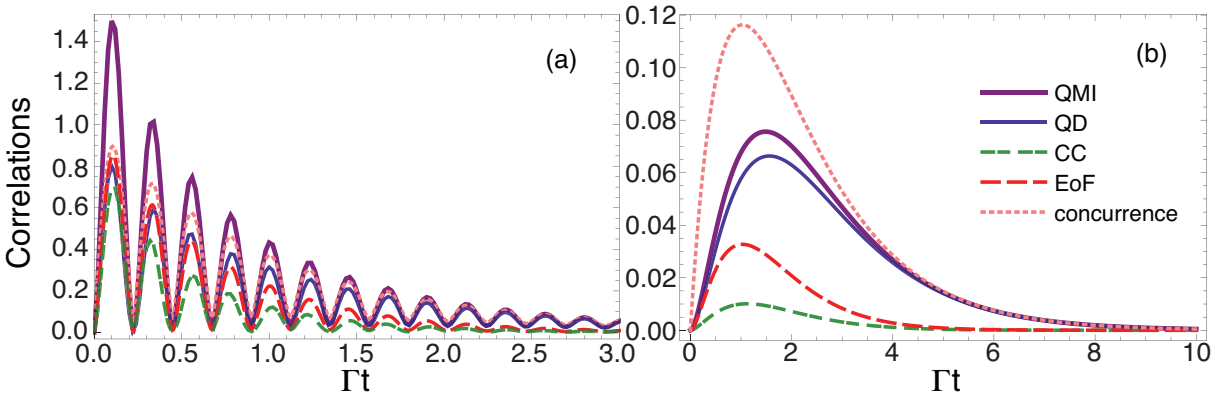

Figure 3.4: Correlations for a two-emitter system in the *absence* of coupling to plasmons. (a) $V = 7\Gamma$ and $\gamma = 0.2\Gamma$. (b) Dipoles parallel to each other and perpendicular to their separation vector; $r_{12} = \frac{3}{4}\lambda_0$, $\lambda_0 \equiv 2\pi/k_0$. The considered initial state is separable: $\rho(0) = |10\rangle\langle 10|$. Total correlation or QMI (purple, thick-solid line), classical correlation (green, double-dashed line), QD (blue, thin-solid line), EoF (red, dashed line), and concurrence (pink, dotted line).

However, note that the correlations decay more rapidly in the plasmon-assisted case because here the emitters distance is such that the collective rate is switched off, and the nonlocal effects are purely due to the weak d-d interaction V_p. In contrast, for the former case, correlations exhibit a longer lifetime in Fig. 3.4(b) because of the presence of the incoherent interaction γ for the distance $r_{12} = \frac{3}{4}\lambda_0$; this implies that the lifetime of the symmetric correlated state $|\Psi^+\rangle = (|01\rangle + |10\rangle)/\sqrt{2}$ (an eigenstate of the bare Hamiltonian $\hat{H}_S$) is more robust ($\gamma < 0$).

The plasmon-mediated coupled emitters become more interesting because for large distances ($d \sim \lambda_p$), the incoherent decay γ_p can take values close to Γ_p, holding the correlations for longer times. A particular case is shown in figure 3.5(a): $d = \lambda_p$, $\gamma_p = 0.82\Gamma_p$, hence V_p is 'switched off'. The correlations are present even for times of the order of $\Gamma_p t \sim 10$ thanks to the slow decay $\Gamma_p - \gamma_p$ of the antisymmetric (subradiant) state $|\Psi^-\rangle = (|01\rangle - |10\rangle)/\sqrt{2}$. For this time scale, EoF is almost zero, and the correlation that prevails is the QD, which in turn tends to the same value as the total correlations. Furthermore, we expect correlations to be enhanced as the collective effects are stronger, for the emitter-plasmon hybrid system, this is understood to happen when $\tilde{\beta} := \beta e^{-\frac{\lambda_p}{2L}}$ tends to 1 (see Eq. (3.2.3) and Eq. (3.2.4)). For an emitter-emitter separation $d = \lambda_p$, the realistic value $\tilde{\beta} = 0.82$ can be obtained for $L = 2\,\mu$m (this is the largest value that is gotten with an optimistic spontaneous emission factor $\beta \sim 0.94$ according to the known dispersion relation [59]). It is shown in Fig. 3.5(a): for this inter-qubit distance, V_p is switched off and the correlations reach larger values than before and are maintained for a much longer time. We also point out that for the parameter window considered in figure 3.5, classical correlations do not play a major role. Interestingly, the QD does play a role and is more robust than the EoF, during the qubit dissipative evolution (this also happens for the scenario considered in Fig. 3.4).

We remark that is not only the existence of quantum correlations, but the way they relate to each other, what is relevant, since it can lead to operational interpretations (see for instance the analysis in terms of the monogamic relations presented in Chapter 2) [95]. In fact, Fig. 3.5(a) shows that for a time $\tau = 10/\Gamma_p$, the EoF (dashed-red curve) has almost vanished and the QD quickly approximates to the value given by the total correlations. In contrast to this, the concurrence (dotted-pink curve) shows that a larger amount of entanglement is generated for this set of parameters. It is evident that the concurrence approximately equals the total correlations, in clear contrast to what is shown by the EoF,.

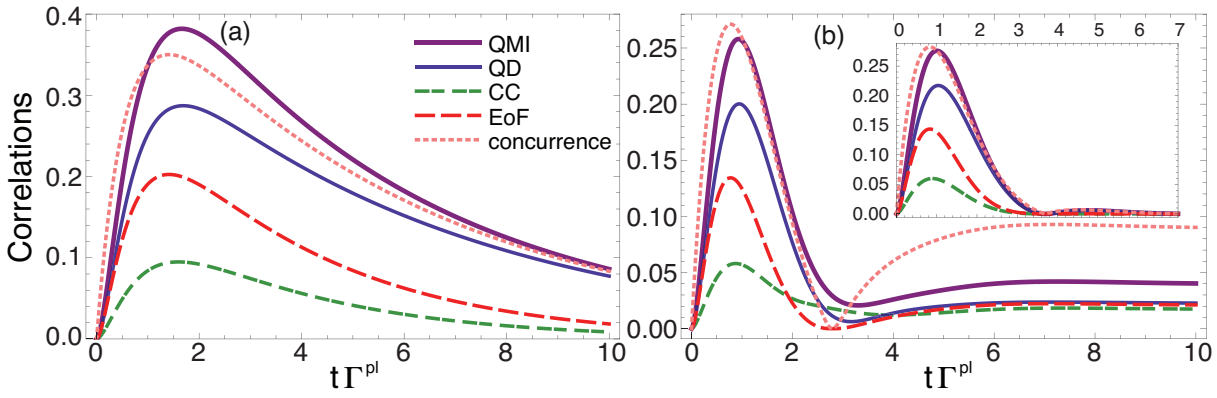

Figure 3.5: Correlations for the emitters interacting with a plasmonic waveguide with the experimentally feasible set of parameters $\beta = 0.94$, $L = 2\mu$m, obtained for an operational wavelength $\lambda_0 = 640$ nm; this gives $\tilde{\beta} \simeq 0.82$, and a plasmonic wavelength $\lambda_p \simeq 542$ nm. (a) Separation between emitters $d = \lambda_p$, $V_p = 0$, (b) $\zeta \equiv d/\lambda_p = 3/4$, $\gamma_p = 0$, and $\ell = 0.2\,\Gamma_p$. The inset corresponds to case (b), but in the absence of laser pumping. The notations for the graphs are as given in figure 3.4.

It is worth noting that this is not an issue concerning to the effects from the plasmon but to the direct monotonic relation of the concurrence with the EoF, (Eq. 1.2.5) [CS2]. Hence, the same behaviour can be also seen in Figure 3.4. More surprisingly, the concurrence reaches higher values than the QMI (solid-purple curve) which is assumed to account for all the correlations (classical and quantum), entanglement included [75, 104] (see Fig. 3.4). Thus, within this framework, concurrence can indicate results that are well above the EoF,, and hence does not allow a direct comparison with other entropic measures such as the QD; in contrast, the latter can be compared, on the same grounds, to the EoF [95].

Furthermore, it is straightforward to show that the density matrix computed at $t = \tau$ (figure 3.5(a)) corresponds to the mixed state $\rho(\tau) = 0.9166|00\rangle\langle 00| + 0.0834|\Psi^-\rangle\langle\Psi^-|$. This state has a very small contribution from the entangled state $|\Psi^-\rangle$, and so it provides a small degree of entanglement. However, the mixture of this with the product state $|0\rangle \otimes |0\rangle$, produces a quantum correlated state with QD, which is different, in its very essence, to entanglement [29, 104].

The qubit correlation dynamics due to the collective effects arising from the emitters coupling to the plasmon modes, V_p and γ_p, become even more interesting when they are pumped with a continuous laser field of amplitude ℓ_i and frequency ω_L (Eq. (1.1.10)). If we consider the laser excitation to be in resonance with the emitters transition frequency $\omega_L = \omega_0$, stationary correlations can be obtained by making the amplitudes $\ell_1 = \ell_2 \equiv \ell$, as shown in figure 3.5(b) for a distance $\zeta = 3/4$, $\gamma_p = 0$. In the same spirit, a higher stationary behaviour of correlations is obtained for $\zeta = 1$, by introducing a relative phase between the laser amplitudes: $\ell_1 = -\ell_2 = \ell$, as shown in figure 3.6(a). The correlations are much larger than those obtained in figure 3.5(b) because the laser excitation assists the very slow decay of the 'naturally created' antisymmetric state $|\Psi^-\rangle$.

For the sake of completeness, in figure 3.6(b) we consider, for a fixed laser amplitude, the role of the initial state preparation on the correlations dynamics. Here, we plot the QD as a function of time, for initial states $\sqrt{\alpha}|01\rangle + \sqrt{1-\alpha}|10\rangle$, $\alpha \in \mathbb{R}$. Although it is clear that, at $t = 0$, the QD takes the value 1 for $\alpha = 1/2$, we have plotted it only for a range up to $\delta^{\leftarrow}_{AB} = 0.3$, in order to appreciate comparatively the correlations behaviour for all α. The trend in correlations is clearly influenced by α but, overall, the states converge to a common stationary value. The QD, CC, and EoF, are plotted for the particular case $\alpha = 1$ in figure 3.6(c), showing how an increment in the laser amplitude may produce a noticeable

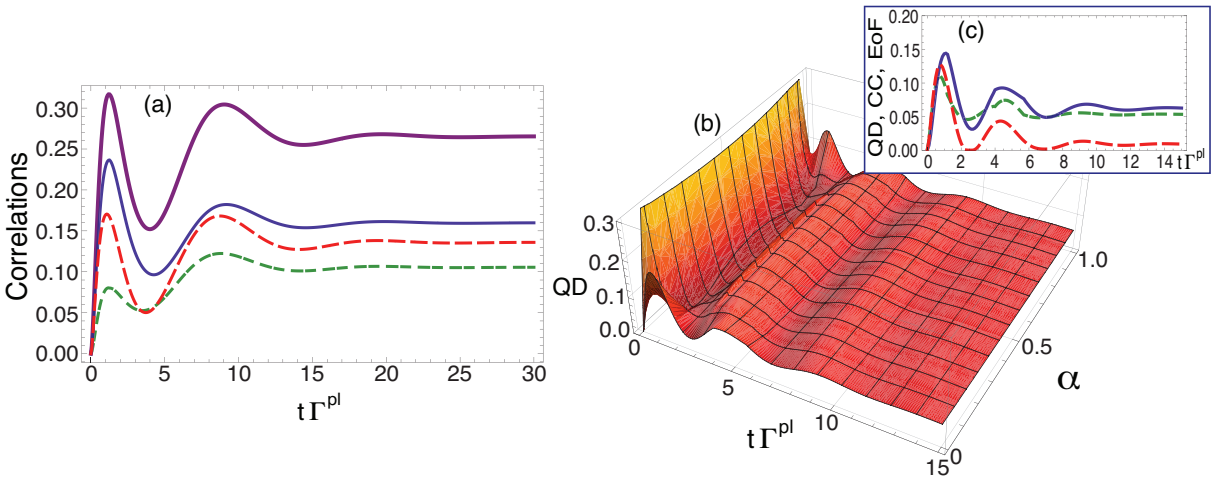

Figure 3.6: Optical control of correlations dynamics. (a) Total spectrum of correlations for laser amplitude $\ell_1 = -\ell_2 = \ell = 0.2\,\Gamma_p$, and initial state $|01\rangle$. (b) QD dynamics for $\ell_1 = -\ell_2 = \ell = 0.4\,\Gamma_p$, and initial state configurations $\sqrt{\alpha}|01\rangle + \sqrt{1-\alpha}|10\rangle$. (c) Comparison between QD, CC, and EoF, for $\alpha = 1$. In all graphs, $\zeta = 1$, $V_p = 0$, $\beta = 0.94$, and $L = 2\mu$m.

difference between the QD and the EoF.

3.3.1 Discussion

We have shown that rather than entanglement, QD is the most robust correlation during the dissipative dynamics, and, depending on the separation between emitters, the qubit-plasmon modes coupling can enhance the degree of correlations via the collective parameter γ_p. Furthermore, pumping with a continuous laser field can be used as an additional means to dynamically control the relationship between entanglement and other quantum correlations present in the register. Such a fact could be used as an important resource in the realisation of non-conventional quantum protocols [12, 13, 72].

Bearing in mind that quantum correlations, as measured by the QD, give the amount of information that is not locally accessible, our results show that most of the information stored in the emitters is purely quantum (compare the thin-solid blue with the doubly-dashed green lines in all the figures). Also, we note that, in most cases, this type of information does not arise from entanglement, which is kept to a minimum, as can be seen in figures 3.4(b), 3.5(a), and 3.6(c). This said, a possible optical control of the amount and class of induced quantum correlations can be carried out with external laser pumping, as depicted in Fig. 3.6.

The relation between the correlations and the physical properties of the hybrid system analysed here is clearly showed in Figs. 3.4-3.6: the lifetime of the correlations is enhanced thanks to the illumination with the coherent laser field; also, a large β-factor (due to the plasmon channel) increases the degree of correlations, especially that of the QD. It is evident from figure 3.6 that an adequate manipulation of the light-matter interaction strength allows control of the dynamics followed by the QD and the EoF. This degree of quantum control is possible due to the interplay between the laser illumination intensity and the coherent emitter-emitter interaction [46, CS1, CS2].

The crucial feature of the dynamics studied here is the large separation between emitters (of the order of or greater than the plasmons wavelength), which could lead to long-distance quantum control and communication: the correlations are purely generated via the emitter-plasmon interaction, which in

turn is reflected in the functional dependence of the collective parameters given by equations (3.2.3) and (3.2.4). An interesting by-product is the feasibility of tailoring the phase difference that exists between the collective parameters, which might allow the switching on/off of the emitters correlations. Here, a parameter configuration where either V_p or γ_p goes to zero, an appropriate choice of initial conditions and laser tailoring, enables the enhancement or suppression of the existing correlations as will be shown in the following section.

3.4 Quantum control and switching of correlations

As shown in section 3.3, we can control the correlations dynamics by tailoring the collective effects and the light-matter interaction properties. It is also clear that the initial state configuration of the pair of qubits plays an important role in this sort of control. In this section, we show how to use the versatility of these parameters to produce a dynamically-controlled mechanism on correlations. For doing so, we ponder a particular set of initial states for qubits. We show that our mechanism works for both resonant and detuned emitters.

A general two-qubit state can be written as $\epsilon = \frac{1}{4}\big(\mathbb{1}_{4\times4} + \vec{a}\vec{\sigma}\otimes\mathbb{1}_{2\times2} + \mathbb{1}_{2\times2}\otimes\vec{b}\vec{\sigma} + \sum_{i=1}^{3} h_i\sigma_i\otimes\sigma_i\big)$, where $\vec{a} = (a_1, a_2, a_3), \vec{b} = (b_1, b_2, b_3) \in \mathbb{R}^3$, and $h_i \in \mathbb{R}$ [105, 106]. The initial density matrix used in our forward calculations adopts an X-like structure with $\vec{a} = (0, 0, a_3), \vec{b} = (0, 0, b_3)$, and $h_1 = h_2 = \eta$:

$$\rho_{AB}(0) \;=\; \begin{pmatrix} \frac{1+c_+ +h_3}{4} & 0 & 0 & 0 \\ 0 & \frac{1+c_- -h_3}{4} & \frac{\eta}{2} & 0 \\ 0 & \frac{\eta}{2} & \frac{1-c_- -h_3}{4} & 0 \\ 0 & 0 & 0 & \frac{1-c_+ +h_3}{4} \end{pmatrix},$$

where $c_\pm = a_3 \pm b_3$, and a_3, b_3, η, and h_3 are chosen such that $\rho_{AB}(0)$ is a well-defined density matrix [105].

3.4.1 Resonant molecules without laser pumping

For the above initial state, and identical emitters with transition frequencies $\omega_1 = \omega_2 \equiv \omega_0$, Eq. (1.1.5) admits an analytical solution in the absence of optical driving. The non-trivial density matrix elements read $a(t) \equiv \rho_{00,00} = 1 - b_+(t) - b_-(t) - f(t)$, where $f(t) \equiv \rho_{44} = \frac{1}{4}pe^{-2\Gamma_p t}$, with $p = 1 + h_3 - c_+$, and

$$\begin{aligned} b_\pm(t) \equiv \left\{ \begin{array}{c} \rho^{+}_{01,01} \\ \rho^{-}_{10,10} \end{array} \right\} &= \frac{e^{-\Gamma_p t}}{4(\Gamma_p^2 - \gamma_p^2)}\Big[-p(\Gamma_p^2 + \gamma_p^2)e^{-\Gamma_p t} - \big(c_+(\Gamma_p^2 + \gamma_p^2) - 2\left(\Gamma_p^2 + h_3\gamma_p^2\right)\big)\cosh(\gamma_p t) \\ &-2\left(p\gamma_p\Gamma_p + \eta(\Gamma_p^2 - \gamma_p^2)\right)\sinh(\gamma_p t) \pm c_-(\Gamma_p^2 - \gamma_p^2)\cos(2Vt)\Big]; \\ z(t) \equiv \rho_{01,10} &= \frac{e^{-\Gamma_p t}}{4(\Gamma_p^2 - \gamma_p^2)}\Big[-2p\gamma_p\Gamma_p e^{-\Gamma_p t} + 2\left(\eta(\Gamma_p^2 - \gamma_p^2) + p\gamma_p\Gamma_p\right)\cosh(\gamma_p t) \\ &+ \big(c_+(\Gamma_p^2 + \gamma_p^2) - 2\left(\Gamma_p^2 + h_3\gamma_p^2\right)\big)\sinh(\gamma_p t) + \mathrm{i}c_-(\Gamma_p^2 - \gamma_p^2)\sin(2Vt)\Big], \end{aligned} \tag{3.4.1}$$

and $z^*(t) \equiv \rho_{10,01}$. Importantly, the initial states $\rho(0)$ contain the eigenstates of the system's Hamiltonian ($\hat{H}_S + \hat{H}_{d-d}$): $|00\rangle$, $|\Psi^\pm\rangle = \frac{1}{\sqrt{2}}(|01\rangle \pm |10\rangle)$, $|11\rangle$, which allows for their experimental generation, control, and read-out [45, 36].

From Eq. (3.4.1) we see that for $c_- = 0$ the density matrix becomes independent of the dipolar interaction V_p ($b_+ = b_- = b$) and, as such, the quantum correlation dynamics is only due to the collective damping γ_p. Such correlations persist for long times and for a large emitters' separation ($d = \lambda_p; \zeta = 1$), as shown in Fig. 3.7. For the plasmon waveguide we used realistic parameters $L = 2\,\mu$m, $\beta = 0.94$, and $\lambda_p \approx 542$ nm, that follows from the dispersion relation reported in Ref. [59], based on an operational wavelength $\lambda_0 = 640$ nm. These parameters can be achieved with e.g. plasmonic wedges (Λ) and V-groove waveguides, as mentioned in section 3.3. Although we have chosen $\zeta = 1$, which makes $V_p = 0$, our results are more general and can be extrapolated to other ζ-values because the considered initial states evolve completely independently of V_p.

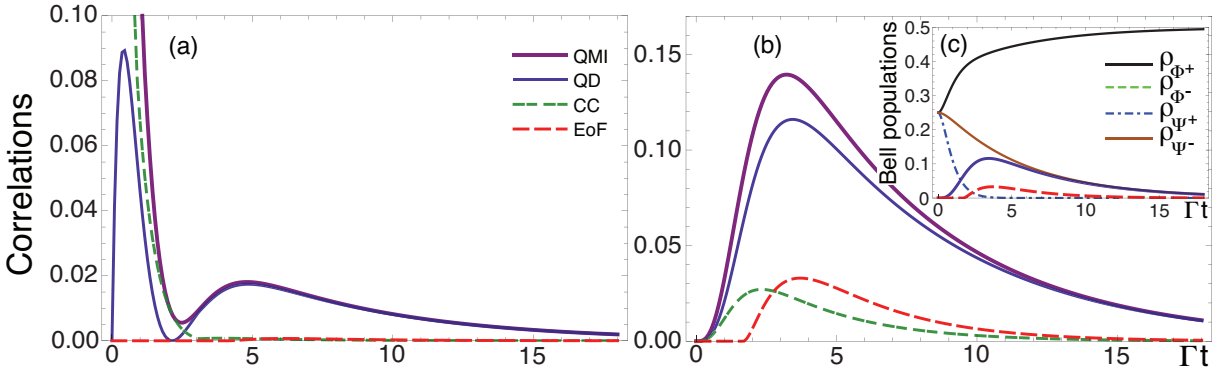

Figure 3.7: Dynamics of correlations for initial states (a) $\rho_{\mathcal{C}}$, and (b) ρ_{MM}. We employ optimal plasmonic waveguide parameters [59]: $L = 2\,\mu$m, $\beta = 0.94$, $\lambda_p = 542$ nm (operational wavelength $\lambda_0 = 640$ nm). The emitters are separated a distance $d = \lambda_p$ ($\zeta = 1$). (c) Bell states populations for the case (b).

Figure 3.7(a) shows the correlations dynamics for the classically correlated initial state $\rho_{\mathcal{C}} = \frac{1}{2}|00\rangle\langle 00| + \frac{1}{2}|11\rangle\langle 11|$ for which $\mathcal{J}^{\leftarrow}_{AB} = \mathcal{I}_{AB} = 1$. Further, in Fig. 3.7(b) we show how the correlations are increased for a completely uncorrelated initial state $\rho_{MM} = \mathrm{diag}\{\frac{1}{4}, \frac{1}{4}, \frac{1}{4}, \frac{1}{4}\}$. Note that while the QD increases from $t = 0$, the emitters follow entanglement sudden birth [38] for $t \sim 4/\Gamma_p$ (Fig. 3.7(a)), and $t \sim 2/\Gamma_p$ (Fig. 3.7(b)). For $t > 10/\Gamma_p$ Fig. 3.7(a) shows that the system becomes disentangled, QD, however, equals $\mathcal{I}_{AB}$ and the nonclassical correlation represents the total correlation in the dimer (i.e., $\mathcal{J}^{\leftarrow}_{AB} = 0$). Figure 3.7(c) plots the population dynamics of the Bell basis states $\rho_{\Psi^\pm} \equiv |\Psi^\pm\rangle\langle\Psi^\pm|$ and $\rho_{\Phi^\pm}$, $|\Phi^\pm\rangle = \frac{1}{\sqrt{2}}(|00\rangle \pm |11\rangle)$, as well as the time evolution of the QD and the EoF for $\rho(0) = \frac{1}{4}(\rho_{\Psi^+} + \rho_{\Psi^-} + \rho_{\Phi^+} + \rho_{\Phi^-})$ (Fig. 3.7(b)): although the EoF eventually vanishes, the dynamics of $\delta^{\leftarrow}_{AB}$ quickly approaches that of the antisymmetric Bell state ρ_{Ψ^-}, which decays at the slowest rate $\Gamma_p - \gamma_p$; this is due to the natural mixture of the Bell populations which spontaneously create quantum correlations beyond entanglement, here captured by the QD. Figure 3.7 thus shows that, for suitable (unentangled) initialisation of the emitters, QD is the most robust and persistent nonclassical correlation available.

Although Lindblad conjectured that, for any quantum state, $\mathcal{J}^{\leftarrow}_{AB}(\rho) \geq \delta^{\leftarrow}_{AB}(\rho)$ [76, 30, 107], we give an entropy condition for which the quantum correlation is always greater than the classical one [108, CS2]: since $\mathcal{I}_{AB} = \delta^{\leftarrow}_{AB} + \mathcal{J}^{\leftarrow}_{AB}$, we ask if the inequality $\mathcal{I}_{AB} - 2\,\mathcal{J}^{\leftarrow}_{AB} \geq 0$ is ever met. The sought entropy bound reads

$$2\mathcal{S}(\rho_{A|\Pi^B_j}) - S(\rho_{AB}) + S(\rho_B) - S(\rho_A) \geq 0\,, \tag{3.4.2}$$

where $\mathcal{S}(\rho_{A|\Pi_j^B}) = \min_{\{\Pi_j^B\}}\{\sum_j p_j S(\rho_{A|\Pi_j^B})\}$, is the optimised entropy associated to the density matrix of subsystem A after the measure (see the definition of CC in Eq. (1.2.13)). Equation (3.4.2) is indeed satisfied, at all times, for suitable resonant emitters.

An important point to note is that for the initial state ρ_{MM} ($c_- = 0$) the quantum correlation is *always* greater than the classical correlation. Under these initial conditions the inequality given by Eq. (3.4.2) is satisfied; they have an associated conditional entropy $\mathcal{S}(\rho_{A|\Pi_j^B}) = \min(S^{(1)}, S^{(2)})$, with

$$
\begin{aligned}
S^{(1)} &= -a\log_2\frac{a}{a+b} - b\log_2\frac{b}{a+b} - b\log_2\frac{b}{b+f} - f\log_2\frac{f}{b+f};\\
S^{(2)} &= -\frac{1}{2}(1-\xi)\log_2\frac{1}{2}(1-\xi) - \frac{1}{2}(1+\xi)\log_2\frac{1}{2}(1+\xi),
\end{aligned}
\tag{3.4.3}
$$

where the marginals $S(\rho_A) = S(\rho_B)$, $\xi^2 = (a-f)^2 + |z|^2$, with a, b and f time-dependent functions coming out from Eq (3.4.1), and we arrive at $2\mathcal{S}(\rho_{A|\Pi_j^B}) - S(\rho_{AB}) \geq 0$. A direct calculation of $S^{(1)}$ and $S^{(2)}$ then demonstrates that the quantum correlation is greater than the classical one, as can be seen in Fig. 3.8(a), where we have plotted the entropy bound (Eq. (3.4.2)). This behaviour has also been shown for other emitters's preparations in section 3.3 (see for instance Fig. 3.6), and for suitable configurations of the sort of system studied in Chapter 2 [CS2].

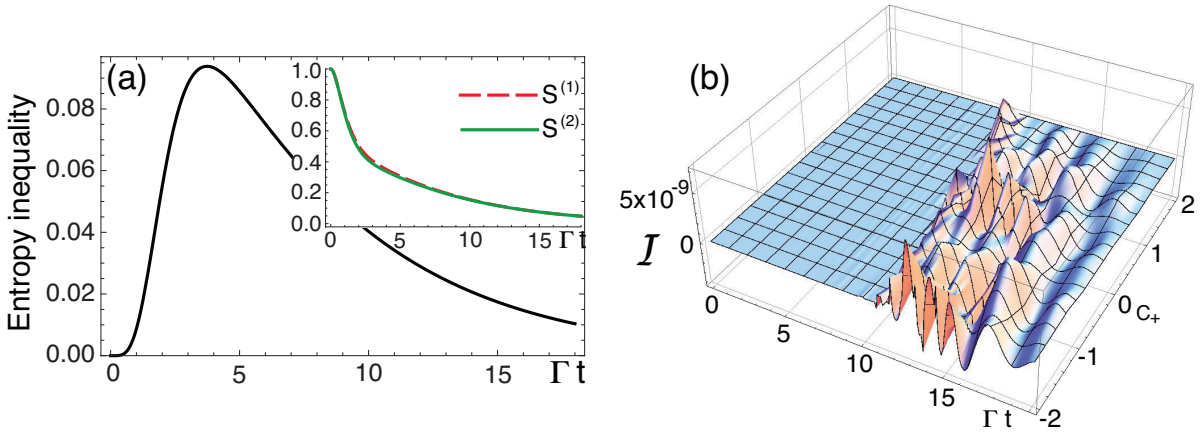

Figure 3.8: (a) Left-hand side of inequality Eq. (3.4.2), for the case shown in Fig. 3.7(b). The inset shows the evolution of the quantities $S^{(1)}$ (dashed red curve) and $S^{(2)}$ (solid green curve), whose minima give the conditional entropy. (b) Numerical simulation of the QMI for the set of initial states $\Xi := \{c_- = 0, \eta = 0, h_3 = c_+^2/4\}$ in Eq. (3.4.1). The same result is obtained for the other correlations.

If we now choose the emitters' mutual separation such that $\zeta_n = \frac{1}{4}(2n+1)$, n integer, the damping γ_p vanishes according to Eq. (3.2.4). As the emitters' dynamics is independent of V_p, the density matrix elements read

$$
\begin{aligned}
&a(x) = 1 + \frac{1}{4}x\left[px + 4\left(\frac{c_+}{2} - 1\right)\right];\quad b_\pm(x) = \frac{1}{4}x\left[2\left(1 - \frac{c_+}{2}\right) - px\right];\\
&f(x) = \frac{1}{4}px^2;\quad z(x) = \frac{1}{2}\eta x,
\end{aligned}
\tag{3.4.4}
$$

where $x \equiv e^{-\Gamma_p t}$. For this family of initial states (which includes the eigenstates of $\hat{H}_{\text{eff}}$ in absence of the coherent external laser), the dynamics of all correlations has an asymptotic decay following the

time parameter x, in contrast to the scenario shown in Fig. 3.7 for which γ_p is non-zero. If we add the conditions $\eta = 0$ and $h_3 = c_+^2/4$, the density matrix adopts a diagonal structure without quantum correlations. This also allows us to show that $\rho_{AB} = \rho_A \otimes \rho_B$, and hence $\mathcal{J}_{AB}^{\leftarrow} = 0$. Since $\mathcal{I}_{AB}(\rho_{AB})$ gives the relative entropy between the matrices ρ_{AB} and $\rho_A \otimes \rho_B$, it can also be seen that $\mathcal{I}_{AB}(\rho_{AB}) = 0$, and hence there are neither quantum nor classical correlations for this time evolution. Figure 3.8(b) shows the numerical simulation for the QMI as a function of the parameter c_+ (the fluctuations around $\sim 10^{-9}$ are due to numerical errors and do not imply $\mathcal{I}_{AB} \neq 0$). Thus the system evolves through a path of product states even though $V_p \neq 0$. This provides a useful method for controlling the dynamics of correlations in two-qubit systems.

3.4.2 Resonant molecules under laser pumping

Illumination with a laser field, in conjunction with the emitter-plasmon coupling, allows a reestablishment of the correlations, which were lost due to the V_p-independence of the matrix elements. This is included throughout the light-emitter interaction given by the Hamiltonian $\hat{H}_L$ as in Eq. (1.1.10).

To illustrate this mechanism, we consider two individual molecules initially in their ground states, with resonance wavelength λ_0 in order to reach the optimal waveguide parameters of Fig. 3.7. We now, however, consider a shorter emitters' separation: $\zeta_1 = 3/4$, such that $\gamma_p = 0$. Figure 3.9 depicts the evolution of the QD (graph (a)) and the EoF (graph (b)) as functions of time (in $1/\Gamma_p$ units), and laser intensity, under the choice $\ell_1 \equiv \ell \gg \ell_2$. As an illustration, we fix $\ell_2 = 0$ and $\ell \in [0.4\Gamma_p, 3.6\Gamma_p]$ such that the effect of the coherent light over the emitter 1 is much stronger than that over emitter 2 (the latter being negligible). This particular choice is meant to highlight our main results and does not imply any restriction on the validity of the mechanism here presented or loss of generality for other choices of laser intensity.

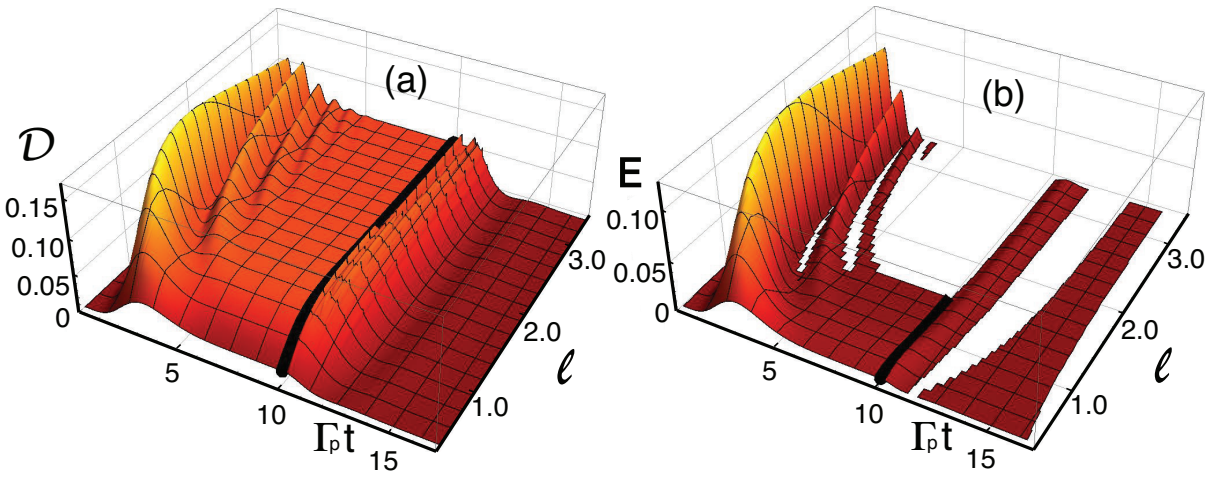

Figure 3.9: (a) QD and (b) EoF as functions of the laser field amplitude ℓ, for resonant qubits $\omega_L = \omega_0$, and initial (ground) state $|00\rangle$. Waveguide parameters are as in Fig. 3.7; $d = 3\lambda_p/4$, so $\gamma_p = 0$. The black solid curve indicates the time at which the laser is turned off.

By turning on the laser field (at $t = 0$) to illuminate emitter 1 with an intensity ℓ, we reach a time regime for which the correlations dynamics stabilises ($\delta_{AB}^{\leftarrow} \sim 0.06$), as conservatively indicated by the thick black curve in Fig. 3.9 at $\Gamma_p t \sim 10$. If we then turn off the laser field at $\Gamma_p t = 10$, the emitters decay again to the ground state well before $\Gamma_p t \sim 15$. The conditional dynamics between the laser field

and the dipolar interaction favours such a behaviour. We point out that if, in the same scenario, the d-d interaction were zero (non-interacting qubits or emitters in vacuum with interqubit separation $d = 3\lambda/4$), the correlations would then equal zero even if the laser were turned on (not shown). We have also checked that the scheme works for other input states which satisfy the initial condition $\Xi := \{c_- = 0, \eta = 0, h_3 = c_+^2/4\}$ (Fig. 3.8(b)). This emphasises the relevance of the plasmon-mediated interaction between the emitters, because this scheme lets us switch on/off the collective parameters V_p (Eq. (3.2.3)) and γ_p (Eq. (3.2.4)).

Figure 3.9 also demonstrates that the QD becomes the 'most relevant' correlation at high laser intensity: The EoF rapidly decays at high intensities and, at about $\ell \sim 1.5\,\Gamma_p$ (see the 'white zone' in graph (b)) the emitters have already experienced collapses, revivals, and early stage disentanglement [38]. In contrast, the QD reaches nonzero stationary values (Fig. 3.9(a)), indicating the presence of nonclassical correlations different to entanglement.

3.4.3 Detuned molecules

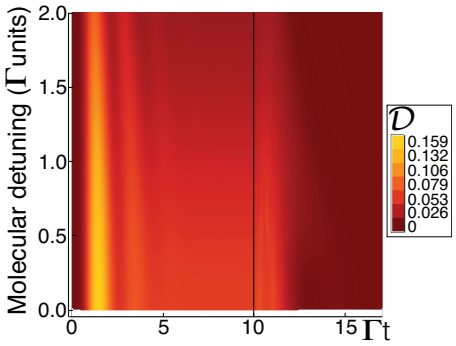

Figure 3.10: Density plot of the switching mechanism for the QD as function of time and molecular detuning Δ_- under laser pumping with amplitude $\ell = 1.5\Gamma_p$, and laser frequency detuning $\Delta = \omega_L - \omega_0$. Initial state and waveguide parameters are as in Fig. 3.9. The black vertical line indicates the time at which the laser is turned off.

As yet, we have assumed identical emitters to show the mechanism for switching correlations. We notice, however, that this quantum control also works in a more general physical setup of two molecules with different transition frequencies, $\omega_1 \neq \omega_2$, i.e. with a frequency detuning $\Delta_- = \omega_1 - \omega_2$. In fact, this situation is encountered in any experiment on molecular systems [45, 34].

In this case, the eigenstates of the emitters Hamiltonian are: $|00\rangle$, $|11\rangle$, and two new entangled states $|\phi^+\rangle = \alpha_1|01\rangle + \alpha_2|10\rangle$, and $|\phi^-\rangle = \alpha_2|01\rangle - \alpha_1|10\rangle$, with $\alpha_1 = \sqrt{V^2/(\kappa^2+V^2)}$, $\alpha_2 = \sqrt{\kappa^2/(\kappa^2+V^2)}$, and $\kappa = \Delta_-/2 + \sqrt{V^2+(\Delta_-/2)^2}$. The new transition frequencies of these eigenstates are, respectively: $\omega_\pm = \omega_0 \pm \sqrt{V^2+(\Delta_-/2)^2} = \omega_0 \pm \Delta^*$. The inclusion of a molecular detuning does not allow for a general analytical solution of the master equation (1.1.5). If we assume, however, that the emitters have interqubit separation ζ_n, and are initialised by $c_- = 0$, in the absence of laser excitation we obtain

$$z(t) = 2\eta \frac{\exp^{-\Gamma t}}{16(\Delta^*)^2}\left[4V^2 + \Delta_-^2\cos\left(2\Delta^* t\right) + 2\mathrm{i}\Delta_-\Delta^*\sin\left(2\Delta^* t\right)\right]; \tag{3.4.5}$$

$$b_\pm(t) = \frac{\exp^{-\Gamma t}}{16(\Delta^*)^2}\Big[\left((2-c_+) - pe^{-\Gamma_p t}\right)\left(4V^2+\Delta_-^2\right) \pm\ 4\eta\left(\cos\left(2\Delta^* t\right)-1\right)\Delta_- V\Big],$$

where $a(t)$ and $f(t)$ are given as in Eq. (3.4.1). In contrast to the previous case of identical molecules, this evolution is not independent of V_p so the correlations may exhibit oscillatory behavior due to the terms in $z(t)$. As we are interested in a rapid switching of correlations, we apply the complete configuration Ξ to the initial condition such that the matrix element $z(t)$ goes to zero, and the factor $(\Delta^*)^2$ simplifies in $b_\pm(t)$. The reduction of Eq. (3.4.6) shows that, under the parameters choice $\{\Xi, \zeta_n\}$, the same result as for identical, resonant molecules is recovered: all correlations remain zero.

To understand the influence of the molecular energy mismatch under laser pumping, we plot the QD in terms of Δ_- in Fig. 3.10. We illuminate emitter 1 with a laser intensity $\ell = 1.5\Gamma_p$, and take into account the eigenenergies of the intermediate states to introduce the laser detuning $\Delta := \omega_L - \omega_0 = \Delta^*$. This choice makes the dynamical action of the two entangled eigenstates effective, so both the QD and the EoF can be enhanced. The value reached by the QD slightly decreases as the molecular detuning increases from 0 to $2.0\,\Gamma_p$, because the emitters start to be uncoupled from each other for $\Delta_- \gg V$.

The plasmon-assisted dipolar interaction V_p, for e.g. $\zeta_1 = 3/4$, in combination with an applied laser field, would then allow the realisation of conditional quantum dynamics. As we have demonstrated, this works for molecules separated by distances of at least 0.4 μm.

3.4.4 Discussion

Recent experiments have demonstrated the control of light-matter interaction by means of plasmonic resonators [109] and silver nanowires [110] to enable the enhancement of the Purcell effect in quantum emitters, and the strength of the coupling to the plasmonic modes of such nanostructures. This offers the possibility of testing the results here reported with state-of-the-art technology. Furthermore, another experimental demonstration of communication between two distant single emitters (organic molecules) via single photons has been recently reported [111]. Thus, the setup proposed in this work has also the potential for demonstrating an additional degree of quantum control in which sensitive quantum information encoded in single photons can be transmitted and processed between coupled (but largely separated) single emitters.

We stress that our approach can be tested in the laboratory with present day technology. The plasmonic structure is modelled with parameters that can be achieved with e.g. either Λ or V-groove channel waveguides [97]. Although we note that our calculations are based on ideal plasmonic structures, the basic phenomena that we have theoretically predicted should still be observable in an experiment using real structures. Perylene dyes are suitable single emitters because they are highly photostable, very bright and well characterised at the single-molecule level [34]. The deterministic placement of single emitters on plasmonic structures [55] can be achieved by lithographic methods or chemical surface functionalisation. For the initialisation and coherent control of this plasmon-coupled dimer system, (high resolution) laser addressing combined with time-correlated single-photon counting techniques are readily available [45, 36, 34]. These allow the quantification of the molecules' dipolar coupling strength, the decay rates, and photon emission required in the generation of the quantum states and the correlations here described.

It is worth pointing out that for other waveguide geometries, β-factor can reach values well below those used here. For example, for a cylindrical waveguide the highest predicted β-factor is ~ 0.6 [59, 56].

In such a case, the parameter window for which both the dimer to waveguide surface distance, and the emitter-emitter separation fall within the plasmonic approximation Eq. (3.2.3) and Eq. (3.2.4) becomes limited, and the losses into the metal, as well as the radiation into vacuum play more significant roles and hence an evaluation of the full Green's tensor is required. This said, the main effect on the results here reported would be a reduction in the degree of quantum correlations in the dimer system, and the protocol for long-distance quantum control here described would continue working.

Chapter 4
Local correlations as a resource for a quantum information protocol

So far we have considered scenarios where quantum entanglement and correlations such as quantum discord act as resources for quantum protocols. In Chapter 2 we explored how to generate entanglement in dimer and trimer molecular systems, and in Chapter 3 we discussed a protocol for switching those quantum correlations. In this Chapter we test these properties from a different viewpoint, within a particular protocol of game theory, the so-called Prisoners' Dilemma (PD) game.

The above-mentioned quantum features have been considered in game theory, e.g., in the increase of efficiency and payoffs, emergence of new equilibria, and novel game strategies which are simply not possible in the classical domain [112, 113]. These achievements signalled an interest about the nature of such a quantum advantage, and introduced questions related to the internal properties of physical systems and the mathematical structure that underlies the novel game strategies [62, 31, 63, 64, 113]. Advantages of different kind became evident when quantisation rules were applied to different sort of games, and most of these scenarios pointed out quantum entanglement as a precursor of such effects [60, 61, 112]. Furthermore, Bell nonlocality has been recently shown to provide an advantage when deciding conflicting interest games [62, 31, 63]. In this regard, and mostly inspired by strategies of this sort, the activation of quantum nonlocality has been put forward [31]. In particular, k-copy nonlocality or superactivation [32, 33], and activation of nonlocality through tensoring and local filtering [115], although seminal for protocols based on nonlocality (e.g., quantum cryptography), are ultimately limited by the presence of entanglement [31]. This said, here we explore other kind of correlations that highlight local states as a possible resource for introducing a quantum advantage (see Fig. 4.1, shaded region). In particular, we ask whether there is, beyond entanglement or nonlocality, another underlying fundamental quantum feature that warrants the emergence of the above-mentioned advantages. This consideration is also motivated by a recent experimental demonstration of a *zero-sum* game that exhibits a quantum gain for players that do not share entanglement [114].

4.1 Prisoners' Dilemma

The Prisoners' Dilemma game is a celebrated bipartite non-zero sum game in classical game theory [65, 66] whereby two parties, say Alice (A) and Bob (B), have to decide between two strategies in an independent way: to defect (D) or cooperate (C). The retribution to the players decision is conditioned to the pair of choices, as shown in TABLE 4.1. The classical PD game reveals the existence of a set of strategies from which unilateral movement of the players diminishes their payoff—a Nash equilibrium (NE)— and a set of strategies whereby the players simultaneously do best—a Pareto optimal [65]. The

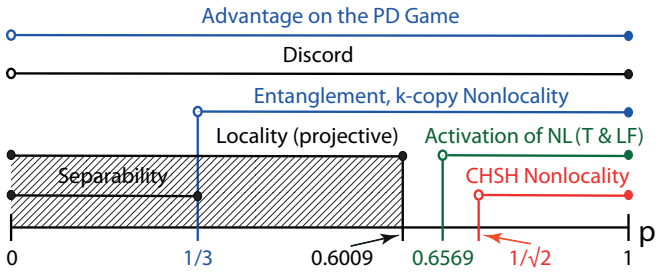

Figure 4.1: The schematics highlights locality, entanglement, CHSH-nonlocality, k-copy nonlocality, activation of nonlocality through tensoring and local filtering, and discord, for the Werner-like states $\rho_{W\text{-}l}(p) = p|\psi\rangle\langle\psi| + \frac{(1-p)}{4}\mathbb{1}\otimes\mathbb{1}$, $|\psi\rangle = \frac{1}{\sqrt{2}}(|00\rangle + i\,|11\rangle)$, $0 \leq p \leq 1$. These states can lead to a PD game advantage in the whole p-region. See Appendix B for definitions.

dilemma arises due to the choice problem between the equilibrium and the optimal gain. This non-zero sum game has been extended to the quantum domain by Eisert *et al.* [61], who proposed the use of initial maximally entangled states and unitary operators to define a strategy of purely quantum character that removes the decision dilemma [61]. Thus, the interaction between players can be cast in a quantum circuit that generates, via the action of a two-qubit operator $\hat{\mathcal{J}}(\delta)$, an initial state of the form:

$$|\psi_{in}(\delta)\rangle = \cos\frac{\delta}{2}|00\rangle + i\sin\frac{\delta}{2}|11\rangle, \tag{4.1.1}$$

where $\delta \in [0, \pi/2]$. Here, the possible outcomes of the classical strategies *C* and *D* are assigned to the computational basis states $|0\rangle$ and $|1\rangle$, respectively, and the strategy space of each player has a Hilbert space structure that couples through a tensor product.

Alice\Bob	C	D
C	(3,3)	(0,5)
D	(5,0)	(1,1)

Table 4.1: Payoff matrix for the PD game. The first (second) entry in the parenthesis denotes Alice's (Bob's) payoff. In the classical game, the strategy (*C*,*C*) defines a Pareto optimal (joint maximum gain), and (*D*,*D*) a Nash equilibrium.

In Fig. 4.2(a), the operator $\hat{\mathcal{J}}(\gamma) = \exp\{i\gamma\hat{D}\otimes\hat{D}/2\}$ generates input entangled states [61]. We introduce the operator $\hat{\tilde{\mathcal{J}}}(\delta)$, such that $\hat{\tilde{\mathcal{J}}} = \hat{\mathcal{J}}^{\dagger}$, as sketched in Fig. 4.2(b). After that, the players execute, unilaterally, their movements acting with the unitary parameterised operator ($i = A, B$),

$$\hat{U}_i(\theta_i, \phi_i) = \begin{pmatrix} e^{i\phi_i}\cos\frac{\theta_i}{2} & \sin\frac{\theta_i}{2} \\ -\sin\frac{\theta_i}{2} & e^{-i\phi_i}\cos\frac{\theta_i}{2} \end{pmatrix}, \tag{4.1.2}$$

particularly, $\hat{C} = \hat{U}(0,0)$ and $\hat{D} = \hat{U}(\pi,0)$ reduce to the classical strategies. Finally, an operator that destroys the entanglement generated by $\hat{\mathcal{J}}(\delta)$ is applied before projecting the output state onto the usual 4-dimensional space basis, giving rise to a probability distribution above the four possible classical states, from which the expected payoff for each player is determined.

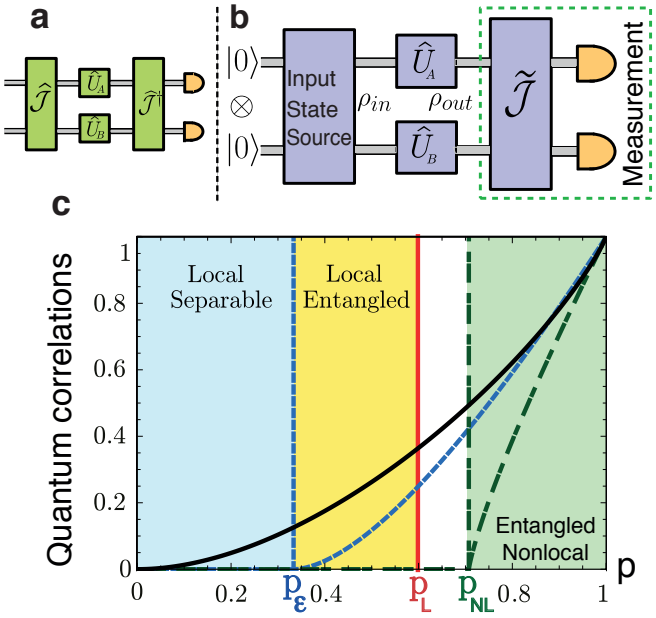

Figure 4.2: Quantum Prisoners' Dilemma setup and classification of input correlations. (a) Eisert *et al.* two players game protocol [61], (b) our setup uses a source of input $\rho_{in} \equiv \rho_{in}(p,\delta)$ (e.g., Werner-like) states, one qubit gates to represent the players' moves, and the measuring process (dashed rectangle). The measurement is taken as the projection onto the basis generated by $\tilde{\mathcal{J}} \equiv \tilde{\mathcal{J}}(\delta)$ in the usual 4-dimensional basis, (c) quantum correlations of input $\rho_{W\text{-}l}(p)$ states: QD (solid-black), EoF (dashed-blue), and CHSH-nonlocality (doubly-dashed green).

In this Chapter, we analyse the PD game and demonstrate that *local*, and even further, *separable* quantum input states suffice to achieve an advantage over any classical strategy. This result is in contrast with previous approaches to quantum games that consider entanglement or Bell nonlocality as required resources for achieving a quantum advantage [60, 61, 62, 31]. The only quantum correlation exhibited for those input states is caught by the QD. However, we also find other input states discord-correlated that do not present any advantage in the PD game, so we show that there exist (non-zero discord) input states for which the discord does not play any role at reaching this advantage. These results have been reported in [CS6].

4.2 Local quantum correlations as a resource in the PD game

In contrast to the use of entangled states as a strategy for 'quantising' the PD game (Fig. 4.2(a)) [61], we explore a different feature and use the following input states (Fig. 4.2(b)) as the feeding resource for performing the quantum PD game:

$$\rho_{in}(p,\delta) = \frac{(1-p)}{4}\mathbb{1} + p|\psi_{in}(\delta)\rangle\langle\psi_{in}(\delta)|, \tag{4.2.1}$$

where $\mathbb{1}$ is the 4×4 identity matrix, and $p \in [0,1]$ acts as a control of the statistical mixture $\rho_{in}(p,\delta)$, and allows a direct comparison with the protocol of Fig. 4.2(a) [61]. In Fig. 4.2(b), the measurement

process is made in a basis controlled by the same δ parameter, which allows the control of the degree of correlations that is 'destroyed' in the final step of the protocol, just before the projection onto the usual basis; i.e., the quantum operator $\tilde{\mathcal{J}} \equiv \tilde{\mathcal{J}}(\delta)$ inside the dashed rectangle of Fig. 4.2(b) is defined in the same way as the entangling operator of Fig. 4.2(a) [61].

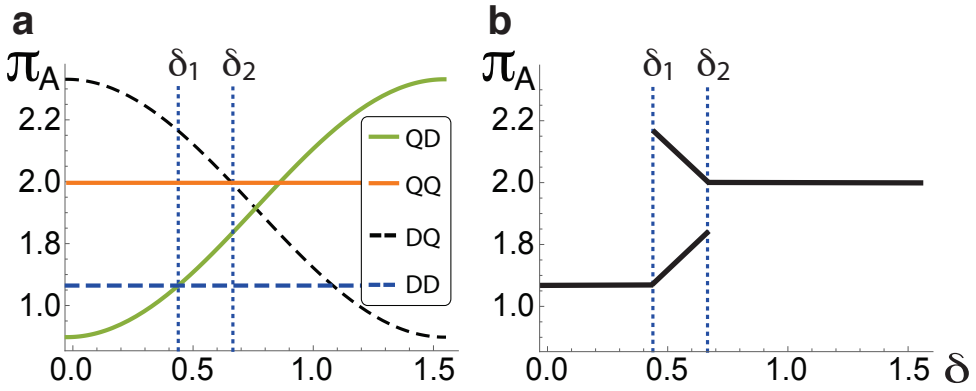

Figure 4.3: Payoffs for general states $\rho_{in}(p,\delta)$: (a) the control of the initial state correlations, and $\tilde{\mathcal{J}}(\delta)$ imply thresholds at $\delta_1 = \sin^{-1}\sqrt{1/5}$, and $\delta_2 = \sin^{-1}\sqrt{2/5}$, (b) strategies reaching the Nash equilibrium in the regions defined by δ_1 and δ_2.

Every separable (non-entangled) state is local. However, there exist entangled states which are also local. For general two-qubit states of the form $\rho := p\rho' + \frac{(1-p)}{4}\mathbb{1}$, $0 \leq p \leq 1$, being ρ' an arbitrary two-qubit state, a projective-locality bound has been reported [116]. In our protocol, we identify $\rho' = |\psi_{in}(\delta)\rangle\langle\psi_{in}(\delta)|$ such that $\rho \equiv \rho_{in}(p,\delta)$, and hence the locality bound reads $p_L \approx 0.6009$; i.e., entangled states with $p \leq p_L$ are local (see for instance the yellow region in Fig. 4.2(c)).

To explore how our input states $\rho_{in}(p,\delta)$ (4.2.1) induce an advantage over any classical strategy in the PD game, we compute the required inequalities to obtain the Nash equilibria; in a finite game of normal form $\{N, \{S_i\}_{i=0}^n, \{\pi_i\}_{i=1}^n\}$, a strategy chain s^* is NE to the i-th player if and only if $\pi_i(s_i^*, s_{-i}^*) \geq \pi_i(s_i, s_{-i}^*), \forall s_i \in S_i$, where S_i is the strategy space of player i, and π denotes the payoff function. For our calculations, we also consider that the entanglement parameter δ varies in the measurement process (Fig. 4.2(b)). We also compute quantum properties as QD, EoF, and CHSH-nonlocality (see Appendix B), to analyse the role of these quantities in the reach of the quantum advantage.

Nash inequality holds as follows: for the strategy $(\hat{D},\hat{Q})$ (or equivalently, for $(\hat{Q},\hat{D})$), $\Delta\pi_A := \frac{p}{2}(-3+5\cos 2\delta_1) \geq 0$, and for the strategy $(\hat{Q},\hat{Q})$, $\Delta\pi_A := \frac{p}{2}(1-5\cos 2\delta_2) \geq 0$. Three regions arise, as indicated in Figs. 4.3(a) and 4.3(b), by means of $\delta_1 = \sin^{-1}\sqrt{1/5}$, and $\delta_2 = \sin^{-1}\sqrt{2/5}$. The payoff for the players in the $(\hat{Q},\hat{Q})$ strategy will be constant in the same way that for the $(\hat{D},\hat{D})$ strategy. This behaviour is crucial for values greater than δ_2 because the Nash equilibrium is reached, and the dilemma is removed. The key parameters δ_1 and δ_2 obtained here for the considered mixed states coincide with those reported by Du *et al.* [112] for just pure states. This is because p only affects the size but not the shape of the payoff functions. For example, by computing the Nash inequality for A's payoff in the $(\hat{Q},\hat{Q})$ and $(\hat{D},\hat{Q})$ strategies, p holds as a global parameter and does not affect the bounds of the inequality. Finally, we show that by considering the *W-l* states $\rho_{in}(p)$ and just controlling the degree of correlations in the final operator $\tilde{\mathcal{J}}(\delta)$, we reach the quantum advantage which removes the game dilemma for δ values smaller than those reported before [112], and, crucially, $\delta^* < \delta_2$, even for separable states.

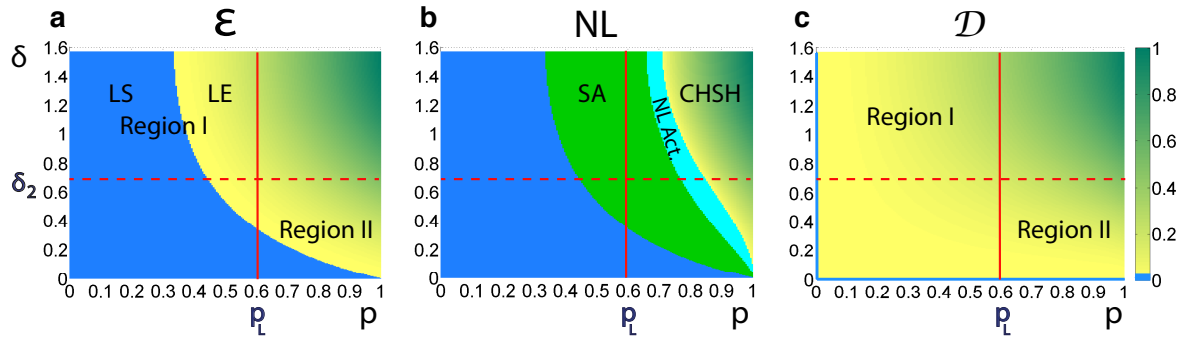

Figure 4.4: Quantum properties of the input states $\rho_{in}(p,\delta)$ and quantum advantage bound. As a function of δ and p, we plot: (a) EoF: the blue area represents the set of separable and therefore local states, and all the states $p \leq p_L \approx 0.6009$, as depicted by the vertical line $p = p_L$, are also local [116]; these allow the identification of the local-entangled (LE) region of states, (b) non-locality (NL) properties: CHSH inequality violation, k-copy nonlocality or superactivation (SA) of non-locality (green-solid area), and activation of non-locality (NL Act.) through tensoring and local filtering (cyan-solid area), (definition of the nonlocal properties is in Appendix B) and (c) QD: the Region I ($\delta \geq \delta_2$, $p \leq p_L$, upper left rectangles) spans non-zero discord states that even though local, allow a quantum advantage; the Region II ($\delta < \delta_2$, $p > p_L$, lower right rectangles) portrays non-local and local non-zero discord states for which the choice dilemma is not removed. The bound $\delta \geq \delta_2 = \sin^{-1}\sqrt{2/5}$, for which the quantum advantage holds, is depicted by a horizontal red-dashed line.

For the sake of completeness, we analyse the quantum advantage in the PD game, i.e., the two regions defined by the δ_2 bound, from which the quantum $(\hat{Q},\hat{Q})$ strategy removes the dilemma, in terms of the quantum properties of the input $\rho_{in}(p,\delta)$ states. We plot the EoF (Fig. 4.4(a)), non-locality given by CHSH inequality violation, k-copy nonlocality (SA) [32, 33], and activation through tensoring and local filtering [115] (NL Act.) (Fig. 4.4(b)), and QD (Fig. 4.4(c)), all of them as functions of the correlation δ, and mixing p parameters (see the Methods section for definitions). We distinguish two principal regions in Fig. 4.4: Region I ($\delta \geq \delta_2$, and $p \leq p_L$, upper left rectangles) in which it is possible to find local-entangled states, and more interestingly, separable states which are able to remove the choice dilemma as they admit the quantum $(\hat{Q},\hat{Q})$ strategy to be the NE and Pareto optimal (see Fig. 4.3). This implies that there exist local quantum states that can be seen as a powering resource for performing quantum strategies that outperform any possible classical strategy in a PD game. In Region II ($\delta < \delta_2$, and $p > p_L$, lower right rectangles), there are states with different nonlocal properties (Fig. 4.4(a) and (b)) admitting no quantum advantage for removing the choice dilemma in the PD game. It is worth pointing out that the nonlocal properties here analysed are bounded by entanglement, i.e., all of them cover sets of states smaller than or equal to the one representing the entangled states. On the other hand, Fig. 4.4(c) clearly shows that even for some discord-correlated states, the dilemma is not removed in this region, hence explicitly showing the existence of non-zero discord states that exhibit no quantum advantage. Thus, discord on its own cannot be regarded as a fundamental measure (beyond entanglement) that underpins the quantum advantage.

4.3 Discussion

Purely *local* and/or *separable* input quantum states have been harnessed as a resource in the PD game, and we have shown that such a strategy gives a clear advantage over the original bipartite non-zero sum game that makes use of just classical resources. In particular, we have also shown that neither entanglement nor any nonlocal property is strictly required at the input of the game in order to achieve a quantum $(\hat{Q}, \hat{Q})$ strategy that removes the PD dilemma and hence outperforms any classical strategy. First, our results have been explored for the general class of correlation-parameter-dependent states (equation (4.2.1)) which comprise the Werner-like states whose quantum properties are depicted in Fig. 4.1 and Fig. 4.2(c). Second, we have shown that within the set of discord-correlated states, there exist some states for which the PD choice problem is not removed, thus implying that QD is neither a necessary condition for achieving the above-described quantum advantage. These results point out the interesting and relevant role played by separable quantum states (and therefore locality) when designing quantum strategies that outperform those based on classical resources, and suggest that such a key resource actually arises from basic quantum interference (superposition) mechanisms.

We remark that we have mainly focused on generating the sufficient conditions for the purely quantum strategy $(\hat{Q}, \hat{Q})$ to solve the dilemma in a realistic scenario. This is why we consider an initial state perturbed by a white noise and discussion the more general case in which not only the entanglement of the measurement basis is varied, but also the entanglement in the ρ' component of the input state, i.e., we consider the variation of the same correlation parameter δ at both the beginning and the end of the PD game.

Our findings are amenable (although not restricted) to being tested with current photonics technology, and basic photon interferometry can be used to demonstrate the locally correlated-quantum advantage here reported. Further work will address a full optical setup and numerical simulations to test our results.

Chapter 5
Complexity of multipartite quantum states

A multipartite system is said to be complex if its properties cannot be inferred from the properties of its parts. Several attempts to define and quantify complexity have been made in Computer Science, Physics, Biology, relying on the assumption that a complex system is highly correlated (for a discussion about several definitions of complexity see e.g., [125]). Yet, a formal link between the concepts of complexity and correlations is still missing. Here, we characterise the complexity of a multipartite system by studying how the correlations between the parts of the system scale with their size. To measure multipartite correlations, we identify a class of metrics satisfying the bona fide criteria proposed in the context of Shannon Information theory [15, 129]. We then define complexity as the nonlinear increase of the correlations between system parts under coarse graining of the system partitioning. We extend the analysis to quantum systems, showing that they can be more complex than classical ones by introducing a computable formula for the complexity in finite dimensional systems. The result calls for further investigation on the potential of quantum complexity as a resource for quantum information processing.

5.1 Known approaches to complexity

We briefly review the celebrated *Neural Complexity* developed by Tononi, Sporns and Edelman (TSE) in 1994 [67] (here, we will refer to this complexity metric as TSE-complexity), and the unified framework for complexity recently proposed by Nihat Ay *et al*. [126]. Both developed within a classical context.

5.1.1 TSE-complexity

TSE-complexity was proposed as a measure of the relationship between two important process in brain activity: segregation (neural activities happening in specialised areas), and integration (interaction of processes from different areas). TSE associated this sort of activities with the statistical dependence of probability distributions and formulated their measure of complexity in terms of the Shannon entropy, they assumed that the statistical properties of these activities did not change with time and did not consider extrinsic inputs from environments. They asked for the deviation from independence among the N components of a system X (e.g. a set of random variables associated to the functionalities of the neural system) and its relation with the deviation from independence among the k components of a subsystem X^k, that is, a partition of the total system X with k elements. Hence, they associated the multi-information

$$I(X) = \sum_{i=1}^{N} H(x_i) - H(X) \tag{5.1.1}$$

with integration activity, and linked the average of multi-information of all the possible subsets X^k with k-out-of-N components with segregation activity. $H(x) = \sum_x p(x) \log p(x)$ is the Shannon entropy and log function is on basis 2.

Within this formalism, TSE-complexity was defined as:

$$C_{\mathrm{TSE}}(X) := \sum_{k=1}^{N} \frac{k}{N} I(X) - \langle I(X_j^k) \rangle, \tag{5.1.2}$$

where j means that the average is over all the possible $C(N,k) = N!/k!(N-k)!$ combinations with k components. Equation (5.1.2) can be written in terms of entropies as:

$$C_{\mathrm{TSE}}(X) = \sum_{k=1}^{N} \langle H(X_j^k) \rangle - \frac{k}{N} H(X). \tag{5.1.3}$$

This approach has been applied in neuroscience to interpret some states of mammal brains as conscious awareness and slow-wave sleep [127].

5.1.2 Geometric approach of complexity

Some other complexity measures under the same context were proposed, for example; the multi-information (5.1.1) was considered a complexity measure on its own [68], and the excess entropy [128], originally introduced in the context of time series as the minimal amount of memory required for an optimal prediction, just to name a few. Recently, a more general approach to complexity measures for finite random fields was developed [126] by using the geometric framework of hierarchies of exponential families [69]. This approach includes an interaction structure at different scales of description and gives the notion of a reconstruction protocol of the given field (be it a classical probability distribution or a quantum state).

Let $\mathcal{S}$ be the set of systems we want to assign a complexity measure, for $s \in \mathcal{S}$, we interpret the reduced description of the system in terms of its parts $D(s)$ as the assignment $D : \mathcal{S} \to \mathcal{D}$. The next step is to reconstruct the system s by means of the parts $D(s)$, for doing so, a reconstruction map $C : \mathcal{D} \to \mathcal{S}$ is required such that the composition function is interpreted as the sum of the parts:

$$P(s) := (C \circ D)(s). \tag{5.1.4}$$

A possible complexity measure is thus defined as the deviation of a system to be just the sum of its parts, i.e., the geometric distance between systems s and $P(s)$. According to Eq. (5.1.4), it is clear that

$$(D \circ C)(s') = s'$$

for all $s' \in \mathcal{D}$, which implies $P^2 = P$.

In order to give a quantitative meaning of complexity, the distance-like metric must satisfy $d(s, s') \geq 0$, with equality if and only if $s = s'$. In agreement with the discussed reconstruction protocol, the desired metric can be defined as [126]:

$$d(s) := d(s, P(s)) = \min_{s' \in \mathcal{N}} d(s, s'), \tag{5.1.5}$$

where $\mathcal{N} = \{s \in \mathcal{S} : P(s) = s\}$ is just the set of non-complex systems.

Ay *et al.* [126] formalised this into an information-geometric framework in terms of the maximum entropy principle and projection onto interaction spaces. The system is considered to be a finite node set

V whose node v can be in many finitely states $\mathcal{H}_v$ and can be modelled by a probability distribution p on the corresponding product configuration set $\mathcal{H}_V = \prod_{v\in V} \mathcal{H}_v$. The parts are the marginals probabilities p_A, for A taken from a set $\mathcal{U}$ of subsets of V. $\mathcal{U} \in s^V$ is called a simplicial complex and is assumed to satisfy

$$\cup_{A\in\mathcal{U}} A = V \text{ and } A \in \mathcal{U},\ B \subseteq A \Rightarrow B \in \mathcal{U}.$$

An interaction space is defined, for the decomposition of $x \in \mathcal{H}_V$ as $x = (x_A\,, x_{V\setminus A})$, for every $A \subseteq V$, as the subspace of functions that do not depend on the configurations $x_{V\setminus A}$:

$$I_A := \left\{ f \in \mathbb{R}^{\mathcal{H}_V} : f(x_A\,, x_{V\setminus A}) = f(x_A\,, x'_{V\setminus A})\, \forall x_A \in \mathcal{H}_V,\, \forall x_{V\setminus A},\, x'_{V\setminus A} \in V \setminus A \right\}.$$

It is known as the space of A-interactions, and has dimension $\prod_{v\in A} \mid \mathcal{H}_v \mid$. For the simplicial complex $\mathcal{U}$, the corresponding interaction space is

$$I_{\mathcal{U}} = \sum_{A\in\mathcal{U}} I_A,$$

and can be associated with an exponential family $\exp(\mathcal{U}) := \exp(I_{\mathcal{U}})$. Given a system with N elements, the particular choice $\mathcal{U}_k = \{A \subseteq V : |A| = k\}$ [69], has the order structure $\mathcal{U}_k \preceq \mathcal{U}_{k+1}$ which implies the hierarchy $\exp(I_{\mathcal{U}_k}) \subseteq \exp(I_{\mathcal{U}_{k+1}})$ on the interaction spaces, for $k = 0, ..., N$.

The main result in [126] is that the minimum geometric distance (5.1.5) measured by the relative entropy; $d(p) = D(p||\exp(I_{\mathcal{U}_k}))$, of an arbitrary probability distribution p with respect to the exponential families $\exp(I_{\mathcal{U}_k})$ corresponds to the one given by the probability distribution $\tilde{p}_k \in \exp(I_{\mathcal{U}_k})$ with the same k-marginals than p and maximally non-commitant (with maximum entropy). After showing this fact, Authors in [126] proposed as complexity measure a weighted sum of relative entropy on the interaction structure given by the exponential families:

$$C_G(p) := \sum_{k=1}^{N-1} \alpha(k) D(p||\tilde{p}_k), \tag{5.1.6}$$

where $D(p||\tilde{p}_k) = \min_{p_k\in\exp(I_{\mathcal{U}_k})} D(p||p_k)$, and $\alpha(k)$ is an arbitrary weight function that depends on k.

5.2 Our approach to complexity

The definitions of the TSE-complexity (5.1.2), and the geometric complexity (5.1.6) originally introduced in classical systems, can be easily quantised; i.e., it is basically enough to change the Shannon entropy with the von Neumann entropy. As they compute complexity as a measure of statistical interdependence (Eq. (5.1.2)), and as a reconstruction protocol from interaction spaces (Eq. (5.1.6)), respectively, we can associate them with the concept of correlations among the parts of the system at different scales of description. It is then worth noting that these measures present some technical issues that do not agree with a well established measure of correlations (see for example the definition of the EoF and the QD in section 1.2, and their formulas for the particular case of qubits).

For more than two-particle systems, correlations among the parts of the system are more complex to be described as they appear at different scales, and furthermore, one can introduce the concept of genuine multipartite correlations, i.e. correlations at a scale or size k (among k particles) that can not be described in terms of correlations at a scale $k-1$. Some approaches to measure genuine multipartite correlations have been developed [14, 129, 131, 132, 133, 134, 135] as extensions of some of the correlations introduced in section 1.2.

We briefly describe the basic criteria we agree for genuine multipartite correlations [129]:

(C1) If an N-partite state does not have genuine N-partite correlations and one adds a party as a product state, then the resulting $N+1$ partite state does not have genuine N-partite correlations.

(C2) If an N-partite state does not have genuine N-partite correlations, then general local operations can not generate genuine N-partite correlations.

(C3) If an N-partite state does not have genuine N-partite correlations, then if one party splits his subsystem into two parts, keeping one part for himself and the other to create a new $N+1$-st subsystem, then the resulting $N+1$ partite state does not have genuine $N+1$-partite correlations.

Hence, considering these criteria as minimal requirements for the contributing terms used in the definition of a complexity measure, it can be shown that those ones in the geometric complexity (5.1.6) fail to satisfy criterium C2 due to every k-contribution increases under local operations [131] (a solution was found by including the closure of the exponential families in the definition of genuine multipartite correlations for every $\mathcal{U}_k$ [136]). Furthermore, even though criterion C2 is taken in the geometric approach of complexity, this latter is difficult to be computed and some algorithms have been proposed in the quantum domain [137].

To try to overcome these technical problems and to give an operational interpretation to complexity, we make a conservative approach to define a new way to compute the complexity of quantum states. For doing so, we also consider to measure how far a given multipartite quantum state is from a set of states with some particular properties at a given size k, being $1 \leq k \leq (N-1)$ the size of an arbitrary partition of the total N-partite system. Hence, we define the set of states that do not present any kind of correlations as the set of all product states, at a size k, as:

$$\underline{\mathcal{P}}_k = \left\{ \rho | \rho = \bigotimes_{i=1}^{m} \rho^{[k_i]};\ \forall k_i \left| \sum_{i=1}^{m} k_i = N\ ; k = \max\{k_i\} \right. \right\}, \tag{5.2.1}$$

where $\rho^{[k_i]}$ is the density matrix of a k_i-partite state. These sets hold the hierarchy $\underline{\mathcal{P}}_1 \subset \underline{\mathcal{P}}_2 \subset \cdots \subset \underline{\mathcal{P}}_{N-1}$, as schematically shown in Fig. 5.1.

Let us illustrate the structure of the sets $\underline{\mathcal{P}}_k$ for some small k; for $k=1$ we have:

$$\underline{\mathcal{P}}_1 = \left\{ \rho | \rho = \rho_{A_1}^{[1]} \otimes \rho_{A_2}^{[1]} \otimes \cdots \otimes \rho_{A_N}^{[1]} \right\},$$

where $A_i \in \mathbb{A}$ labels the i-th particle, with $\mathbb{A} = \{A_1, A_2, \cdots, A_N\}$. $\underline{\mathcal{P}}_1$ represents the set of all single-particle product states.

For $k=2$:

$$\underline{\mathcal{P}}_2 = \left\{ \rho | \rho = \rho_{A_1}^{[1]} \otimes \rho_{A_2}^{[1]} \otimes \cdots \otimes \rho_{A_N}^{[1]};\ \rho_{A_1 A_2}^{[2]} \otimes \rho_{A_3}^{[1]} \otimes \cdots \otimes \rho_{A_N}^{[1]} \right\},$$

an so on, such that the maximum number of particle allowed to interact are two. We can write this set as:

$$\underline{\mathcal{P}}_2 = \underline{\mathcal{P}}_1 \bigcup \left\{ \beta^{[2]} \right\},$$

where $\left\{ \beta^{[2]} \right\}$ is the set of all product states with 2-particle correlations, i.e. with *at least* one superscript $k=2$. In general, we can write:

$$\left\{ \beta^{[2]} \right\} = \left\{ \bigotimes_{i=1}^{m} \rho_{A_{2i-1}A_{2i}}^{[2]} \otimes \bigotimes_{j=2m+1}^{N} \rho_{A_j}^{[1]};\ m = 1, \cdots,\ \begin{array}{ll} \frac{N-1}{2} & \text{if } N \text{ odd} \\ \frac{N}{2} & \text{if } N \text{ even} \end{array} \ + \text{ combinations} \right\},$$

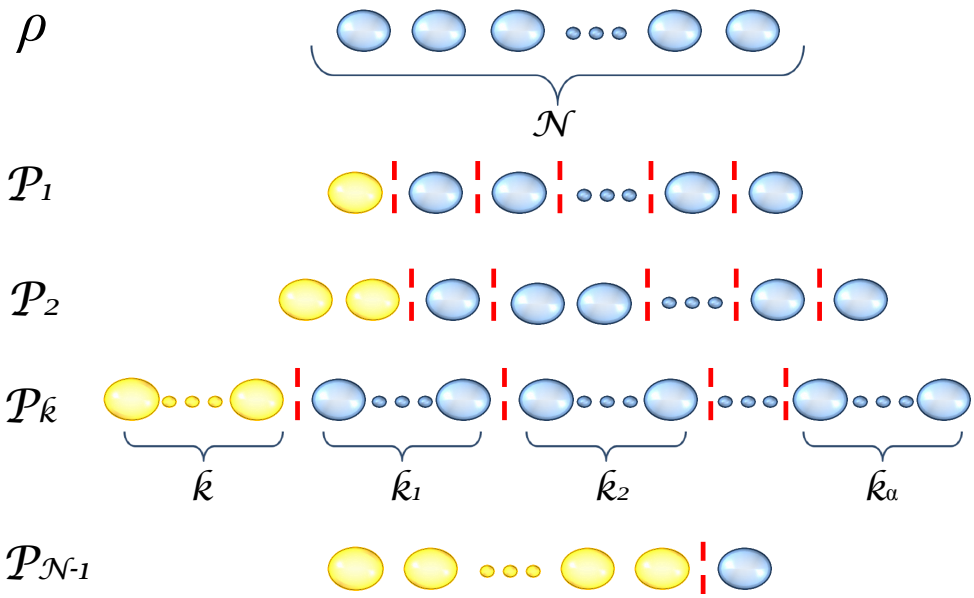

Figure 5.1: Scheme of the hierarchy of sets $\underline{\mathcal{P}}_k$. The given N-party quantum state ρ is analysed at different scale of descriptions in terms of the uncorrelated sets of product states $\underline{\mathcal{P}}_k$.

where the combinations run over the particles (the subscripts A_i).

Following this structure for higher values of k, it is easy to see that we can always write:

$$\underline{\mathcal{P}}_k = \underline{\mathcal{P}}_{k-1} \bigcup \left\{ \beta^{[k]} \right\},$$

where $\left\{ \beta^{[k]} \right\}$ is the set of all possible states with *at least* one k-particle joint contribution.

Now, for building our measure of complexity, we ask about how far is a given state from the different sets $\underline{\mathcal{P}}_k$, for doing so, we use the relative entropy as our distance-like metric and define the distance as the minimum of the relative entropy with respect to the states in a particular set, as follows:

$$D_k(\sigma) := \min_{\rho_k \in \underline{\mathcal{P}}_k} D(\sigma || \rho_k), \tag{5.2.2}$$

where $D(\sigma||\rho_k) = -S(\sigma) - \mathrm{Tr}(\sigma \log \rho_k)$, and $S(\sigma) = -\mathrm{Tr}(\sigma \log \sigma)$ is the von Neumann entropy.

To give an analytical result of the minimisation process in Eq. (5.2.2), we extend the result of Lemma 1 in Ref. [104] that establishes: *The closest product state for any generic state, σ, as measured by relative entropy, is its reduced states (its marginals) in the product form, i.e. $\pi_\sigma = \pi_1 \otimes \pi_2 \otimes ... \otimes \pi_N$.*

Here, we follow the proof of Lemma 1 in [104] to demonstrate the following Lemma for some arbitrary partition of size k:

Lemma: For any partition k of any generic state, σ_N, the closest state in the product form: $\rho^{[k]} \otimes \rho^{[N-k]}$, masured by relative entropy, is its reduced k- and $(N-k)$-partite states in the product form,

i.e. $\pi_\sigma^{[k]} = \pi_{\{A_k\}}^{[k]} \otimes \pi_{\mathbb{A}\setminus\{A_k\}}^{[N-k]}$, where $\pi_{\{A_k\}}^{[k]} = \mathrm{Tr}_{\mathbb{A}\setminus\{A_k\}}(\sigma_N)$ is the reduced state of σ_N for a particular partition of k particles.

Proof: Let $\alpha = \alpha^{[k]} \otimes \alpha^{[N-k]}$ be the closest product-form state to σ_N, consider the difference $D(\sigma_N||\pi_\sigma^{[k]}) - D(\sigma_N||\alpha) \geq 0$. Now, as $\mathrm{Tr}(\rho \log(\alpha_1 \otimes \alpha_2)) = \mathrm{Tr}(\mathrm{Tr}_2(\sigma)\log\alpha_1) + \mathrm{Tr}(\mathrm{Tr}_1(\sigma)\log\alpha_2)$ by linearity of trace and additivity of log function, the above inequality can be written as: $-D(\pi_{\{A_k\}}^{[k]}||\alpha^{[k]}) - D(\pi_{\mathbb{A}\setminus\{A_k\}}^{[N-k]}||\alpha^{[N-k]}) = -D(\pi_\sigma^{[k]}||\alpha) \geq 0$.

Hence, for all σ, we have shown that $\pi_\sigma^{[k]} = \alpha$ is the minimiser of the relative entropy. Note that we have assumed a particular partition for a given size k, thus, the result of the Lemma is valid for all the α states in the Hilbert spaces associated to the subsystems of the particular partition. Consequently, our metric to catch the distance of the given state from the sets $\underline{\mathcal{P}}_k$ (Eq. (5.2.2)), can be rewritten as:

$$D_k(\sigma) = \min_{C(N,k)} D(\sigma||\pi_\sigma^{[k]}), \tag{5.2.3}$$

where the minimum is taken over all the possible $C(N,k)$ combinations of particles for a given size k. This gives a simplified formula for $D_k(\sigma)$. Then, our approach to compute the complexity of a given multipartite quantum state can be defined as:

$$\mathcal{C}(\sigma) := \sum_{k=1}^{N-1} \alpha(k) D_k(\sigma), \tag{5.2.4}$$

where the coefficients $\alpha(k)$ are arbitrary chosen.

The above lemma allows us to write sets $\underline{\mathcal{P}}_k$ in a more compact form as the closest state has a particular structure for every k. For understanding this, let us consider the case of a 5-particle state σ and compute the relative entropy with respect to $\underline{\mathcal{P}}_2$:

$$D_2(\sigma) \equiv D(\sigma||\tilde{\rho}^{[2]}) = \min_{\rho \in \underline{\mathcal{P}_2}} D(\sigma||\rho).$$

There are two possibilities for the minimiser $\tilde{\rho}^{[2]}$ according to Eq. (5.2.1). Firstly, let's assume that $\tilde{\rho}_1^{[2]} = \rho_{A_1A_2}^{[2]} \otimes \rho_{A_3A_4}^{[2]} \otimes \rho_{A_5}^{[1]}$, where $\sigma_{A_1A_2}^{[2]} = \mathrm{Tr}_{A_3,A_4,A_5}(\sigma)$. Without loss of generality, we have chosen this particular combination of particles to be the minimiser of the relative entropy in agreement with the above lemma. The explicit form of the relative entropy is:

$$\begin{aligned} D(\sigma||\tilde{\rho}_1^{[2]}) &= D(\sigma||\sigma_{A_1A_2}^{[2]} \otimes \sigma_{A_3A_4}^{[2]} \otimes \sigma_{A_5}^{[1]}) \\ &= -S(\sigma) - \mathrm{tr}(\sigma \log(\sigma_{A_1A_2}^{[2]} \otimes \sigma_{A_3A_4}^{[2]} \otimes \sigma_{A_5}^{[1]})) \\ &= S(\sigma_{A_1A_2}) + S(\sigma_{A_3A_4}) + S(\sigma_{A_5}) - S(\sigma). \end{aligned} \tag{5.2.5}$$

On the other hand, if we assume that $\tilde{\rho}_2^{[2]} = \rho_{A_1A_2}^{[2]} \otimes \rho_{A_3}^{[1]} \otimes \rho_{A_4}^{[1]} \otimes \rho_{A_5}^{[1]}$ satisfies the above lemma, we have that the minimum relative entropy is instead:

$$\begin{aligned} D(\sigma||\tilde{\rho}_2^{[2]}) &= D(\sigma||\sigma_{A_1A_2}^{[2]} \otimes \rho_{A_3}^{[1]} \otimes \rho_{A_4}^{[1]} \otimes \rho_{A_5}^{[1]}) \\ &= -S(\sigma) - \mathrm{tr}(\sigma \log(\sigma_{A_1A_2}^{[2]} \otimes \rho_{A_3}^{[1]} \otimes \rho_{A_4}^{[1]} \otimes \rho_{A_5}^{[1]})) \\ &= S(\sigma_{A_1A_2}) + S(\sigma_{A_3}) + S(\sigma_{A_4}) + S(\sigma_{A_5}) - S(\sigma). \end{aligned} \tag{5.2.6}$$

Hence, let's observe the following:

$$D(\sigma||\tilde{\rho}_2^{[2]}) - D(\sigma||\tilde{\rho}_1^{[2]}) = S(\sigma_{A_3}) + S(\sigma_{A_4}) - S(\sigma_{A_3A_4}) = D(\sigma_{A_3A_4}||\sigma_{A_3} \otimes \sigma_{A_4}) \geq 0,$$

which means that, in general, the minimiser has the form $\tilde{\rho}_1^{[2]}$, and that, as expected, $\tilde{\rho}_2^{[2]}$ is a particular case; in our example, when $\sigma_{A_3A_4} = \sigma_{A_3} \otimes \sigma_{A_4}$.

Taking into account the above observation, it is easy to write Eq. (5.2.1) in a particular and more compact form, as follows:

$$\underline{\mathcal{P}}_k = \left\{ \rho | \rho = \left(\bigotimes_{j=1}^{\lfloor N/k \rfloor} \rho_j^{[k]} \right) \otimes \rho_{\lfloor N/k \rfloor + 1}^{[r]} \right\}, \tag{5.2.7}$$

where $\lfloor N/k \rfloor$ stands for the floor integer part of the fraction N/k, and the reminder r satisfies $N = j_{\max} k + r$, with $j_{\max} = \lfloor N/k \rfloor$.

The relative entropy also acquires a close formula in terms of the size k:

$$\begin{aligned} D_k(\sigma) &= D\left(\sigma || \left(\bigotimes_{j=1}^{j_{max}} \sigma^{[k]}_{A_{(j-1)k+1}A_{(j-1)k+2}...A_{jk}} \right) \otimes \sigma^{[r]}_{A_{j_{max}k+1}...A_N} \right) \\ &= \sum_{j=1}^{j_{max}} S(\sigma^{[k]}_{A_{(j-1)k+1}A_{(j-1)k+2}...A_{jk}}) + S(\sigma^{[r]}_{A_{j_{max}k+1}...A_N}) - S(\sigma), \end{aligned} \tag{5.2.8}$$

where the subscript $A_{(j-1)k+1}A_{(j-1)k+2}...A_{jk}$, $j = 1, ..., j_{max}$ just indicates that it is the particular partition giving the minimum of the relative entropy of the arbitrary state σ with respect to $\underline{\mathcal{P}}_k$. As a particular case, if $N = nk$, n integer, Eq. (5.2.8) reads:

$$D_k(\sigma) = \sum_{j=1}^{n} S(\sigma^{[k]}_{A_{(j-1)k+1}A_{(j-1)k+2}...A_{jk}}) - S(\sigma). \tag{5.2.9}$$

5.2.1 Complexity of N-partite GHZ states

Having such a close formula to compute the relative entropy, we now proceed to evaluate our approach of complexity in a simple but very interesting case of qubits. Hence, we first consider the case of N qubits in the mixed GHZ state:

$$\sigma^{\mathrm{GHZ}} = \frac{p}{2^N} \mathbb{1}^{\otimes N} + (1-p) |\mathrm{GHZ}_N\rangle\langle \mathrm{GHZ}_N|, \tag{5.2.10}$$

where $\mathbb{1}$ is the identity matrix in the one-qubit Hilbert's space and $|\mathrm{GHZ}_N\rangle = (|0\rangle^{\otimes N} + |1\rangle^{\otimes N})/\sqrt{2}$ is the pure Greenberger-Horne-Zeilinger (GHZ) state [130]. The partial trace of this state over some amount of qubits is symmetric with respect to the chosen partition, that is, the reduced state (marginal) of k qubits is the same for all the possible partitions, and it is:

$$\begin{aligned} \sigma_k^{\mathrm{GHZ}} &= \mathrm{Tr}_{\{N-k\}} \sigma^{\mathrm{GHZ}} \\ &= \frac{p}{2^k} \mathbb{1}^{\otimes k} + \frac{(1-p)}{2} (|0\rangle\langle 0|^{\otimes k} + |1\rangle\langle 1|^{\otimes k}), \end{aligned} \tag{5.2.11}$$

where the subscript $\{N-k\}$ means that the partial trace has been applied over $N-k$ qubits for some specific partition of k elements, $k = 1, ..., N-1$. Due to the symmetry of the state with respect to the partial trace, the minimisation over all the possible partitions with the same size k does not take place anymore and Eq. (5.2.8) can be written as:

$$D_k(\sigma^{\mathrm{GHZ}}) = \lfloor N/k \rfloor S(\sigma_k^{\mathrm{GHZ}}) + S(\sigma_r^{\mathrm{GHZ}}) - S(\sigma^{\mathrm{GHZ}}), \tag{5.2.12}$$

where,

$$S(\sigma_k^{\mathrm{GHZ}}) = -2\left(\frac{p}{2^k}+\frac{1-p}{2}\right)\log\left(\frac{p}{2^k}+\frac{1-p}{2}\right)-\left(2^k-2\right)\frac{p}{2^k}\log\frac{p}{2^k} \tag{5.2.13}$$
$$= -\left(\frac{p}{2^{k-1}}+1-p\right)\log\left(\frac{p}{2^{k-1}}+1-p\right)-\frac{2^{k-1}-1}{2^{k-1}}p\log p+\frac{p(k-1)(2^{k-1}-1)}{2^{k-1}}+1\,,$$

$$S(\sigma^{\mathrm{GHZ}}) = -\left(2^N-1\right)\frac{p}{2^N}\log\frac{p}{2^N}-\left(1-\frac{2^N-1}{2^N}p\right)\log\left(1-\frac{2^N-1}{2^N}p\right) \tag{5.2.14}$$
$$= -\frac{2^N-1}{2^N}p\log p-\frac{2^N(1-p)+p}{2^N}\log\left(2^N(1-p)+p\right)+N,$$

and $S(\sigma_r^{\mathrm{GHZ}})$ has the same form of $S(\sigma_k^{\mathrm{GHZ}})$ but with the remainder r instead of k.

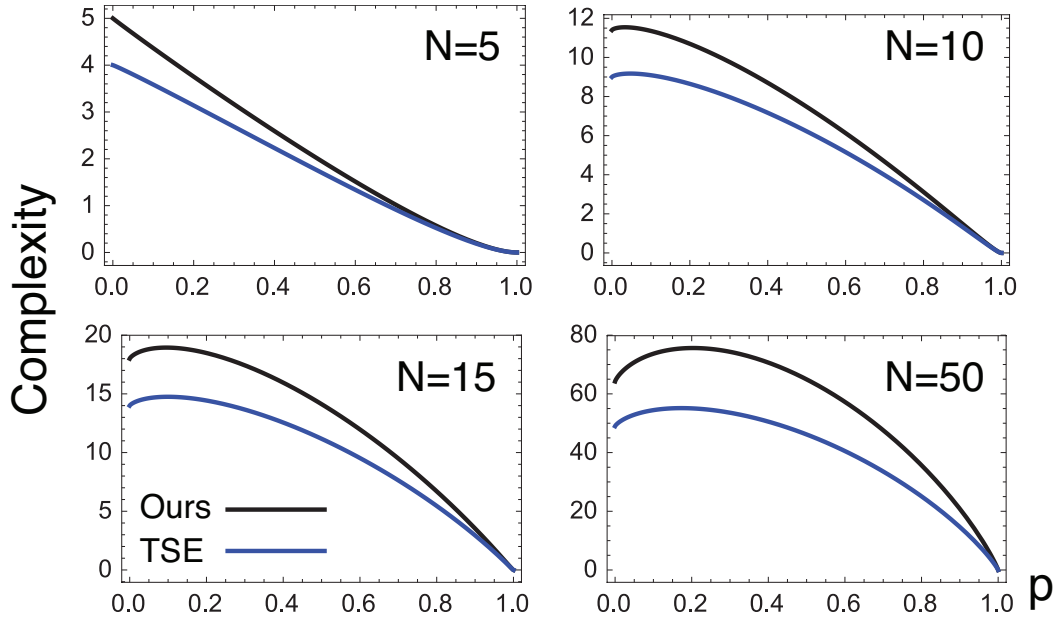

Figure 5.2: Our measure of complexity (black) and TSE-complexity (blue) for $N = 5,\ 10,\ 15,\ 50$. The behaviour is the same for both metrics but $\mathcal{C} \geq C_{TSE}$.

For comparison purposes, let's remember the TSE-complexity. The quantum version of the contributing terms to the TSE-complexity can be written as [126]:

$$C^{(k)}(\rho) = \frac{N}{k\,C(N,k)}\sum_{1\leq i_1<\ldots<i_k\leq N} S(\rho_{i_1},\ldots,\rho_{i_k}) - S(\rho), \tag{5.2.15}$$

where $S(\rho_{i_1},\ldots,\rho_{i_k})$ is the von Neumann entropy of some marginal with k particles, and the sum runs over the $C(N,k)$ possible partitions.

For the particular case of the mixed GHZ state, Eq. (5.2.15) reduces to:

$$C^{(k)}(\sigma^{GHZ}) = \frac{N}{k}S(\sigma_k^{\mathrm{GHZ}}) - S(\sigma^{\mathrm{GHZ}}), \tag{5.2.16}$$

as the sum in the first term gives just $C(N,k)\,S(\sigma_k^{\rm GHZ})$. Replacing $\lfloor N/k \rfloor = (N-r)/k$ and Eq. (5.2.16) in Eq. (5.2.12), we have the direct relationship between each term in our measure of complexity and the corresponding term in the TSE-complexity:

$$D_k(\sigma^{GHZ}) = C^{(k)}(\sigma^{GHZ}) + S(\sigma_r^{\rm GHZ}) - \frac{r}{k} S(\sigma_k^{\rm GHZ}). \tag{5.2.17}$$

It is clear that in the cases for which N is a multiple of k, i.e. $r = 0$, both terms are the same ($D_k = C^{(k)}$). In general, our measure of complexity differs from the TSE-complexity; if we multiply Eq. (5.2.17) by $\alpha(k) = k/N$ and sum over all the contributions k, according to Eq. (5.2.4), we have:

$$\mathcal{C}(\sigma^{\rm GHZ}) = C_{TSE}(\sigma^{\rm GHZ}) + \sum_{k=1}^{N-1} \frac{1}{N} \left(kS(\sigma_r^{\rm GHZ}) - rS(\sigma_k^{\rm GHZ}) \right), \tag{5.2.18}$$

where C_{TSE} is the TSE-complexity, and r depends on k.

Figure 5.2 shows the behaviour of our complexity metric (Eq. (5.2.4)) vs the TSE-complexity for four different amount of qubits in the corresponding mixed GHZ state. In this case, our complexity metric behaves in the same way than the TSE's, but taking higher values as the parameter p goes from one to zero.

To understand the behaviour of our complexity metric, we show every contribution D_k (Eq. (5.2.12)) in Fig. 5.3, for $N = 4,\ 5,\ 10,\ 50$. Note that for small amount of qubits ($N = 4, 5$) all the curves are concave downward, but for the other two cases of 10 and 50 qubits, the contributions have a concave upward profile; this explains the change in behaviour of our complexity metric from 5 to 10 qubits in Fig. 5.2. Note that some of the contributions are very close to each other as k increases, and particularly, some contributions have the same value for the pure GHZ state ($p = 0$).

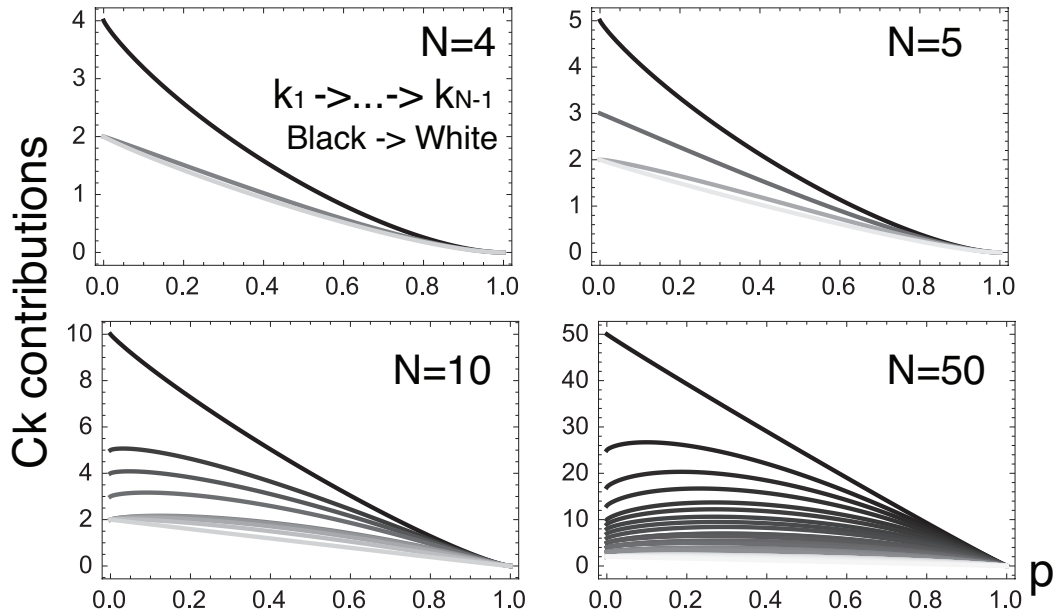

Figure 5.3: Contributions of D_k for $N = 4,\ 5,\ 10$ and 50 qubits. The grey scale goes from black to white as k increases.

5.2.2 Discussion

Thinking in each term D_k as a measure of how much correlated are the parts of a system for a given size k, this result partially agrees with the work reported in [131], where the analysis of irreducible correlations in multipartite systems in terms of the maximum entropy principle, showed that the pure $\rho_0 = |\mathrm{GHZ}_N\rangle\langle\mathrm{GHZ}_N|$ state had just N- and 2-party correlations. Let us understand *irreducible* as correlations that exist in a k-particle partition that can not be described in terms of correlations existing in the $k-1$-party subsystem. By defining irreducible correlations as $D_{k-1} - D_k \equiv S(\tilde{\pi}^{k-1}) - S(\tilde{\pi}^k)$, in our approach, we can see that some irreducible correlations are zero as k increases due to $D_{k-1} = D_k$ according to Eq. (5.2.12). For example, for $N = 10$ we have that D_1, D_2, D_3, D_4 and D_5 have different values, so we would say that the 10-qubit GHZ state has irreducible multipartite correlations for $k = 2, 3, 4, 5$ and zero irreducible multipartite correlations for $k = 6, 7, 8, 9$. Furthermore, it is clear that $D_9 \neq 0$ and thus, the system also has irreducible 10-party correlations.

In Ref. [131], irreducible multiparty correlations were defined as:

$$C_Z^{(k)}(\rho) = S(\tilde{\rho}^{[k-1]}) - S(\tilde{\rho}^{[k]}), \tag{5.2.19}$$

where $\tilde{\rho}^{[k]}$ is the state with the same k-party marginals as ρ and that is maximally noncommittal (with maximal von Neumann entropy). Zhou [131] then showed that ρ_0 has zero irreducible multipartite correlations for $k = 2, 3, ..., N-1$ and

$$C_Z^{(2)}(\rho_0) = N - 1 \ , \ C_Z^{(N)}(\rho_0) = 1.$$

In other words, the pure GHZ state has only N- and 2-party correlations. This result comes from the fact that the maximiser of the von Neumann entropy are: $\tilde{\rho}^{[1]} = \mathbb{1}^{\otimes N}/2^N$, $\tilde{\rho}^{[k]} = 1/2(|00...0\rangle\langle 00...0| + |11...1\rangle\langle 11...1|)$ for $k = 2, 3, 4, ..., N-1$, and clearly, $\tilde{\rho}^{[N]} = \rho_0$ (the same original state). A direct computation of entropies gives the result for $C_Z^{(2)}$ and $C_Z^{(N)}$. Noting that our definition of irreducible multiparty correlations is quite similar to Eq. (5.2.19), the crucial difference lies in the states that our approach considers to reconstruct the original state in a tensor product form; for every size k, the minimiser of relative entropy in our approach always has the form:

$$\tilde{\pi}^k = \underbrace{1/2(|0\rangle\langle 0|^{\otimes k} + |1\rangle\langle 1|^{\otimes k}) \otimes ... \otimes 1/2(|0\rangle\langle 0|^{\otimes k} + |1\rangle\langle 1|^{\otimes k})}_{\lfloor N/k \rfloor \text{ times}} \otimes 1/2(|0\rangle\langle 0|^{\otimes r} + |1\rangle\langle 1|^{\otimes r}), \tag{5.2.20}$$

for $k = 1, ..., N-1$. While the states used in Ref. [131] are:

$$\begin{aligned} &1/2(|0\rangle\langle 0|^{\otimes N} + |1\rangle\langle 1|^{\otimes N}) \ ; \ k = 2, ..., N-1 \\ &\mathbb{1}^{\otimes N}/2^N \ ; \ k = 1. \end{aligned}$$

In our approach, Eq. (5.2.20) implies that all the consecutive contributions with the same value for the integer part $\lfloor N/k \rfloor$ give the result $D_{k-1} - D_k = 0$, thus implying that for these terms, the system does not present genuine k-partite correlations.

In contrast to the geometric complexity, the principal lemma of our approach is based on tensor product states that give a close formula to compute our definition of complexity. This is thanks to the contributing terms of relative entropies (Eq. (5.2.3)). Furthermore, these terms satisfy the basic postulates or requirements for multipartite correlations.

Concluding remarks and outlook

Summary

We have demonstrated how to generate and control entanglement in dimer and trimer molecular systems which comprise currently synthesised organic molecules. The study in terms of the eigenenergies of the bare molecular Hamiltonian revealed that entanglement 'naturally' appears due to the physical coupling between the molecules, that in our description is described as a dipolar interaction. With the information extracted from the detection of the PBI molecules [35, 77, 34], we were able to predict the entanglement dynamics for both dimers and trimers. As it is experimentally feasible to excite a particular eigenstate of the dimer/trimer Hamiltonian by means of an external laser field, our findings indicate that we could know whether the state is entangled, how much entangled it is, and how robust its entanglement is. This is possible as we can access the dynamics followed by each eigenstate.

We have shown that the way in which quantum systems correlate or share information can be understood from the dynamics followed by the register-environment correlations. This has been done via the KW relations established for the Entanglement of Formation (EoF) and the Quantum Discord (QD). Particularly, we have shown that the distribution of entanglement between each qubit and the environment signals the results for both the prior- and post-measure conditional entropy (partial information) shared by the qubits. As a consequence of this link, we have also shown that some information (the distribution of quantum correlations—$\mathcal{L}_{\circlearrowleft}$) about the whole tripartite system can be extracted by performing local operations over one of the bipartitions, say AB, and by knowing the EoF in the same subsystem (see Eq. (2.3.15)). We stress that these two remarks are completely independent of the considered physical model as they have been deduced from the original definition of the monogamy KW relations. On the other hand, by considering the properties of the specific model here investigated (which may be applicable to e.g., atoms, small molecules, and quantum dots arrays), the study of the dynamics of the distribution of qubit-environment correlations led us to establish that qubit energy asymmetry induces entanglement oscillations, and that we can extract partial information about AB entanglement by analysing the way in which information flows between each qubit and the environment, for suitable initial states. Particularly, we have shown that the qubits early stage disentanglement may be understood in terms of the laser strength asymmetry which determines the entanglement distribution between the qubits and the environment. In addition, we have also shown that the extrema of the qubit-environment $A\mathcal{E}$ and $B\mathcal{E}$ EoF oscillations exactly match the AB EoF minima. The study here presented has been done without need to explicitly invoque any knowledge about the state of the environment at any time $t > 0$.

We have also computed entanglement, classical, quantum, and total correlations for a hybrid system composed of largely separated quantum emitters coupled to the plasmonic modes of a one-dimensional waveguide, which is externally driven by a laser field. We have illustrated, by direct calculation, that Classical Correlations (CC) are the least assisted by the plasmon bus and that the QD is the dominant

correlation that prevails throughout the whole dissipative dynamics. This latter can be enhanced by the presence of the plasmonic collective excitations and by the external laser pumping. This tendency in the correlations has been analytically demonstrated for the case of bare emitters coupled to the vacuum electromagnetic field in [CS2].

We have emphasised the entropic origin of the EoF, the QD, and the Quantum Mutual Information (QMI), as quantifiers of correlations. By direct computation of the concurrence, we found that this quantity can reach values well above the EoF, and the QMI (total correlations). This shows that care must be taken when confronting or using specific quantifiers of entanglement for describing a physical process, especially because the interpretation of the EoF, as the cost of creation of an entangled state (with no regularisation), leads to an upper bound on the actual degree of entanglement in a quantum system. On the other hand, the concurrence is an entanglement monotone but is not an 'actual' entanglement metric in the sense that it obtains its meaning from its relation to the EoF and not the opposite [139].

Furthermore, we have demonstrated a mechanism for controlling and switching nonclassical correlations between qubits. Our mechanism is based on a set of distant quantum emitters, that are coupled via the interaction with the plasmon modes of a waveguide and driven by an external laser field. We have shown that QD plays a key role in the proposed emitters conditional quantum dynamics protocol. We have also given a suitable qubit preparation for which the emitters quantum correlation is always greater than the classical one. Our results could be exploited for quantum computing and communication at long interqubit distances, with the potential for long-range quantum circuitry integration.

Regarding the use of quantum states as a resource for performing quantum games, we have tested entanglement and quantum discord in the so-called Prisoners' Dilemma. We have computed nonlocality properties via the Bell's inequalities, and explored the role played by entangled (be it local or nonlocal) states in reaching a quantum advantage in the game that outperforms any classical strategy. We have shown that there exist some quantum states for which nonlocality, entanglement, and more interestingly, quantum discord *do not* play any role at all at reaching the quantum advantage: It suffices to resort to local quantum states as a resource.

In the last part of this Thesis, we have proposed a new measure of complexity for multipartite quantum systems. Our definition of complexity belongs the class devoted to understand the structure of a multipartite system and to describe the system itself by means of the knowledge of its structure. Hence, we defined as a measure of complexity the weighted sum of the relative entropy between the total state of the original multipartite system and the state given by tensor product combinations of substates at different scale of description, i.e., considering all the possible partitions of the big state, from 1 to $N-1$ parties. The use of tensor product to reconstruct a version of the total state from the information of its parts assures that our definition does not increase by introducing new parties in a tensor product way. Furthermore, for the particular case of considering partitions with just one party, our mesure reduces to the well-known multi-information metric, as expected. We have evaluated our measure for the interesting multipartite GHZ states under white noise, and have shown that the behaviour of such metric is 'similar' to the expected behaviour followed by the TSE-complexity. Even though the geometry complexity derived in [126] gives a nice interaction structure description, it is very difficult to be computed. In this aspect, we have also found an advantage of our measure of complexity with respect to the former.

Future work

The results here reported are part of a very active field of research and are worthy of further investigations. With regard to generation and control of quantum correlations in physical systems, a point to develop is to investigate quantum nonlocality in the considered organic molecules. In a first instance, for the dimer

case, as much of the known nonlocality metrics are well defined. A detailed analysis of these quantum properties has been developed as part of a master dissertation in the QuanTIC Group. Nowadays, Bell's nonlocality is not the unique way to prove nonlocality in quantum states and other criteria have been proposed, thus giving a new classification of nonlocality. On the other hand, the proper quantification of nonlocality in states of more than two particles is still an open question. Another interesting point to be explored is related to the link between entanglement and the observables associated to measurements in molecular spectroscopy. As it is known, fluorescence, for example, is related to the steady state of the density matrix elements, and thus it can be related to the entanglement supported by the evolved states. In this direction, very recently, a relation between Fisher information and susceptibility in condensed matter physics was derived, thus providing with a practical way of detecting multipartite entanglement [140].

Regarding quantum complexity, there is much work to do. We are currently computing our measure of complexity in another important set of states in quantum information theory, it is the set of W-like states that provides a different kind of entanglement than that one exhibited by the GHZ states. Relating our measure of complexity with the concept of correlations, each contributing term in our definition could be associated with the amount of total correlations in the state of a particular partition of the system, be it quantum or classical. In this regard, alternative definitions of complexity could be developed such that they are able to distinguish between classical correlations, entanglement or other form of quantum correlations. Another important point to deal with is the fact that a "measure of something" needs an operational interpretation so that it can be tested in the Lab. In our case, we look to forward develop an operational interpretation in the context of quantum metrology. We expect to relate our measure of complexity to the robustness of a state with phase estimation protocols. So far, Fisher information, that is arduously used in phase estimation theory, can not tell us how robust a state is in the protocol, e.g., GHZ and W-like states seem equally good. Hence, complexity as a weighted sum of contributions of Fisher information could, in principle, deal with this problem.

Appendix A
Markovian master equation

The derivation of the Markovian master equation (1.1.4) is typically made in the interaction picture. For doing it, Hamiltonian (1.1.1) is rewritten as

$$\hat{H}_{Full} = \hat{H}_0 + \hat{H}_{S\mathcal{E}}(t), \tag{A.0.1}$$

with $\hat{H}_0 = \hat{H}_S \otimes \mathbb{1}_{\mathcal{E}} + \mathbb{1}_S \otimes \hat{H}_{\mathcal{E}}$. The transformation from the Schrödinger to the interaction picture is defined, for some operator in $\mathcal{H}_{Full}$, by

$$\tilde{A}(t) = e^{\mathrm{i}\hat{H}_0 t} A(t) e^{-\mathrm{i}\hat{H}_0 t}.$$

Hence, the interaction picture version of the Liouville-von Neumann equation (1.1.2) is

$$\dot{\tilde{W}}(t) = -\mathrm{i}\left[\tilde{H}_{S\mathcal{E}}(t), \tilde{W}(t)\right], \tag{A.0.2}$$

or, in an integral form

$$\tilde{W}(t) = \tilde{W}(0) - \mathrm{i}\int_0^t dt' \left[\tilde{H}_{S\mathcal{E}}(t'), \tilde{W}(t')\right]. \tag{A.0.3}$$

Inserting eq. (A.0.3) into eq. (A.0.2) and tracing out over the environment, one finds

$$\dot{\tilde{\rho}}(t) = -\mathrm{i}\mathrm{Tr}_{\mathcal{E}}\left\{\left[\tilde{H}_{S\mathcal{E}}(t), \tilde{W}(0)\right]\right\} - \int_0^t dt' \mathrm{Tr}_{\mathcal{E}}\left\{\left[\tilde{H}_{S\mathcal{E}}(t), \left[\tilde{H}_{S\mathcal{E}}(t'), \tilde{W}(t')\right]\right]\right\}. \tag{A.0.4}$$

This equation is exact but still intractable. The first two approximations carried out on eq. (A.0.4) are: the initial factorable condition; $W(0) = \rho(0) \otimes \rho_{\mathcal{E}}(0) \equiv \rho(0)\rho_{\mathcal{E}}$, which means that at $t = 0$ there is not any correlation between the system and its environment. The Born (weak-coupling) approximation establishing that the system-environment interaction is weak such that only the system S follows a time evolution. It is written as

$$\tilde{W}(t') = \tilde{\rho}(t')\rho_{\mathcal{E}}. \tag{A.0.5}$$

Under these two assumptions, the master equation (A.0.4) leads

$$\dot{\tilde{\rho}}(t) = -\mathrm{i}\mathrm{Tr}_{\mathcal{E}}\left\{\left[\tilde{H}_{S\mathcal{E}}(t), \tilde{\rho}(0)\rho_{\mathcal{E}}\right]\right\} - \int_0^t dt' \mathrm{Tr}_{\mathcal{E}}\left\{\left[\tilde{H}_{S\mathcal{E}}(t), \left[\tilde{H}_{S\mathcal{E}}(t'), \tilde{\rho}(t')\rho_{\mathcal{E}}\right]\right]\right\}. \tag{A.0.6}$$

A further simplification of Eq. (A.0.6) is obtained doing the Markov approximation. It establishes that the time scale τ_R over the state of the system S evolves, is large compared with the time scale $\tau_{\mathcal{E}}$ over which the reservoir correlations decay. The corresponding changes in Eq. (A.0.6) are: $\tilde{\rho}(t')$ is replaced by $\tilde{\rho}(t)$. t' is changed by $t - t'$ and the upper integral limit is extended to infinity (This is permissible provided the integral disappears sufficiently fast for $t' \gg \tau_{\mathcal{E}}$) [74, 138].

The Markovian quantum master equation in the *Born-Markov approximation* is

$$\dot{\tilde{\rho}}(t) = -\mathrm{i}\mathrm{Tr}_{\mathcal{E}}\left\{\left[\tilde{H}_{S\mathcal{E}}(t), \tilde{\rho}(0)\rho_{\mathcal{E}}\right]\right\} - \int_0^\infty dt' \mathrm{Tr}_{\mathcal{E}}\left\{\left[\tilde{H}_{S\mathcal{E}}(t), \left[\tilde{H}_{S\mathcal{E}}(t-t'), \tilde{\rho}(t)\rho_{\mathcal{E}}\right]\right]\right\}. \quad \text{(A.0.7)}$$

To transform Eq. (A.0.7) to the form of Eq. (1.1.4), one writes in the Schrödinger picture, the most general form of the interaction Hamiltonian, which is

$$\hat{H}_{S\mathcal{E}} = \sum_k A_k \otimes B_k, \quad \text{(A.0.8)}$$

where A_k acts on $\mathcal{H}_S$ and B_k on $\mathcal{H}_{\mathcal{E}}$, respectively. For simplicity, one defines the operators

$$A_k(\omega) = \sum_{\epsilon'-\epsilon=\omega} \Pi(\epsilon) A_k \Pi(\epsilon'), \quad \text{(A.0.9)}$$

where ϵ's are the eigenvalues of $\hat{H}_S$ and $\Pi(\epsilon)$ the projection onto the eigenspace belonging to the eigenvalue ϵ. The sum is over eigenvalues ϵ and ϵ' with a fixed energy difference ω. From definition (A.0.9) one has:

$$\begin{aligned}
\left[\hat{H}_S, A_k(\omega)\right] &= -\omega A_k(\omega) \\
\left[\hat{H}_S, A_k^\dagger(\omega)\right] &= \omega A_k^\dagger(\omega) \\
\left[\hat{H}_S, A_k^\dagger(\omega) A_l(\omega)\right] &= 0.
\end{aligned} \quad \text{(A.0.10)}$$

The corresponding interaction picture operators following (A.0.10) are

$$\begin{aligned}
e^{\mathrm{i}\hat{H}_S t} A_k(\omega) e^{-\mathrm{i}\hat{H}_S t} &= e^{-\mathrm{i}\omega t} A_k(\omega) \\
e^{\mathrm{i}\hat{H}_S t} A_k^\dagger(\omega) e^{-\mathrm{i}\hat{H}_S t} &= e^{\mathrm{i}\omega t} A_k^\dagger(\omega),
\end{aligned}$$

with $A_k^\dagger \equiv A_k(-\omega)$. Thus, the interaction Hamiltonian in the interaction picture takes the form

$$\tilde{H}_{S\mathcal{E}}(t) = \sum_{k,\omega} e^{-\mathrm{i}\omega t} A_k(\omega) \otimes \tilde{B}_k(t) \equiv e^{-\mathrm{i}\omega t} A_k^\dagger(\omega) \otimes \tilde{B}_k^\dagger(t), \quad \text{(A.0.11)}$$

where $\tilde{B}_k(t) = e^{\mathrm{i}\hat{H}_{\mathcal{E}} t} B_k e^{-\mathrm{i}\hat{H}_{\mathcal{E}} t}$.

Inserting Eq. (A.0.11) into Eq. (A.0.7) one obtains

$$\dot{\tilde{\rho}}(t) = \sum_{\omega',\omega} \sum_{k,l} e^{\mathrm{i}(\omega'-\omega)t} \gamma_{kl}(\omega) \Big(A_l(\omega)\tilde{\rho}(t) A_k^\dagger(\omega') - A_k^\dagger(\omega') A_l(\omega)\tilde{\rho}(t) \Big) + \mathrm{H.c.} \quad \text{(A.0.12)}$$

Here, H.c. means the Hermitian conjugate of the expression. Note the first term in Eq. (A.0.7) has disappeared because of the assumption that the average of $\tilde{B}(t)$ vanishes, i.e.

$$< \tilde{B}_k(t) > \equiv tr\left\{\tilde{B}_k(t)\rho_{\mathcal{E}}\right\} = 0,$$

and the one-sided Fourier transform of the environment correlations

$$\gamma_{kl}(\omega) = \int_0^\infty dt' e^{\mathrm{i}\omega t'} < \tilde{B}_k^\dagger(t) \tilde{B}_l(t-t') > \quad \text{(A.0.13)}$$

has been introduced. Supposing $\rho_{\mathcal{E}}$ is a stationary state of the environment ($[\hat{H}_{\mathcal{E}}, \rho_{\mathcal{E}}] = 0$) the environment correlation functions are homogeneous in time:

$$< \tilde{B}_k^\dagger(t)\tilde{B}_l(t-t') >=< \tilde{B}_k^\dagger(t')\tilde{B}_l(0) >,$$

showing that the quantities $\gamma_{kl}(\omega)$ are time-independent.

In Eq. (A.0.12), $|\omega - \omega'|^{-1}$ defines the typical time scale of the intrinsic evolution of the system S. When this time scale is very quick compared to the relaxation time scale τ_R of the open system, the non-secular terms, i.e., terms for which $\omega' \neq \omega$ can be neglected. This is the rotating wave approximation. Hence,

$$\dot{\tilde{\rho}}(t) = \sum_{\omega} \sum_{k,l} \gamma_{kl}(\omega) \Big(A_l(\omega)\tilde{\rho}(t)A_k^\dagger(\omega') - A_k^\dagger(\omega')A_l(\omega)\tilde{\rho}(t) \Big) + \text{H.c.} \tag{A.0.14}$$

By writing the Fourier transform (A.0.13) as $\gamma_{kl}(\omega) = (1/2)\Gamma_{kl}(\omega) + \mathrm{i}S_{kl}(\omega)$ for fixed ω, the interaction picture master equation leads to

$$\dot{\tilde{\rho}}(t) = -\mathrm{i}\big[H_{\text{Coh}}, \tilde{\rho}(t)\big] - \sum_{\omega} \sum_{k,l} \frac{\Gamma_{kl}(\omega)}{2} \Big(\big\{ A_k^\dagger(\omega')A_l(\omega), \tilde{\rho}(t) \big\} - 2A_l(\omega)\tilde{\rho}(t)A_k^\dagger(\omega') \Big), \tag{A.0.15}$$

where $H_{\text{Coh}} = \sum_{\omega} \sum_{k,l} S_{kl}(\omega) A_k^\dagger(\omega) A_l(\omega)$ has a diagonal part known as the Lamb shift, and non-diagonal coherences induced by the environment ($l \neq k$).

The master equation (A.0.15) is brought into the Lindblad form (1.1.4) by turning back to the Schrödinger picture and by diagonalization of matrices $\Gamma_{kl}(\omega)$. Finally, the first term in the right hand side of Eq. (A.0.15) comprises the energies of the bare open system and the coherent effects such as interactions (the physical interaction experienced by the system considered in this Thesis is the d-d interaction). This term also contains the interaction of the open system with coherent fields as it is the case of the continuous laser included throughout this Thesis. The dissipative part is all covered by the second term of the right hand side of Eq. (A.0.15) that in the model used in this Thesis reduces to the relaxation rates, also known as the spontaneous emission of the considered qubits, and to the collective damping rate.

Appendix B
Quantum nonlocality-related properties

A general finite-dimensional bipartite AB system is represented by a density matrix or quantum state $\rho \in D(\mathbb{C}^{d_A} \otimes \mathbb{C}^{d_B})$, with $d_A, d_B \geq 2$, where $D(\mathcal{H}) := \{\rho \in PSD(\mathcal{H}) | \mathrm{Tr}(\rho) = 1\}$ stands for the set of density matrices of the complex Hilbert space $\mathcal{H}$, with PSD the set of *positive semidefinite* complex matrices, i.e., the matrices ρ such that $\forall\, |\phi\rangle \in \mathcal{H} : \langle\phi|\, \rho\, |\phi\rangle \geq 0$. Here, we focus on the quantum properties of our two-qubit input states $\rho_{in}(\delta, p)$ (4.2.1) as shown in Fig. 4.4, where we have emphasised the projective-locality region ($p \leq p_L$) which is limited by the value $p_L \approx 0.6009$ (vertical line), according to the best known bound [116]. The aforementioned nonlocal quantum features of the input states plotted in Fig. 4.4 for performing the PD game are described as follows.

CHSH-Nonlocality. Given $\rho \in D(\mathbb{C}^2 \otimes \mathbb{C}^2)$, the Clauser-Horne-Shimony-Holt (CHSH) inequality [117] considers two dichotomic observables per party (eigenvalues ± 1), namely (A_1, A_2, B_1, B_2), and it takes the form:

$$|B_\rho(A_1, A_2, B_1, B_2)| \quad := \quad |E_{11} + E_{12} + E_{21} - E_{22}| \leq 2, \tag{B.0.1}$$

where $E_{ij} := \mathrm{Tr}\left[(A_i \otimes B_j)\, \rho\right]$, $i, j = 1, 2$. It is said that ρ violates the CHSH inequality if and only if $M(\rho) := \mu + \widetilde{\mu} > 1$, where $\mu, \widetilde{\mu}$ are the biggest two eigenvalues of the matrix $U_\rho := T_\rho^T T_\rho \in M_{3\times 3}(\mathbb{R})$, with $T_\rho := [t_{nm}] \in M_{3\times 3}(\mathbb{R})$, with elements $t_{nm} := \mathrm{Tr}[\rho(\sigma_n \otimes \sigma_m)]$, σ_k, $k = 1, 2, 3$, the Pauli matrices. This arises from the fact that $\max B_\rho := |\max_{A_1,A_2,B_1,B_2} B_\rho| = 2\sqrt{M(\rho)}$ [118]. Then, using the Tsirelson's bound [119], $\max B_\rho \leq 2\sqrt{2}$, it follows $0 \leq M(\rho) \leq 2$, showing nonlocality in the interval $1 < M(\rho) \leq 2$. Instead of $M(\rho)$, we could work with $B(\rho) := \sqrt{\max\{0, M(\rho) - 1\}}$ given that, for pure states, the former equals the concurrence: $C(|\psi\rangle) = B(|\psi\rangle)$ [120]. However, in order to have a direct comparison with $\mathcal{E}$, in Fig. 4.4(b), we compute nonlocality through the CHSH inequality, by plotting $\mathrm{CHSH}(\rho) := h([1 + \sqrt{1 - B(\rho)^2}]/2)$, where $h(x)$ is the binary entropy.

k-copy nonlocality (superactivation). Given $\rho \in D(\mathbb{C}^2 \otimes \mathbb{C}^2)$, if ρ is useful to teleportation then is k-copy nonlocal, i.e., ρ admits *superactivation* of nonlocality [32, 33]. Usefulness to teleportation can be numerically tested by computing the Fidelity of Teleportation, which can be written as $\mathcal{F}(\rho) = \frac{2F(\rho)+1}{3}$, where F denotes the Fully Entangled Fraction [121], which for two qubits reads $F(\rho) = \max\{\eta_i, 0\}$, with η_i's the eigenvalues of the matrix $M = [M_{mn}]$, of elements $M_{mn} = \mathrm{Re}\left(\langle\psi_m|\, \rho\, |\psi_n\rangle\right)$, and $\{|\psi_n\rangle\}$ the so-called magic basis $|\psi_{ab}\rangle := i^{(a+b)}(|0, b\rangle + (-1)^a\, |1, 1 \oplus b\rangle)/\sqrt{2}$ [122]. ρ is useful to teleportation if and only if $\mathcal{F} > 2/3$ [121]. In our case, as shown in Fig. 4.4(b), the set of states that can be superactivated coincides with the whole set of entangled states (although this fact does not hold in general).

Activation of nonlocality through tensoring and local filtering. Given $\rho \in D(\mathbb{C}^{d_1} \otimes \mathbb{C}^{d_2})$ for subsystems A and B with arbitrary dimensions d_1 and d_2 respectively and, defining P_{CHSH} as the set of states that do not violate the CHSH inequality, even after local filtering, we say that $\rho \in P_{CHSH}$ admits *activation* of nonlocality through tensoring and local filtering [115] if there exists a state $\tau_\rho \in P_{CHSH}$ such that $\rho \otimes \tau_\rho \notin P_{CHSH}$. The latter is equivalent to have $\mathrm{Tr}\left(\tau_\rho \left(\rho^{\mathrm{T}} \otimes H_{\pi/4}\right)\right) < 0$, with $H_{\pi/4} := \mathbb{I}_2 \otimes \mathbb{I}_2 - \frac{1}{\sqrt{2}}(\sigma_x \otimes \sigma_x + \sigma_z \otimes \sigma_z)$, with T denoting transposition [115]. A theorem [115] establishes the existence of such matrices τ_ρ in the space $D\big(\bigotimes_{i=1}^{2}(\mathbb{C}^{d_i} \otimes \mathbb{C}^2)\big)$ for any entangled ρ. Although the existence of such a matrix τ_ρ is already guaranteed, the theorem does not explicitly tell us how to calculate it. We have numerically tested this activation [115] by looking for a state τ_ρ with positive partial transpose with respect to the first subsystem, $\tau_\rho^{T_1} \geq 0$ (say $\mathbb{C}^{d_A} \otimes \mathbb{C}^2$) [79, 123], since this implies $\tau_\rho \in P_{CHSH}$ [124]. Thus, we solved the optimisation problem $\sigma(\rho) := \min_{\tau_\rho} \mathrm{Tr}\left(\tau_\rho \left(\rho^{\mathrm{T}} \otimes H_{\pi/4}\right)\right)$ under constrains $\tau_\rho \geq 0 \ \wedge \ \tau_\rho^{T_1} \geq 0$ [115]. Even though the considered activation of the nonlocality region covers the whole entangled states [115], the region for which we are indeed able to find the ancillary matrix required for the activation is represented by the cyan solid area (which covers the CHSH inequality violation region) in Fig. 4.4(b).

Papers

The principal papers whose results are presented in this Thesis are:

1. John H. Reina, **Cristian E. Susa** and Felipe F. Fanchini, 2014, "Extracting information from qubit-environment correlations", *Scientific Reports* 4, 7443.

2. **Cristian E. Susa**, John H. Reina and Richard Hildner, 2014, "Plasmon-assisted quantum control of distant emitters", *Physics Letters A* 378, 2371.

3. **Cristian E. Susa**, John H. Reina and Luis L. Sánchez-Soto, 2013, "Correlations in emitters coupled to plasmonic waveguides", *Journal of Physics B* 46, 224022.

4. Carlos A. Melo, **Cristian E. Susa**, Andrés Ducuara, Astrid Barreiro and John H. Reina, 2017, "Quantum locality in game strategy", *Sci. Rep.* **7**, 44730 (2017).

5. Davide Girolami, **Cristian E. Susa** and Tomasso Tuffareli, 2016, "Quantum states are more complex than classical ones", to be submitted.

As further work developed during my doctoral studies, I also coauthored the following papers:

6. Andrés Ducuara, **Cristian E. Susa** and John H. Reina, 2016 (September), "PBR theorem under noisy channels", submitted to *Journal of Physics A*.

7. (In spanish) **Cristian E. Susa** and John H. Reina, 2013, "Coherence and entanglement in non-Markovian dynamics of qubits", *Universitas Scientiarum* 18:2, 141.

Participation in conferences

1. **Cristian E. Susa** and John. H. Reina, Quantum control and information processing in organic dimers/trimers, *Workshop I: Optical and Molecular Spectroscopy*, Universidad del Valle, Cali, Colombia, 14-18 March (2016).

2. **Cristian E. Susa** *et al.* Quantum locality in game strategies, *XIV ENO & V CANCOA*, Universidad del Valle, Cali, Colombia, 16-20 November (2015).

3. **Cristian E. Susa** and Davide Girolami, Quantifying complexity in quantum systems, *XXVI National Physics Congress*, Universidad Nacional de Colombia, Sede Manizales, Colombia, 29 September-02 October (2015).

4. Davide Girolami and **Cristian E. Susa**, Quantum systems are more complex than classical ones, *British Mathematical/Applied Mathematical Colloquium*, University of Cambridge, Cambridge, England, 30 March-02 April (2015).

5. John H. Reina, **Cristian E. Susa** and Felipe F. Fanchini, Quantum information flow: qubit-qubit and qubit-environment correlations, *International Workshop on Quantum Coherence and Decoherence II*, Universidad de Antioquia, Medellín, Colombia, 25-29 August (2014).

6. **Cristian E. Susa**, John H. Reina and Felipe F. Fanchini, Maximizing information flow between coupled qubits under dissipation, *Escuela de Física Matemática: The Mathematics of Entanglement*, Universidad de los Ándes, Bogotá, Colombia, 27-31 May (2013).

7. **Cristian E. Susa**, John H. Reina and Richard Hildner, Plasmon-assisted quantum correlations in distant emitters, *International Conference on Squeezed States and Uncertainty Relations*, Max Planck Institute for the Science of Light, Hotel Sheraton-Carlton, Nuremberg, Germany, 24-28 July (2013).

8. **Cristian E. Susa**, John H. Reina and Luis L. Sánchez-Soto, Plasmon-assisted switching of correlations in distant emitters, *International Workshop on Quantum Coherence and Decoherence I*, Universidad del Valle, Cali, Colombia, 24-28 September (2012).

9. **Cristian E. Susa** and John H. Reina, Dissipative dynamics of correlations in emitters coupled to plasmonic waveguides, *Workshop on Quantum Correlations: Entanglement, Discord and Beyond*, Brazilian National Institute for Science and Technology in Quantum Information (Poster), Natal, Brasil, 13-15 June (2012).

Bibliography

[CS1] C. E. Susa, and J. H. Reina, Nonlocal fluctuations and control of dimer entanglement dynamics. *Phys. Rev. A* **82**, 042102 (2010).

[CS2] C. E. Susa and J. H. Reina, Correlations in optically controlled quantum emitters, *Phys. Rev. A* **85**, 022111 (2012).

[CS3] C. E. Susa, J. H. Reina, and L. L. Sánchez-Soto, Correlations in emitters coupled to plasmonic waveguides, J. Phys. B **46**, 224022 (2013).

[CS4] C. E. Susa, J. H. Reina and R. Hildner, Plasmon-assisted quantum control of distant emitters. *Phys. Lett. A* **378**, 2371-2376 (2014).

[CS5] J. H. Reina, C. E. Susa and F. F. Fanchini, Extracting information from qubit-environment correlations, *Sci. Rep.* **4**, 7443 (2014).

[CS6] C. A. Melo, C. E. Susa, A. Ducuara, A. Barreiro and J. H. Reina, Quantum locality in game strategy, *Sci. Rep.* **7**, 44730 (2017).

[CS7] C. E. Susa and J. H. Reina, "Coherence and entanglement in non-Markovian dynamics of qubits", *Universitas Scientiarum* **18**:2, 141 (2013).

[1] D. Deutsch, Quantum theory, the Church-Turing principle and the universal quantum computer. *Proc. Roy. Soc. Lond. A* **400**, 97-117 (1985).

[2] C. Bennett and D. DiVincenzo, Quantum information and computation, *Nature* **404**, 247 (2000).

[3] M. A. Nielsen and I. L. Chuang, *Quantum Computation and Quantum Information*, Cambridge University Press (2000).

[4] T. D. Ladd, F. Jelezko, R. Laflamme, Y. Nakamura, C. Monroe, and J. L. O'Brien, Quantum Computers, *Nature* **464**, 45 (2010).

[5] E. Knill, Physics: Quantum computing, *Nature* **463**, 441-443 (2010).

[6] R. Horodecki, P. Horodecki, M. Horodecki and K. Horodecki, Quantum Entanglement, *Rev. Mod. Phys.* **81** 865 (2009).

[7] F. De Martini, F. Sciarrino and C. Vitelli, Entanglement test in a microscopic-macroscopic system, *Phys. Rev. Lett.* **100**, 253601(2008); E. Pomarico, B. Sanguinetti, P. Sekatski, H. Zbinden and N. Gisin, Experimental amplification of an entangled photon: what if the detection loophole is ignored? *New J. Phys.* **13**, 063031 (2011).

[8] E. Togan, *et al.* Quantum entanglement between an optical photon and a solid-state spin qubit, *Nature* **466**, 730-734 (2010).

[9] B Julsgaard, A. Koshekin and E. S. Polzik, Experimental long-lived entanglement of two macroscopic objects, *Nature* **413**, 400-403 (2001).

[10] N. Brunner, D. Cavalcanti, S. Pironio, V. Scarani and S. Wehner, Bell nonlocality. *Rev. Mod. Phys.* **86**, 419-478 (2014).

[11] H. Buhrman, Ł. Czekajd, A. Grudka, M. Horodecki, P. Horodecki, M. Markiewicz, F. Speelman and S. Strelchuk, Quantum communication complexity advantage implies violation of a Bell inequality, *PNAS* **113**, 3191-3196 (2016).

[12] E. Knill and R. Laflamme, Power of one bit of quantum information, *Phys. Rev. Lett.* **81**, 5672-5675 (1998).

[13] A. Datta, A. Shaji, and C. M. Caves, Quantum discord and the power of one bit, *Phys. Rev. Lett.* **100**, 050502 (2008); V. Madhok and A. Datta, Quantum discord as a resource of quantum communication, *Int. J. Mod. Phys. B* **27**, 1245041 (2013).

[14] K. Modi, A. Brodutch, H. Cable, T. Paterek and V. Vedral, The classical-quantum boundary for correlations: Discord and related measures. *Rev. Mod. Phys.* **84**, 1655-1707 (2012).

[15] G. Adesso, T. R. Bromley, M. Cianciaruso, Measures and applications of quantum correlations, *J. Phys. A* **49**, 473001 (2016).

[16] W. K. Wootters, Entanglement of formation of an arbitrary state of two qubits, *Phys. Rev. Lett.* **80**, 2245-2248 (1998).

[17] A. Ferraro, L. Aolita, D. Cavalcanti, F. M. Cucchietti, and A. Acín, Almost all quantum states have nonclassical correlations, *Phys. Rev. A* **81**, 052318 (2010).

[18] T. Schreiber, Measuring information transfer. *Phys. Rev. Lett.* **85**, 461-464 (2000).

[19] M. Prokopenko, and J. T. Lizier, Transfer entropy and transient limits of computation. *Sci. Rep.* **4**, 5394 (2014).

[20] W. H. Zurek, Decoherence, einselection, and the quantum origins of the classical. *Rev. Mod. Phys.* **75**, 715-775 (2003).

[21] J. H. Reina, L. Quiroga, and N. F. Johnson, Decoherence of quantum registers. *Phys. Rev. A* **65**, 032326 (2002); C. Wang, and Q.-H. Chen, Exact dynamics for quantum correlations of two qubits coupled to bosonic baths. *New J. Phys.* **15**, 103020 (2013).

[22] W. G. Unruh, Maintaining coherence in quantum computers. *Phys. Rev. A* **51**, 992-997 (1995).

[23] D. Aharonov, A. Kitaev and J. Preskill, Fault-tolerant quantum computation with long-range correlated noise. *Phys. Rev. Lett.* **96**, 050504 (2006).

[24] J. Preskill, Sufficient condition on noise correlations for scalable quantum computing. *Quant. Inf. Comput.* **13**, 0181-0194 (2013).

[25] R. Hanson, L. P. Kouwenhoven, J. R. Petta, S. Tarucha, and L. M. K. Vandersypen, Spins in few-electron quantum dots, *Rev. Mod. Phys.* **79**, 1217 (2007); K. Roszak, P. Mazurek, and P. Horodecki, Anomalous decay of quantum correlations of quantum-dot qubits, *Phys. Rev. A* **87**, 062308 (2013).

[26] Y. Makhlin, G. Schön, and A. Shnirman, Quantum-state engineering with Josephson-Junction devices, *Rev. Mod. Phys.* **73**, 357 (2001); M. Herrera and J. H. Reina, Quantum entanglement and correlations in superconducting flux qubits, *J. Supercod. Nov. Magn.* **25**, 2149 (2014).

[27] J. M. Raimod, M. Brune, and S. Haroche, Manipulating quantum entanglement with atoms and photons in a cavity, *Rev. Mod. Phys.* **793** (2001) 565; C. Monroe, Quantum information processing with atoms and photons, *Nature* **416** (2002) 238.

[28] M. Thorwart, J. Eckel, J. H. Reina, P. Nalbach, and S. Weiss, Enhanced quantum entanglement in the non-Markovian dynamics of biomolecular excitons. *Chem. Phys. Lett.* **478**, 234 (2009).

[29] H. Ollivier and W. H. Zurek, Quantum discord: A measure of the quantumness of correlations, *Phys. Rev. Lett.* **88**, 017901 (2001).

[30] L. Henderson and V. Vedral, Classical, quantum and total correlations, *J. Phys. A* **34**, 6899 (2001).

[31] N. Brunner, and N. Linden, Connection between Bell nonlocality and Bayesian game theory, *Nat. Commun.* **4**, 2057 (2013).

[32] C. Palazuelos, Superactivation of quantum nonlocality, *Phys. Rev. Lett.* **109**, 190401 (2012).

[33] D. Cavalcanti, A. Acín, N. Brunner and T. Vértesi, All quantum states useful for teleportation are nonlocal resources, *Phys. Rev. A* **87**, 042104 (2013).

[34] E. Lang, R. Hildner, H. Engelke, P. Osswald, F. Würthner, and J. Köhler, Comparison of the photophysical parameters for three Perylene Bisimide derivatives by single-molecule spectroscopy, *Chem. Phys. Chem.* **8**, 1487 (2007).

[35] A. Issac, R. Hildner, C. Hippius, F. Würthner, and J. Köhler, Stepwise decrease of fluorescence versus sequential photobleaching in a single multichromophoric system, *ACS NANO* **8**, 1708-1717 (2014).

[36] R. Hildner, D. Brinks, and N. F. van Hulst, Femtosecond coherence and quantum control of single molecules at room temperature, *Nature Phys.* **7**, 172 (2011).

[37] B. Bellomo, R. Lo Franco and G. Compagno, Non-Markovian effects on the dynamics of entanglement, *Phys. Rev. Lett.* **99**, 160502 (2007).

[38] T. Yu and J. H. Eberly, Sudden death of entanglement, *Science* **323**, 598-601 (2009).

[39] T. Yu and J. H. Eberly, Finite-Time disentanglement via spontaneous emission. *Phys. Rev. Lett.* **93**, 140404 (2004); *ibid.*, Quantum open system theory: Bipartite aspects, *Phys. Rev. Lett.* **97**, 140403 (2006).

[40] M, Gessner and H-P. Breuer, Detecting nonclassical system-environment correlations by local operations. *Phys. Rev. Lett.* **107**, 180402 (2011).

[41] K. Modi, Operational approach to open dynamics and quantifying initial correlations. *Sci. Rep.* **2**, 581 (2012).

[42] M. Gessner, M. Ramm, T. Pruttivarasin, A. Buchleitner, H-P. Breuer and H. Häffner, Local detection of quantum correlations with a single trapped ion. *Nat. Phys.* **10**, 105-107 (2014).

[43] A. Z. Chaudhry, and J. Gong, Amplification and suppression of system-bath-correlation effects in an open many-body system. *Phys. Rev. A* **87**, 012129 (2013); *ibid.* Role of initial system-environment correlations: A master equation approach. *Phys. Rev. A* **88**, 052107 (2013).

[44] L. Mazzola, C. A. Rodríguez-Rosario, K. Modi and M. Paternostro, Dynamical rule of system-environment correlations in non-Markovian dynamics. *Phys. Rev. A* **86**, 010102(R) (2012).

[45] C. Hettich, C. Schmitt, J. Zitzmann, S. Kühn, I. Gerhardt and V. Sandoghdar, Nanometer resolution and coherent optical dipole coupling of two individual molecules, *Science* **298**, 385-389 (2002).

[46] J.H. Reina, R. G. Beausoleil, T. P. Spiller and W. J. Munro, Radiative corrections and quantum gates in molecular systems, *Phys. Rev. Lett.* **93**, 250501 (2004).

[47] D. E. Chang, S. Sorensen, P. R. Hemmer and M. D. Lukin, Quantum optics with surface plasmons, *Phys. Rev. Lett* **97**, 053002 (2006).

[48] J. H. Reina, L. Quiroga and N. F. Johnson, NMR-based nanostructure switch for quantum logics, *Phys. Rev. B* **62**, R2267(R) (2000).

[49] J. H. Reina, L. Quiroga and N. Johnson, Quantum entanglement and information processing via excitons in optically driven quantum dots, *Phys. Rev. A* **62**, 012305 (2000); B. Lovett, J. H. Reina, A. Nazir and A. Briggs, Optical schemes for quantum computation in quantum dot molecules, *Phys. Rev. B* **68**, 205319 (2003).

[50] S. A. Maier, *Plasmonic: fundamentals and applications*, Springer New York, USA (2007)

[51] W. L. Barnes, A. Dereux and T. W. Ebbesen, Surface plasmon subwavelength optics, *Nature* **424**, 824-830 (2003).

[52] M. I. Stockman, Nanoplasmonics: the physics behind the applications, *Phys. Today* **64**, 39 (2011).

[53] A. V. Akimov *et al.*, Generation of single optical plasmons in metallic nano wires coupled to quantum dots, *Nature* **450**, 402-406 (2007).

[54] R. Kolesov *et al.*, Wave-particle duality of single surface plasmon polaritons, *Nature Phys.* **5**, 470-474 (2009).

[55] A. G. Curto, G. Volpe, T. H. Taminiau, M. P. Kreuzer, R. Quidant and N. F. van Hulst, Unidirectional emission of a quantum dot coupled to a nanoantenna, *Science* **329**, 930-933 (2010).

[56] D. Martín-Cano, L. Martín-Moreno, F. J. García-Vidal, and E. Moreno, Resonance energy transfer and superradiance mediated by plasmonic nanowaveguides, *Nano Lett.* **10**, 3129-3134 (2010).

[57] R. F. Oulton, G. Bartal, D. F. P. Pile, and X. Zhang, Confinement and propagation characteristics of subwavelendth plasmonic modes, *New J. Phys.* **10**, 105018 (2008).

[58] D. Dzsotjan, J. Kästel, and M. Fleischhauer, Dipole-dipole shift of quantum emitters coupled to surface plasmons of a nanowire, *Phys. Rev. B* **84**, 075419 (2011); D. Dzsotjan, A. S. Sorensen, and M. Fleischhauer, Quantum emitters coupled to surface plasmons of a nanowire: A Green's function approach, *Phys. Rev. B* **82**, 075427 (2010).

[59] A. González-Tudela, D. Martín-Cano, E. Moreno, L. Martín-Moreno, C. Tejedor and F. J. García-Vidal, Entanglement of two qubits mediated by one-dimensional plasmonic waveguides, *Phys. Rev. Lett.* **106**, 020501 (2011); *ibid.* Dissipation-driven generation of two-qubit entanglement mediated by plasmonic waveguides, *Phys. Rev. B.* **84**, 235306 (2011).

[60] D. A. Meyer, Quantum strategies, *Phys. Rev. Lett.* **82,**, 1052 (1999).

[61] J. Eisert, M. Wilkens, and M. Lewenstein, Quantum games and quantum strategies, *Phys. Rev. Lett.* **83**, 3077 (1999).

[62] A. Pappa, *et al.*, Nonlocality and conflicting interest games, *Phys. Rev. Lett.* **114**, 020401 (2015).

[63] A. Iqbal, and D. Abbott, Constructing quantum games from a system of Bell's inequalities, *Phys. Lett. A* **374**, 3155 (2010).

[64] S. Zhang, S. Quantum strategic game theory, *Proceeding of the 3rd Innovations in Theoretical Computer Science Conference* pp. 39-59, Cambridge, Massachusetts (2012); Doi:10.1145/2090236.2090241.

[65] R. B. Meyerson, *Game Theory: An Analysis of Conflict*, MIT Press, Cambridge (1991).

[66] M. J. Osborne, *An Introduction to Game Theory*, Oxford University Press, Oxford (2002).

[67] G. Tononi, O. Sporns, and G. M. Edelman, A measure for brain complexity: Relating functional segregation and integration in the nervous system, *Proc. Natl. Aca. Sci.* **91**, 5033 (1994).

[68] M. Studený, Multiinformation and the problem of characterization of conditional independence relations, *Problems of Control and Information Theory* **18**(1), 3-16 (1989).

[69] S. Amari, Information geometry of hierarchy of probability distributions, *IEEE Trans. IT* **47**, 1701-1711 (2001).

[70] S. Lloyd, Measures of Complexity: a non–exhaustive list, *http://web.mit.edu/esd.83/www/notebook/Complexity.PDF*

[71] A. Einstein, B. Podolsky, and N. Rosen, Can Quantum-Mechanical Description of Physical Reality Be Considered Complete?, *Phys. Rev.* **47**, 777-780 (1935).

[72] C. Zu, Y-X. Wang, X-Y. Chang, Z-H. Wei, S-Y. Zhang and L-M. Duan, Experimental demonstration of quantum gain in a zero-sum game, *New J. Phys.* **14**, 033002 (2012).

[73] U. Weiss, *Quantum Dissipative Systems*, 2nd ed., World Scientific, Singapore (1999).

[74] H. P. Breuer and F. Petruccione, *The Theory of Open Quantum Systems*, Oxford University Press, Oxford (2002).

[75] S. Hamieh, R. Kobes and H. Zaraket, Positive-operator-valued measure optimization of classical correlations, *Phys. Rev. A* **70**, 052325 (2004).

[76] B. Groisman, S. Popescu, and A. Winter, Quantum, classical, and total amount of correlations in a quantum state, *Phys. Rev. A.* **72**, 032317 (2005).

[77] A. Issac, R. Hildner, D. Ernst, C. Hippius, F. Würthner, and J. Köhler, Single molecule studies of calix[4]arene-linked perylene bisimide dimers: relationship between blinking, lifetime and/or spectral fluctuations,

[78] W. Dür, G. Vidal, and J. I. Cirac, Three qubits can be entangled in two inequivalent ways, *Phys. Rev. A* **62**, 062314 (2000).

[79] A. Peres, Separability Criterion for Density Matrices, *Phys. Rev. Lett.* **77**, 1413-1415 (1996).

[80] G. Vidal, and R. F. Werner, Computable measure of entanglement, *Phys. Rev. A* **65**, 032314 (2002).

[81] P. Agrawal, and A. Pati, Perfect teleportation and superdense coding with W states, *Phys. Rev. A* **74**, 062320 (2006).

[82] A. T. Haedler, *et. al.*, Long-Range Energy Transport in Single Supramolecular Nanofibres at Room Temperature, *Nature* **523**, 196-199 (2015).

[83] F. F. Fanchini, M. F. Cornelio, M. C. de Oliveira and A. O. Caldeira, Conservation law for distributed entanglement of formation and quantum discord. *Phys. Rev. A* **84**, 012313 (2011).

[84] G. L. Giorgi, Monogamy properties of quantum and classical correlations. *Phys. Rev. A* **84**, 054301 (2011).

[85] A. Sen, D. Sarkar and A. Bhar, Monogamy of measurement-induced nonlocality. *J. Phys. A* **45**, 405306 (2012).

[86] A. Streltsov, G. Adesso, M. Piani and D. Bruss, Are general quantum correlations monogamous?. *Phys. Rev. Lett.* **109**, 050503 (2012).

[87] Sudha, A. R. Usha Devi and A. K. Rajagopal, Monogamy of quantum correlations in three-qubit pure states. *Phys. Rev. A* **85**, 012103 (2012).

[88] K. Salini, R. Prabhu, A. Sen(De) and U. Sen, Monotonically increasing functions of any quantum correlation can make all multiparty states monogamous. *Ann. Phys.* **348**, 297-305 (2014).

[89] V. Coffman, J. Kundu and W. K. Wootters, Distributed entanglement. *Phys. Rev. A* **61**, 052306 (2000).

[90] M. Koashi and A. Winter, Monogamy of quantum entanglement and other correlations. *Phys. Rev. A* **69**, 022309 (2004).

[91] C. H. Bennett, D. P. DiVincenzo, J. A. Smolin and W. K. Wootters, Mixed-state entanglement and quantum error correction, *Phys. Rev. A* **54**, 3824-3851 (1996).

[92] T. J. Osborne and F. Verstraete, General monogamy inequality for bipartite qubit entanglement. *Phys. Rev. Lett.* **96**, 220503 (2006).

[93] K. Berrada, F. F. Fanchini and S. Abdel-Khalek, Quantum correlations between each qubit in a two-atom system and the environment in terms of interatomic distance. *Phys. Rev. A* **85**, 052315 (2012).

[94] M. Horodecki, J. Oppenheim and A. Winter, Partial quantum information. *Nature* **436**, 673-676 (2005).

[95] F. F. Fanchini, L. K. Castelano, M. F. Cornelio and M. C. de Oliveira, Locally inaccessible information as a fundamental ingredient to quantum information, *New J. Phys.* **14**, 013027 (2012).

[96] F. F. Fanchini, *et al.* Non-Markovianity through accessible information. *Phys. Rev. Lett.* **112**, 210402 (2014).

[97] S. I. Bozhevolnyi, V. S. Volkov, E. Devaux, J-Y. Laluet, and T. W. Ebbesen, Channel plasmon subwavelength waveguide components including interferometers and ring resonators, *Nature* **440**, 508 (2006).

[98] H. Ditlbacher, J. R. Krenn, A. Leitner, and F. R. Aussenegg, Surface plasmon polariton-based optical beam profiler, *Opt. Lett.* **29** (2004) 1408-1410.

[99] D. K. Gramotnev, Adiabatic nanofocusing of plasmons by sharp metallic grooves: Geometrical optics approach, J. Appl. Phys. **98**, 104302 (2005).

[100] T. Hümmer, F. J. García-Vidal, L. Martín-Moreno, and D. Zueco, Weak and strong coupling regimes in plasmonic QED, Phys. Rev. B **87**, 115419 (2013).

[101] A. González-Tudela, P. A. Huidobro, L. Martín-Moreno, C. Tejedor, and F. J. García-Vidal, Theory of strong coupling between quantum emitters and propagating surface plasmons, Phys. Rev. Lett. **110**, 126801 (2013).

[102] K. C. Vernon, *Strongly localised plasmons in metallic nanostructures*, Ph.D. Thesis, Queensland University of Technology, Australia (2008).

[103] D. M. Cano, *Plasmonic waveguides: classical applications and quantum phenomena*, Ph.D. Thesis, Universidad Autónoma de Madrid, Spain (2013).

[104] K. Modi, T. Paterek, W. Son, V. Vedral, and M. Williamson, Unified View of quantum and classical correlations, *Phys. Rev. Lett.* **104**, 080501 (2010).

[105] U. Fano, Pairs of two-level systems, *Rev. Mod. Phys.* **55** 855-874 (1983); *ibid.* Description of states in quantum mechanics by density matrix and operator techniques, *Rev. Mod. Phys.* **29** 74-93 (1957).

[106] S. Luo, Quantum discord for two-qubit systems, *Phys. Rev. A* **77**, 042303 (2008).

[107] G. Lindblad, *Quantum entropy and quantum measurements*, Lecture notes in physics Vol *378*, (eds. Bendjaballah C. *et al.*) 71-78, Springer (1991).

[108] S. Luo and Q. Zhang, Observable correlations in two-qubit states, *J. Stat. Phys.* **136**, 165-177 (2009).

[109] N. P. de Leon, *et al*. Tailoring light-matter interaction with a nanoscale plasmon resonator, *Phys. Rev. Lett.* **108**, 226803 (2012).

[110] S. Kumar, A. Huck and U. L. Andersen, Efficient coupling of a single diamond color center to propagating plasmonic gap modes, *Nano Lett.* **13**, 1221-1225 (2013).

[111] Y. L. A. Rezus, *et al*, Single-photon spectroscopy of a single molecule, *Phys. Rev. Lett.* **108**, 093601 (2012).

[112] J. Du, *et al.*, Experimental realization of quantum games on a quantum computer, *Phys. Rev. Lett.* **88**, 137902 (2002).

[113] R. Prevedel, A. Stefavov, P. Whalter, and A. Zeilinger, Experimental realization of a quantum game on a one-way quantum computer, *New J. Phys.* **9**, 205 (2007).

[114] C. Zu, *et al.*, Experimental demonstration of quantum gain in a zero-sum game, *New J. Phys.* **14**, 033002 (2012).

[115] Y. C. Liang, L. Masanes, and D. Rosset, All entangled states display some hidden nonlocality, *Phys. Rev. A* **86**, 052115 (2012).

[116] Acín, A., Gisin, N. and Toner, B. Grothendieck's constant and local models for noisy entangled quantum states. *Phys. Rev. A* **73,** 062105 (2006).

[117] J. F. Clauser, M. A. Horne, A. Shimony, and R. Holt, Proposed experiment to test local hidden-variable theories, *Phys. Rev. Lett.* **23**, 880 (1969).

[118] R. Horodecki, P. Horodecki, and M. Horodecki, Violating Bell inequality by mixed spin-$1/2$ states: necessary and sufficient condition, *Phys. Lett. A* **200**, 340-344 (1995).

[119] B. S. Cirel'son, Quantum generalizations of Bell's inequality, *Lett. Math. Phys.* **4**, 93 (1980).

[120] A. Miranowicz, Violation of Bell inequality and entanglement of decaying Werner states, *Phys. Lett. A* **327**, 272 (2004).

[121] M. Horodecki, P. Horodecki, and R. Horodecki, General teleportation channel, singlet fraction, and quasidistillation, *Phys. Rev. A* **60**, 1888 (1999).

[122] J. Grondalski, D. M. Etlinger, and D. F. V. James, The fully entangled fraction as an inclusive measure of entanglement applications, *Phys. Lett. A* **300**, 573 (2002).

[123] M. Horodecki, P. Horodecki, and R. Horodecki, Separability of mixed states: necessary and sufficient conditions, *Phys. Lett. A* **223**, 1 (1996).

[124] L. Masanes, Asymptotic violation of Bell inequalities and distillability, *Phys. Rev. Lett.* **97**, 050503 (2006).

[125] J. P. Crutchfield and J. Machta, Introduction to focus issue on "randomness, structure, and causality: measures of complexity from theory to applications", *Chaos* **21**, 037101 (2011).

[126] N. Ay, E. Olbrich, N. Bertschinger and J. Jost, A geometric approach to complexity, *Chaos* **21**, 037103 (2011). *ibid.* in Proceedings of ECCSÕ06, Santa Fe Institute, Working Paper 06-08-028 (2006)

[127] G. Tononi, G. M. Edelman, and O. Sporns, Complexity and coherency: integrating information in the brain, *Trends in Cognitive Science* **2**(12), 474 (1998).

[128] P. Grassberger, Toward a quantitative theory of self-generated complexity, *Int. J. Theor. Phys.* **25**(9), 907-938 (1986).

[129] C. H. Bennet, A. Grudka, M. Horodecki, P. Horodecki and R. Horodecki, Postulates for measures of genuine multipartite correlations, *Phys. Rev. A* **83**, 012312 (2011).

[130] D. M. Greenberger, M. A. Horne, A. Zeilinger in M. Kafatos (ed.), *Bell's Theorem, Quantum Theory, and Conceptions of the Universe*, Kluwer, Dordrecht, 73-76 (1989); D. M. Greenberger, M. A. Horne, A. Zeilinger, and A. Shimony, Bell's Theorem without Inequalities, *Am. J. Phys.* **58**, 1131-43 (1990).

[131] D. L. Zhou, Irreducible multiparty correlations in quantum states without maximal rank, *Phys. Rev. Lett.* **101**, 180505 (2008).

[132] G. L. Giorgi, B. Bellomo, F. Galve and R. Zambrini, Genuine quantum and classical correlations in multipartite systems, *Phys. Rev. Letts.* **107**, 190501 (2011).

[133] J. Mazeiro and F. M. Zimmer, Genuine multipartite system-environment correlations in coherent dynamics, *Phys. Rev. A* **86**, 042121 (2012).

[134] B. Li, L. C. Kwek and H. Fan, Detecting genuine multipartite correlations in terms of the rank of coefficient matrix, *J. Phys. A: Math. Theor.* **45**, 505301 (2012).

[135] A. Brodutch and K. Modi, Criteria for measures of quantum correlations, *Quantun Information and Computation* **12**, 721-742 (2012).

[136] T. Galla and O. Gühne, Complexity measures, emergence, and multiparticle correlations, *Phys. Rev. E* **85**, 046209 (2012).

[137] S. Niekamp, T. Galla, M. Kleinmann and O. Gühne, Computing complexity measures for quantum states based on exponential families, *J. Phys. A* **46**, 125301 (2013).

[138] Z. Ficek, and S. Swain, *Quantum interference and coherence: Theory and experiments*, Springer Series in Optical Sciences, Springer, New York (2005).

[139] M. B. Plenio and S. Virmani, An introduction to entanglement measures, *Quantum Information and Computation* **7**, 1-51 (2007).

[140] P. Hauke, M. Heyl, L. Tagliacozzo and P. Zoller, Measuring multipartite entanglement through dynamic susceptibility, *Nature Phys.* **Advance online publication** DOI:10.1038/nphys3700 (2016).